THE AEROSPACE CORPORATION

Submitted for Publication

The Physical Review

DIFFERENTIAL AND INTEGRAL CROSS SECTIONS FOR EXCITATION OF THE 2^1S STATE OF HELIUM BY ELECTRON IMPACT*

August 1971 SPL-2307

James K. Rice
Sandia Laboratories, Albuquerque, New Mexico 87115

Donald G. Truhlar
Department of Chemistry
University of Minnesota, Minneapolis, Minnesota 55455

David C. Cartwright
Space Physics Laboratories
The Aerospace Corporation, El Segundo, California 90045

and

Sandor Trajmar
Jet Propulsion Laboratory
California Institute of Technology, Pasadena, California 91103

*This research was supported in part by the United States Atomic Energy Commission through Sandia Laboratories and through the Department of Chemistry of the California Institute of Technology (Report Code No. CALT-767P4-84), by the Department of Chemistry of the University of Minnesota, by the U. S. Air Force Space and Missile Systems Organization (SAMSO) Contract No. F0-4701-70-C-0059, and by the National Aeronautics and Space Administration under Contract No. NAS7-100.

SC-RR-710474

DIFFERENTIAL AND INTEGRAL CROSS SECTIONS FOR EXCITATION OF THE 2^1S STATE OF HELIUM BY ELECTRON IMPACT*

James K. Rice
Sandia Laboratories, Albuquerque, New Mexico 87115

Donald G. Truhlar
Department of Chemistry
University of Minnesota, Minneapolis, Minnesota 55455

David C. Cartwright
Space Physics Laboratories
The Aerospace Corporation, El Segundo, California 90045

and

Sandor Trajmar
Jet Propulsion Laboratory
California Institute of Technology, Pasadena, California 91103

August 1971

ABSTRACT

Experimental measurements of the differential scattering cross sections for excitation of helium by electron impact from its ground state to its 2^1S state are given at four incident electron energies in the range 26-55.5 eV for scattering angles between 10° and 70° and at 81.6 eV for scattering angles between 10° and 80°. These differential cross sections are normalized by using previously determined 2^1P cross sections and measured

*This research was supported in part by the United States Atomic Energy Commission through Sandia Laboratories and through the Department of Chemistry of the California Institute of Technology (Report Code No. CALT-767P4-84), by the Department of Chemistry of the University of Minnesota, by the U. S. Air Force Space and Missile Systems Organization (SAMSO) Contract No. FO-4701-70-C-0059, and by the National Aeronautics and Space Administration under Contract No. NAS7-100.

$2^1S/2^1P$ cross section ratios. These experimental cross sections and cross section ratios are compared with results predicted by the Born approximation, the polarized Born approximation, and several other first-order approximations in which direct excitation is calculated in the Born approximation and exchange scattering in various Ochkur-like approximations. Calculations based on these approximations are also compared to the data of other experimenters. The effect on the small-angle scattering of several nonadiabatic dipole-polarization potentials is examined. For the 34-81.6 eV energy range, it is shown that the inclusion of polarization is necessary for accurate predictions of the angle dependence of the 2^1S cross sections at small angles. The cross sections resulting from the use of analytic self-consistent-field wave functions for both the ground and excited states agree well with those obtained from more accurate correlated wave functions.

ACKNOWLEDGMENTS

We are grateful to Professor Aron Kuppermann and Dr. Walter Williams for their contributions to the experimental work at 26.5-55.5 eV and 81.6 eV, respectively. We are grateful to Dr. Gordon W. F. Drake of the University of Windsor and to Dr. Robert Yaris of Washington University (St. Louis) for valuable discussions of the transition polarizability and to Dr. Drake for performing and sending his unpublished calculations mentioned in the text. Some of the work reported here was initiated while one of the authors (D.C.C.) was associated with the Institute for Extraterrestial Physics of the Max Planck Institute for Physics and Astrophysics in Munich, Germany, and with the Department of Physics of the University of Colorado in Boulder, Colorado, and while two of the authors (J.K.R. and D.G.T.) were associated with the Department of Chemistry of the California Institute of Technology. We would like to express our appreciation to Mrs. Monica Mate of the California Institute of Technology for her invaluable and excellent secretarial assistance with parts of this and many other manuscripts.

TABLE OF CONTENTS

LIST OF FIGURES

LIST OF TABLES

I. INTRODUCTION

In many cases, the first Born approximation has been successful in explaining the differential cross sections for electronic excitation of atoms and molecules by electron impact at high energies (E greater than about 150 eV) and small scattering angles (less than about 15°).[1-4a,5] This is the region where a study of the assumptions behind the first Born approximation leads us to expect it to be most valid, although the quantitative validity of the theory depends on the particular nature of the transition.[5,6] It is desirable to find a calculational scheme, as simple to apply as the first Born approximation, which represents the essential features of the scattering process at intermediate impact energies ($E \cong 15$-150 eV).

In a previous article[7] we presented a theoretical and experimental study of the electron scattering differential cross sections (DCS's) for the $(1s^2)\ 1^1S \rightarrow (1s2p)\ 2^1P$ transition in helium. In that paper we showed that the angle dependence of the DCS for $\theta \lesssim 40°$ and E = 34-82 eV was accurately predicted in the first Born approximation. The success of this approximation indicates that electron exchange, distortion of the scattering electron wave function, and polarization of the target by the incoming electron need not be included in calculating the angle dependence of the small-angle DCS for the $1^1S \rightarrow 2^1P$ transition. In the present article we use similar methods to study the $(1s^2)\ 1^1S \rightarrow (1s2s)\ 2^1S$ transition. We find, however, that it is necessary to include polarization of the target. The most important effect is the dipole polarization induced in the target, and we use the polarized Born approximation (a first Born calculation augmented by polarization)[8] to explain the experimental data. The polarized Born approximation includes the effect of monopole and dipole polarization

of the target. We again show that it is not necessary to treat exchange and distortion accurately to explain the main features of the angular dependence of the small-angle DCS. We discuss experimental and theoretical results for the ratios of the cross sections for these two excitations and both the differential and integral cross sections for excitation of the 2^1S state.

The previous differential cross section studies[2,9-14] of the 2^1S state are limited to small scattering angles $\theta \leq 20°$ (except for energies near threshold and for the data of Ref. 12 which may be in error at large θ due to double scattering[15]). These studies are summarized in Table I, where they are compared with the present experimental conditions. Pre-1940 experimental work on excitation of the n = 2 states of He is critically discussed in Appendix II. There are several previous experimental determinations of the $2^1S/2^1P$ differential cross section ratios.[16-25] These are summarized in Table II, where the energy and angular ranges are compared to the present work. By using our experimental cross section ratios and our approximate normalization of the 2^1P DCS's (Ref. 7) we can put our 2^1S DCS's on an absolute scale. Further, we integrate our 2^1S DCS's to obtain experimental estimates of the absolute 2^1S integral cross sections for impact energies E = 26.5-81.6 eV. The only previous experimental estimates of this quantity were obtained by Dugan, Richards, and Muschlitz[26] for E = 25-135 eV and Vriens, Simpson, and Mielczarek[2] for E = 100-400 eV.

Kim and Inokuti[5] concluded from a study of the available low-angle data in the 200-400 eV incident energy range that the Born approximation is valid down to lower energies for excitation of the 2^1P state than it is for excitation of the 2^1S state. We study this question further in this paper. Moiseiwitsch and Smith[27] pointed out that the Born-Oppenheimer approximation,

TABLE I. Measurements of the differential cross sections for the $1^1S \rightarrow 2^1S$ transition in helium.

Ref.	E(eV)	θ(deg)
9[a]	604	7.6 - 8.6
9[a]	511	3.8 - 8.8
9[a]	417	7.4 - 9.4
10[a]	500	4.7 -15.3
11	500	0.5 - 2.5
14	50 - 400	5
2	300 - 400	5 - 10
2	150 - 225	5 - 15
2	100	5 - 20
12[b]	56.5	5 - 60
13[b]	22	20 - 145
Present	81.6	10 - 80
Present	26.5 - 55.5	10 - 70

[a]The 2^1S and 2^1P peaks were not completely resolved in all the spectra reported in these references.

[b]The cross sections are given in relative units.

TABLE II. Measurements of the differential cross section ratios $2^1S/2^1P$.

Ref.	E(eV)	θ(deg)
23	25,000	0
9	511	4.0 - 8.8
10	500	6.3 - 15.3
11	500	0.5 - 2.5
2	300 - 400	5 - 10
17	235	9
2	150 - 225	5 - 15
18	202	0
2	100	5 - 20
19	22 - 80.7	0
12	56.5	5 - 60
16	50	0
24	48,500	0 - 12
25	48	0 - 12
22	46	90
14	50 - 400	5
Present	81.6	10 - 80
Present	26.5 - 55.5	0 - 70

which includes exchange effects, is much worse for S → S transitions than for S → P transitions. This fault occurs because the Born-Oppenheimer approximation greatly overestimates the effect of exchange for the former case. We bypass this difficulty by accounting for exchange using several Ochkur-like theories.[7,28-36] These theories give more reasonable predictions for the magnitude of the exchange effect and show that for qualitative purposes we may neglect exchange at small scattering angles.

In this paper we present and discuss new experimental and theoretical results and give an extensive analysis and re-evaluation of the experimental data of Rice, Trajmar, and Kuppermann.[37-39]

II. EXPERIMENTS

The electron impact spectrometer and data collection procedures used to obtain the experimental results reported here have been described previously in Ref. 7.

The basic experimental measurements consist of the determination of the intensity of electrons scattered after losing an energy corresponding to excitation of the 2^1S state relative to the intensity resulting from excitation of the 2^1P state as a function of scattering angle for a fixed incident energy. These intensity measurements were taken from the same energy-loss spectra used to obtain much of the data presented in Ref. 7. The $2^1S/2^1P$ intensity ratios are determined by dividing the height of the 2^1S energy-loss peak by that of the 2^1P peak at each angle and energy ($0° \leq \theta \leq 70°$ for E = 26, 34, 44, and 55.5 eV and $10° \leq \theta \leq 80°$ for E = 81.6 eV). Peak heights rather than areas can be used since the peak shapes were found to be independent of scattering angle. The instrumental factors relating the peak intensities to their respective differential cross sections are the same to a good approximation for both the 2^1S and the 2^1P energy-loss features in any one spectrum; therefore, these intensity ratios equal the corresponding differential cross section ratios. These experimentally determined ratios are shown in Figs. 1-3 along with the results of several theoretical calculations which are discussed in Secs. III and IV. The error limits assigned to the 26-55.5 eV ratios are the average deviations of 4 to 7 determinations at each angle. Each data point at 81.6 eV represents a single determination.

The $2^1S/2^1P$ (and $2^3S/2^1P$, $2^3P/2^1P$ and $3^3S/2^1P$) intensity ratios at $\theta = 0°$ agreed well with those of Chamberlain, Heideman, Simpson, and Kuyatt[19] at E = 55.5, 44, and 34 eV but disagreed with theirs at E = 26 eV.

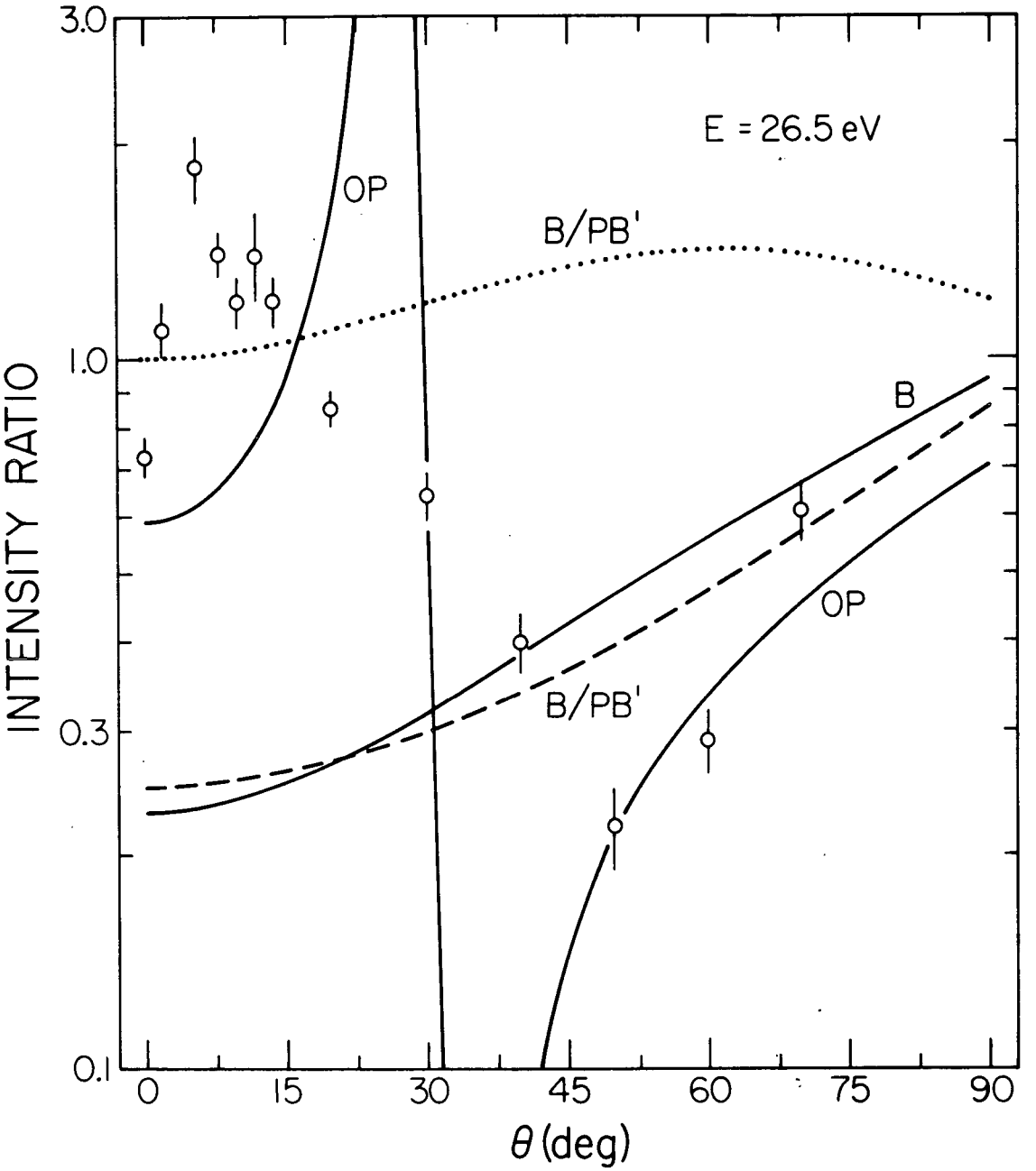

Fig. 1. Ratio of differential cross section of the $1^1S \rightarrow 2^1S$ transition to that of the $1^1S \rightarrow 2^1P$ transition as a function of scattering angle θ for E = 26.5 eV. The circles (with error bars) are the present experimental results and the curves are calculated by the indicated method. The dotted line was obtained with $b = (5/4)\, b_1^{FW} = 1.93\, a_o$ and the dashed line with $b = 2(5/4)\, b_1^{FW} = 3.86\, a_o$. The value of α is $1.584\, a_o^3$ in both cases.

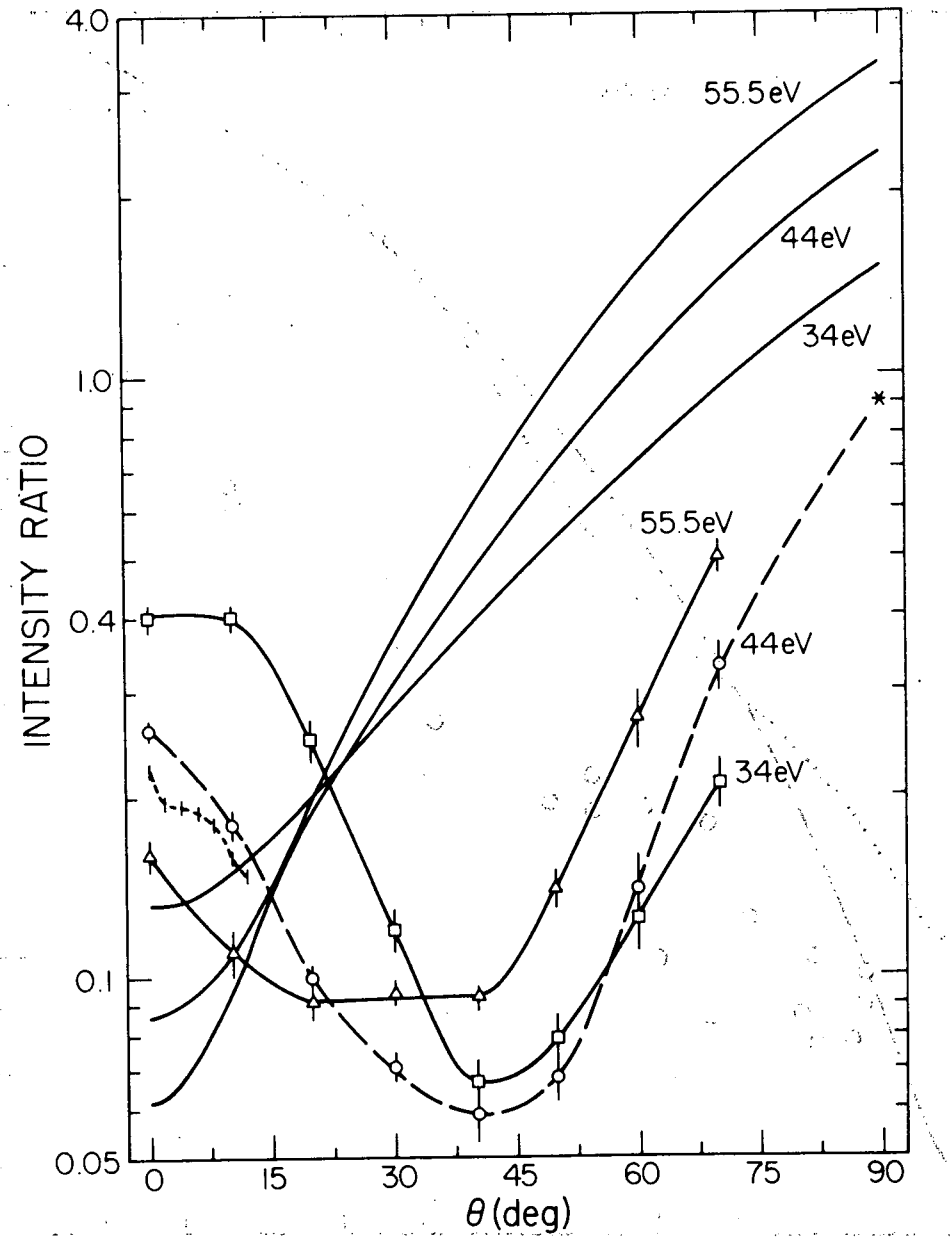

Fig. 2. Ratio of differential cross section of the $1^1S \rightarrow 2^1S$ transition to that of the $1^1S \rightarrow 2^1P$ transition as a function of scattering angle θ. The present experimental results at E = 55.5 eV (triangles with error bars and connected by a solid curve), 44 eV (circles with error bars and connected by a dashed curve), and E = 34 eV (squares with error bars and connected by a solid curve); the results of Lassettre, Skerbele, Dillon, and Ross (Ref. 25) at E = 48 eV (short dashed curve) and a value from Doering (Ref. 22) at 46 eV (asterisk) are shown. The monotonic solid curves are calculated at 34, 44, and 55.5 eV in the Born approximation.

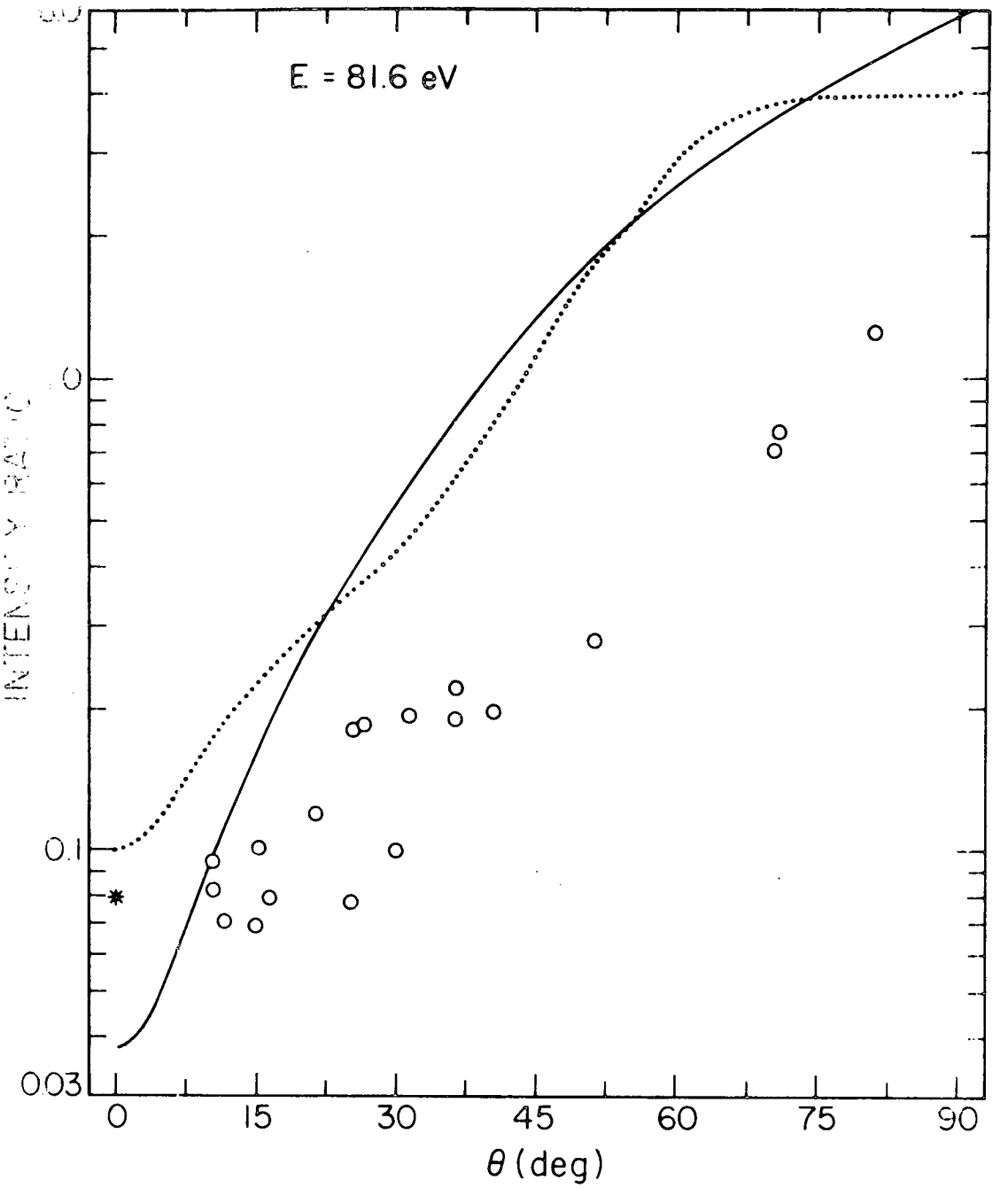

Fig. 3. Same as Fig. 1 except that E = 81.6 eV. The circles are the present experimental results; the asterisk is the 0° result of Chamberlain, Heideman, Simpson, and Kuyatt (Ref. 19) at E = 80.7 eV. The solid curve is calculated in the Born approximation (B) and the dotted curve in the polarized Born approximation (B/PB′) with $\alpha = 1.584\ a_o^2$ and $b = (5/4)\ b_1^{FW} = 3.39\ a_o$.

Since a change in our E of + 0.5 eV (which is within our uncertainty in E, see Ref. 7) completely resolves this discrepancy, we shall assume that E = 26.5 eV in this case.

The absolute 2^1S differential cross sections are computed from the above intensity ratios and the renormalized absolute 2^1P differential cross sections from Ref. 7 as discussed below. The extrapolation procedure used in Ref. 7 to facilitate normalization of the 2^1P differential cross sections assumed that the cross sections decrease monotonically with increasing angle. However, close coupling calculations of electron-hydrogen atom 1s-2p scattering predict differential cross sections which rise significantly at high angles.[40] Consequently, we renormalized the 2^1P differential cross sections presented in Ref. 7 by assuming a constant cross section for angles greater than those for which data were obtained. These renormalized values are lower than those of Ref. 7 by 1.6% at E = 86.3 eV, 7.6% at E = 55.5 eV, 8.0% at E = 44 eV, 7.8% at E = 34 eV, and 19.5% at E = 26.5 eV.

The experimental 2^1S differential cross sections are presented in Figs. 4-8 along with the results of several theoretical calculations which are discussed in Secs. III and IV.

The error bars assigned to the 2^1S differential cross section data include the errors in the ratios and uncertainties in the shape but not the magnitude of the 2^1P differential cross sections. Therefore, these error bars include the uncertainty in the angular dependence of the 2^1S differential cross sections but only part of the uncertainty in their magnitude. The percentage uncertainty in the overall scale at each energy is approximately equal to the "estimated percent error" in the integral of the 2^1P differential cross sections given in Table II of Ref. 7.

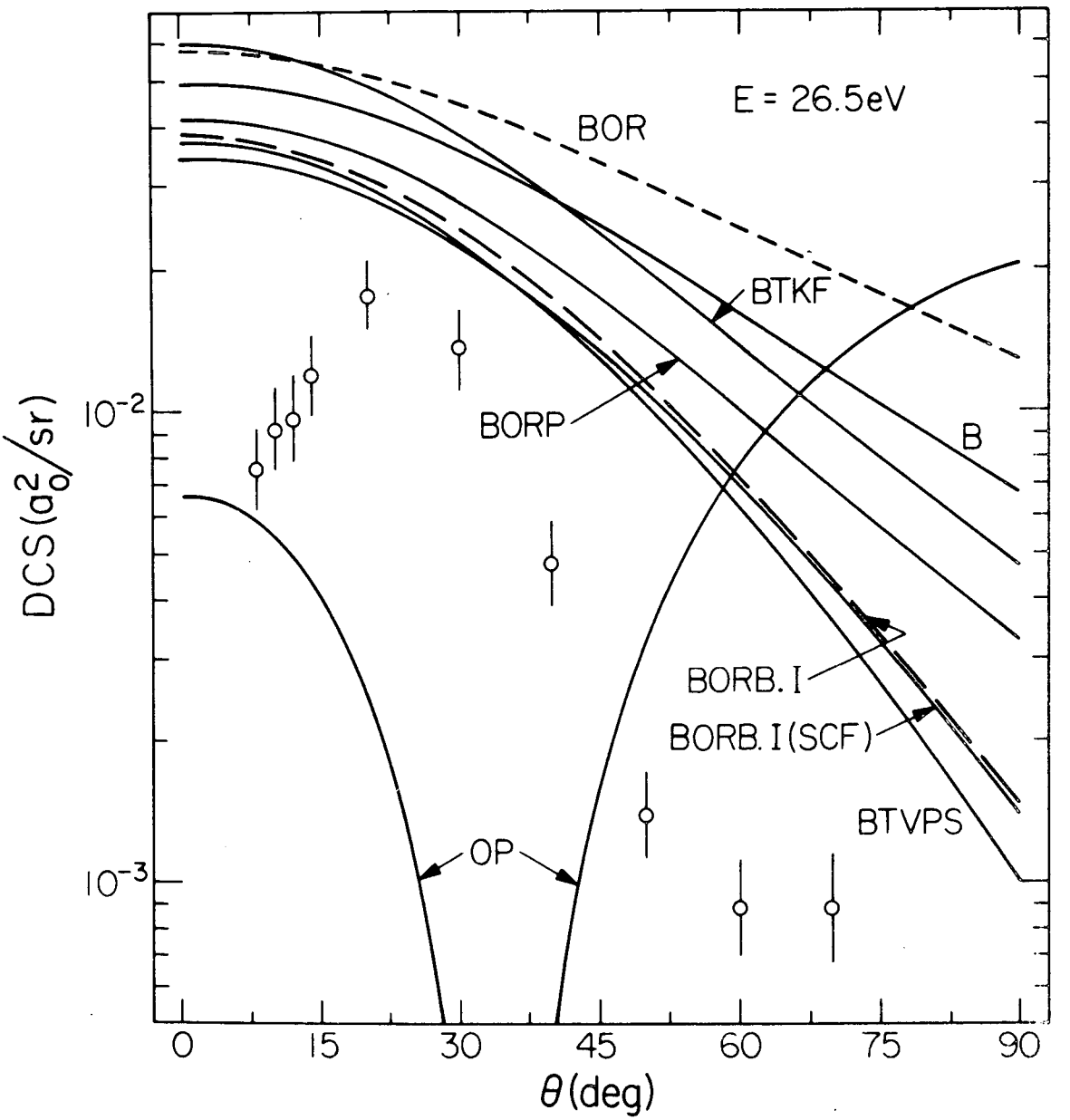

Fig. 4. Differential cross section versus scattering angle for E = 26.5 eV. The circles (with error bars) are the present experimental results. The curve labeled BORB.I(SCF) is calculated in he symmetrized Born-Ochkur-Rudge approximation with the SCF wave functions. The other curves are calculated in the indicated approximations using the accurate generalized oscillator strengths (Refs. 5 and 86).

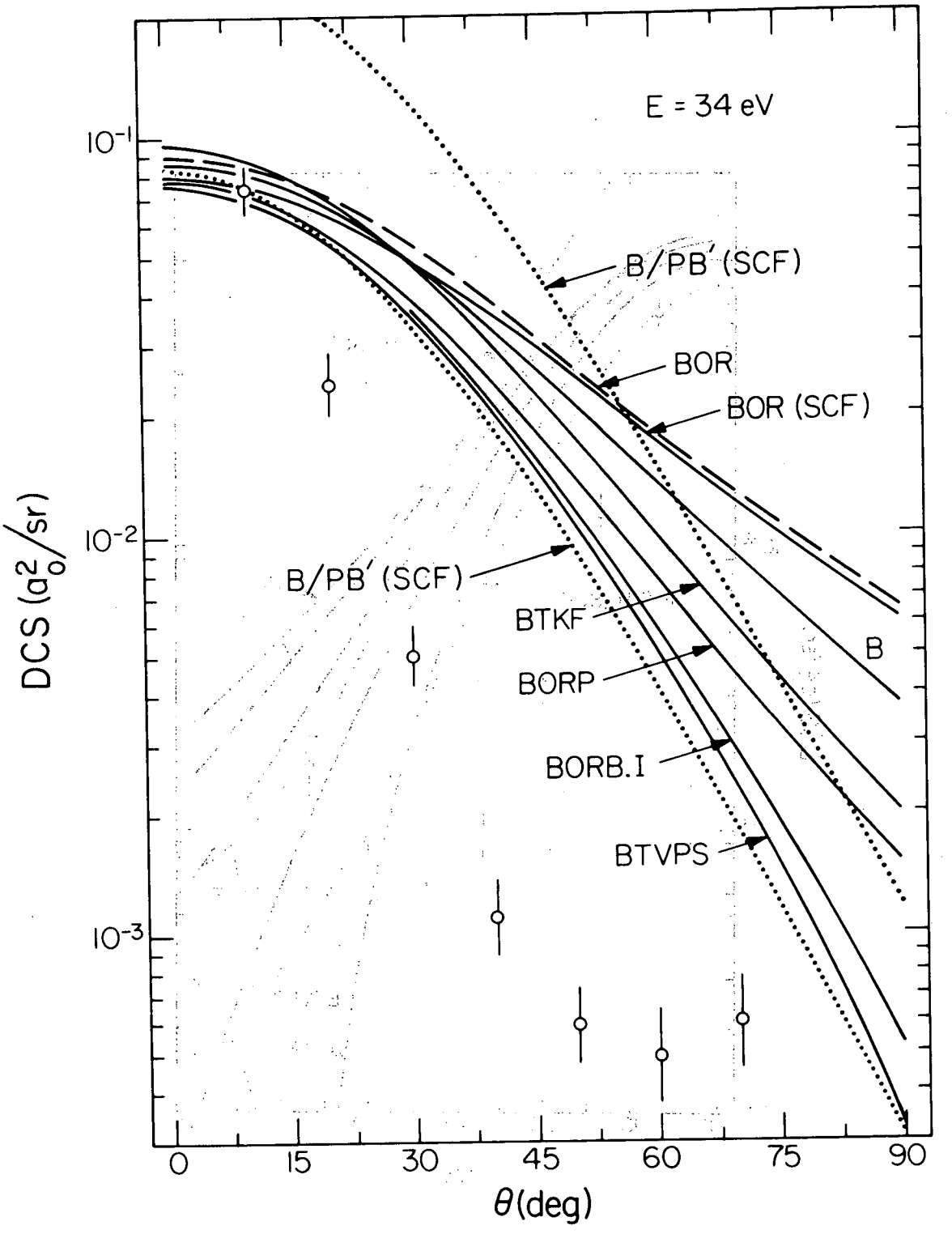

Fig. 5. Differential cross section versus scattering angle θ for E = 34 eV. The circles (with error bars) are the present experimental results. The curves are calculated using the accurate generalized oscillator strengths (Refs. 5 and 86). The upper dotted curve is calculated in the dipole-polarized Born approximation with $\alpha = 1.584\ a_0^3$ and $b = (5/4)\ b_1^{FW} = 2.19\ a_0$. The lower dotted curve is the same but renormalized to experiment at $\theta = 10°$. No other calculation is renormalized.

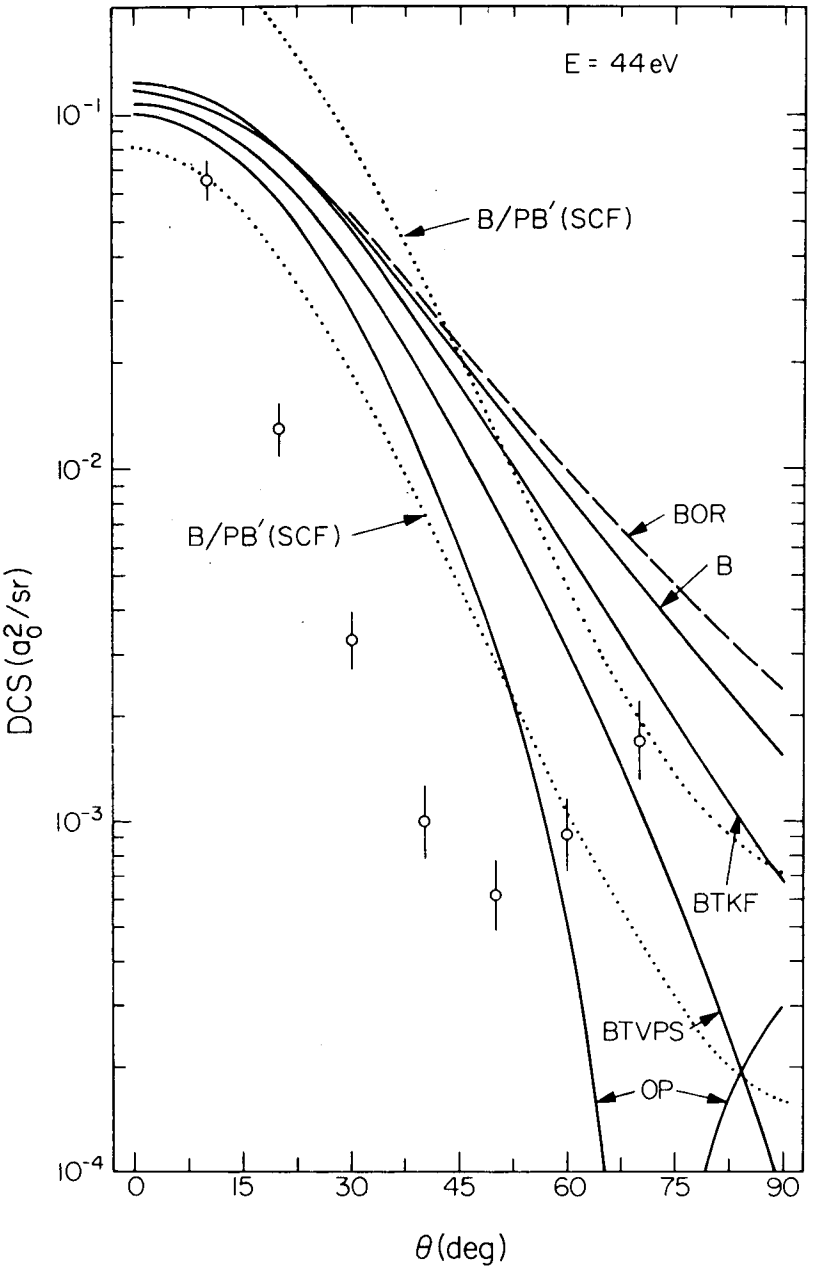

Fig. 6. Same as Fig. 5 except E = 44 eV and b = 2.49 a_o.

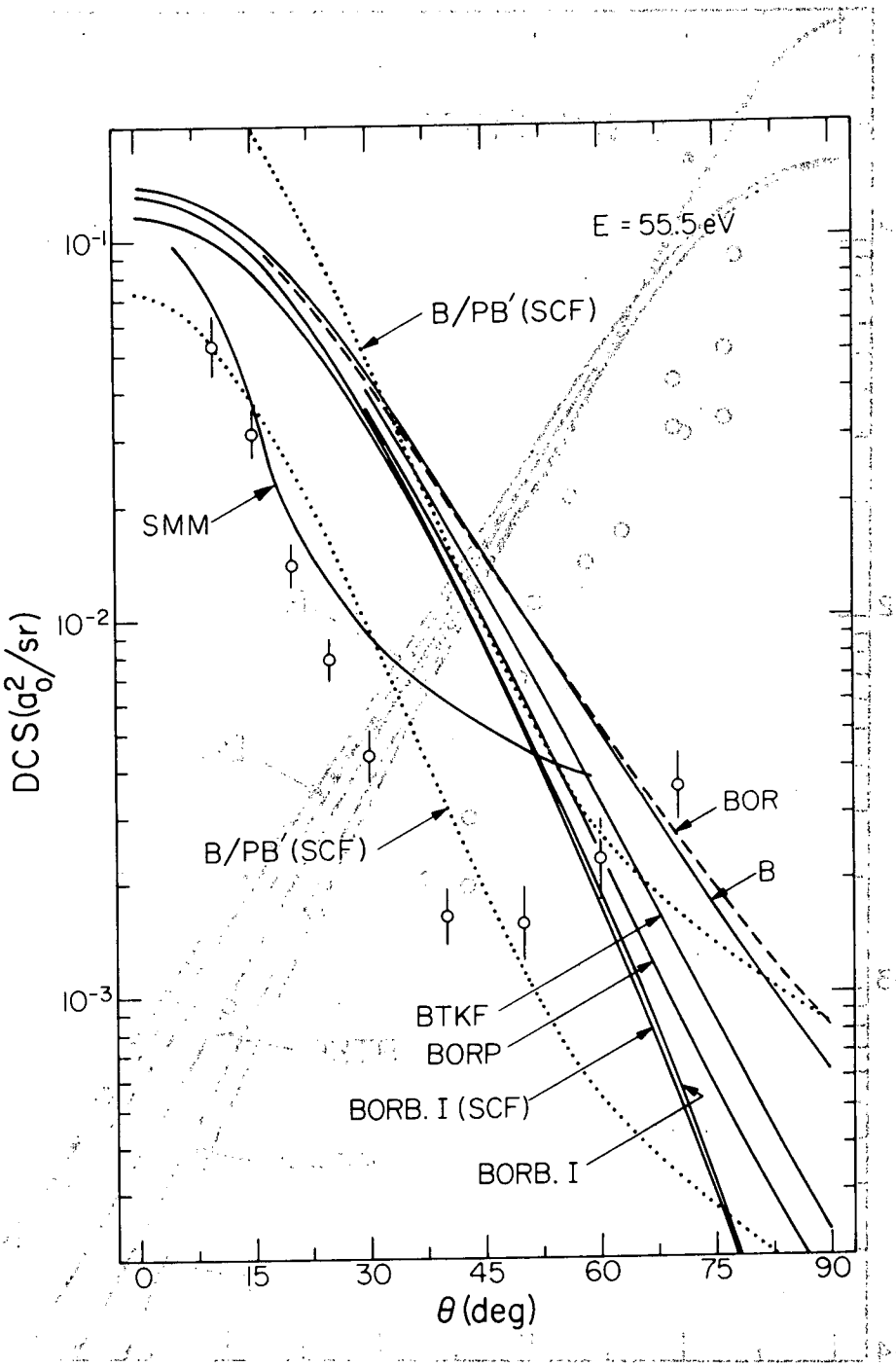

Fig. 7. Same as Fig. 5 except E = 55.5 eV and b = 2.79 a_o. The curve labeled SMM is an experimental result from Ref. 12 (56.5 eV) and is normalized to the lower dotted curve at 30°.

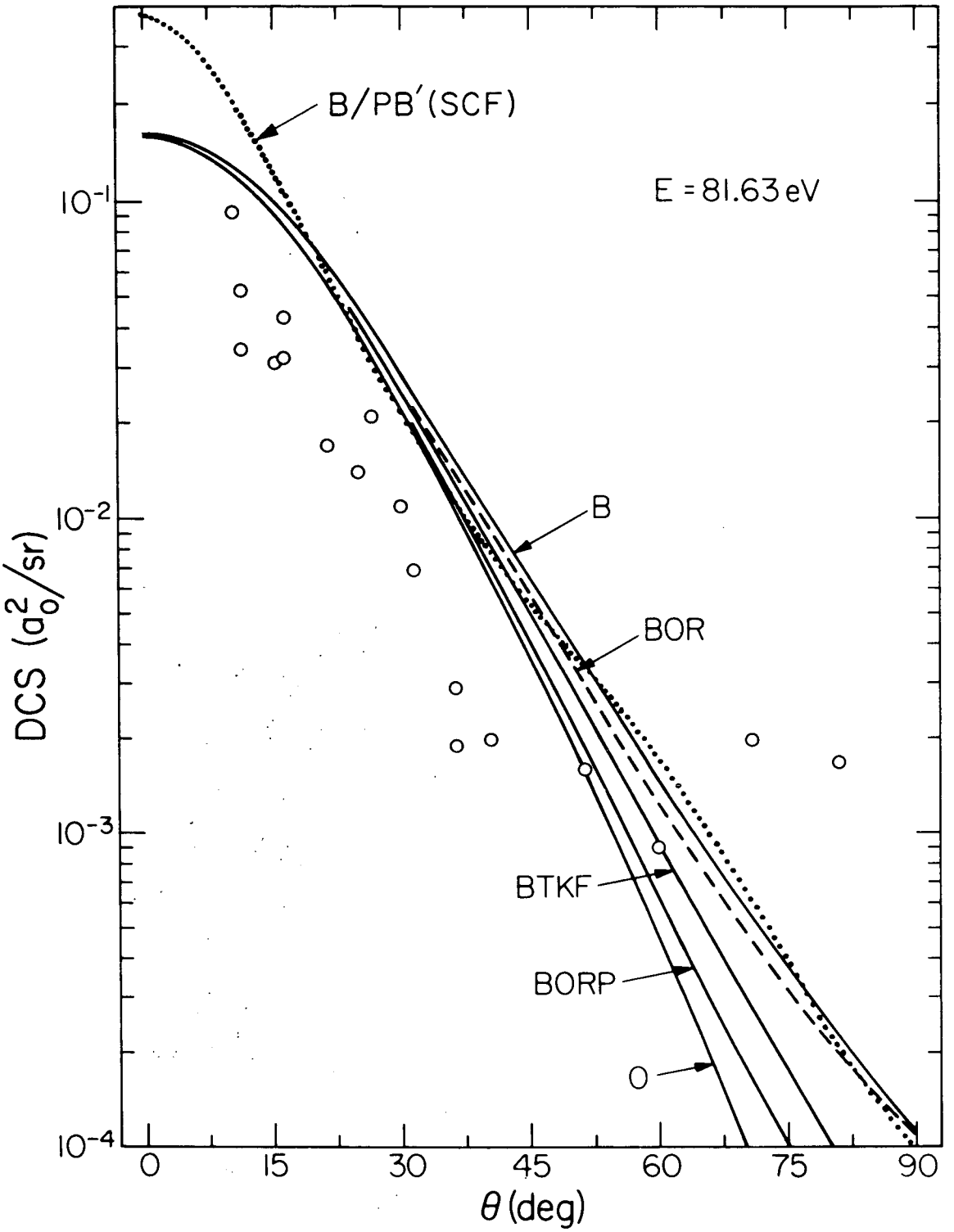

Fig. 8. Same as Fig. 5 except E = 81.6 eV, b = 3.39 a_0, the data are shown as circles without error bars, and no renormalized calculations are presented.

The 2^1S integral cross section $Q(E)$ is related to the differential cross section $I(E,\theta)$ by

$$Q(E) = 2\pi \int_0^{\pi} I(E,\theta) \sin\theta \, d\theta \quad . \tag{1}$$

In order to perform this integral, the 2^1S differential cross sections are extrapolated to 0° and to 180°. The extrapolation to 0° introduces little uncertainty into the integral (see Ref. 7) but the extrapolation to 180° is subject to large uncertainties since the 2^1S DCS's are generally rising at the highest angles for which data are obtained. The contribution to Eq. (1) of the extrapolation to 180° is assumed to be

$$Q_{ext}(E) = 2\pi \, I(E,\theta_{max}) \int_{\theta_{max}}^{\pi} \sin\theta \, d\theta \quad , \tag{2}$$

where θ_{max} is the largest angle for which data are obtained. Table III gives the contributions to (1) from angles less and greater than θ_{max} and the resulting 2^1S integral cross sections. The estimated percent error given in this table includes contributions from both regions of the integral and includes the uncertainty in both the shape and scale of the 2^1S differential cross sections.

TABLE III. Integration of the 2^1S differential cross sections to obtain integral cross sections $Q(10^{-2}\ a_o^2)$.

E(eV)	θ (deg) max	Contributions to Q		Q	Estimated percent error
		$\theta \leq \theta_{max}$	$\theta \geq \theta_{max}$		
26.5	70	2.2	0.7	2.9	50
34	70	2.8	0.4	3.2	35
44	70	2.5	1.5	4.0	48
55.5	70	2.6	3.0	5.6	52
81.6	80	2.5	0.9	3.4	58

III. THEORY

A. Scattering Equations

The theory of electron scattering by the helium atom is well developed.[4,27] Consider the close-coupling equations for this problem. As written by Burke, Cooper, and Ormonde,[41] the coupled integro-differential equations (in hartree atomic units) for the radial functions $F_{m\sigma}^{LS}$ are

$$\left(\frac{d^2}{dr^2} - \frac{\ell_2(\ell_2+1)}{r^2} + \frac{4}{r} + k_m^2\right) F_{m\sigma}^{LS}(r) \tag{3}$$

$$= \sum_n \left[2V_{mn}(r)F_{n\sigma}^{LS}(r) + \int_0^\infty K_{mn}(r,r')F_{n\sigma}^{LS}(r')dr'\right] ,$$

where L and S are the total orbital and spin angular momentum quantum numbers, respectively, r is the separation between the scattering electron and the atomic nucleus, m denotes the state of the atom, ℓ_2 is the orbital angular momentum of the electron, σ denotes the initial state of the atom, and the sum is over all atomic eigenstates in the (necessarily truncated) expansion of the wave function. The wave number k_m and the matrix elements V_{mn} and K_{mn} are defined in Ref. 41. We make the approximation that the eigenfunction expansion is truncated to include M states of S symmetry and N states of P symmetry. We denote unspecified S states by i and j, and unspecified P states by β. Further we use 1, 2, and α to denote the 1^1S, 2^1S, and 2^1P states, respectively. If we specifically consider scattering from ground state helium, Eq. (3) becomes

$$\left(\frac{d^2}{dr^2} - \frac{\ell_2(\ell_2+1)}{r^2} + \frac{4}{r} + k_m^2\right) F_{m1}^{LS}(r)$$

$$= \sum_{i=1}^{M} \left[2V_{mi}(r) + K_{mi}(r)\right] F_{i1}^{LS}(r)$$

$$+ \sum_{\beta=\alpha}^{N} [2V_{m\beta}(r) + K_{m\beta}(r)] F^{LS}_{\beta 1}(r) \quad , \tag{4}$$

where we denote the nonlocal exchange potential by

$$K_{mn}(r)F^{LS}_{ni}(r) \equiv \int_0^\infty K_{mn}(r,r')F^{LS}_{ni}(r')dr' \quad . \tag{5}$$

We do not want to solve these equations exactly but rather to find simple approximations. We next consider the terms in Eq. (4) for some special cases to show which terms can be neglected and which terms should be approximated.

1. Elastic Scattering in the 1^1S State

For elastic scattering in the ground state, the Born-Oppenheimer[4,27,42] approximation corresponds to truncating the sums at M = 1 and N = 0 (no P states) and approximating the radial function in Eq. (4) as a radial function for a free particle with wave number k_1

$$F^{LS}_{11}(r) = j_{\ell 2}(k_1 r) \quad . \tag{6}$$

Then the scattering amplitude is the matrix element between free particle states of the nonlocal potential

$$2V_{11}(r) + K_{11}(r) \quad . \tag{7}$$

The Born (B) approximation[4] consists in further neglecting $K_{11}(r)$.

In these approximations we neglect completely the effect of virtual and real excitations of the P states, i.e., the dipole-polarization of the target. It is well known that this is a serious error.[4,43-44] (Virtual excitation of excited S- and D-states, i.e., monopole and quadrupole polarization, are less important processes.) The polarization

effect is especially important for small angle scattering.[4b,8,43-46] The polarization effect can be included by using the optical potential

$$2V_{11}(r) + K_{11}(r) + 2U_{11}(r) \tag{8}$$

instead of the potential (7) in the matrix element. $U_{11}(r)$ is chosen to simulate the polarization effect, This is the polarized Born-Oppenheimer approximation, and neglecting $K_{11}(r)$ yields the polarized Born (B/P) approximation. It can be shown that the long range behavior of $U_{11}(r)$ can be obtained in the adiabatic approximation,[47-49] in which it is assumed that fluctuations in the incident particle's kinetic energy are small compared to fluctuations in the energy E(n) of the target (virtual excitations).[47-51] In this way it can be shown that

$$U_{11} \sim \frac{-\alpha_{11}}{2r^4}, \quad r \to \infty \tag{9}$$

$$\alpha_{11} = 2 \sum_{\beta=\alpha}^{\infty} \frac{Z_{1\beta} Z_{\beta 1}}{\Delta E_1^{\beta}} \tag{10}$$

$$Z_{j\beta} = \langle j^1S | z_1 + z_2 | \beta^1P \rangle \tag{11}$$

$$\Delta E_j^{\beta} = E(\beta^1P) - E(j^1S) \quad . \tag{12}$$

In Eq. (11), z_1 and z_2 are the z-components of the position vectors of the two bound electrons. The large-r behavior of U_{11} can be compared with that of V_{11},

$$V_{11} \sim c_{11} \exp(-c'_{11} r), \quad r \to \infty \tag{13}$$

with $c'_{11} > 0$. It is because U_{11} is a long range potential compared with V_{11} that polarization is so important for elastic scattering in the ground state.

At very high energy the nonadiabatic effects become very large (so that (9) holds only at such large distances so as to be unimportant), and the polarization potential is vanishingly small.

2. $1^1S \rightarrow 2^1P$ Excitation

For excitation of the 2^1P state from the ground state, the Born-Oppenheimer approximation to the transition amplitude is the matrix element between free particle wave functions of

$$2V_{1\alpha}(r) + K_{1\alpha}(r) \quad . \tag{14}$$

Since

$$V_{i\beta}(r) \sim \frac{c_{i\beta}}{r^2} \ , \ r \rightarrow \infty, \quad \text{all } \beta \quad , \tag{15}$$

is a long range potential, the effects of polarization and exchange on the small angle scattering for this excitation are much smaller than for elastic scattering. Indeed, the Born approximation, which neglects these effects, predicts the angle dependence of the differential cross section for excitation of the 2^1P state quite well for small scattering angles.[7]

3. $1^1S \rightarrow 2^1S$ Excitation

a. Born-Oppenheimer Approximation

For excitation of the 2^1S state from the ground state, the Born-Oppenheimer approximation can be obtained by truncating the sums in (4) at $M = 2$ and $N = 0$ (no P states), making the further approximations (6) and

$$F_{21}^{LS}(r) = j_{\ell_2}(k_2 r) \quad , \tag{16}$$

and approximating the transition amplitude as the matrix element between the free-particle wave functions (6) and (16) of the non-local transition

potential

$$2V_{12}(r) + K_{12}(r) \quad . \tag{17}$$

For this optically forbidden transition[52]

$$V_{12}(r) \sim c_{12} \exp(-c'_{12} r), \quad r \to \infty \tag{18}$$

with $c'_{12} > 0$. This potential is shorter-range than the transition potential (15) corresponding to the optically allowed transtion to the 2^1P state.

b. Born Approximation

The Born approximation is the same as the Born-Oppenheimer approximation except $K_{12}(r)$ is neglected in (17).

c. Polarized Born Approximation

Because of the different ranges of the transition potentials V_{12} and $V_{i\beta}(i = 1,2)$, the second order process $1^1S \to \beta^1P \to 2^1S$ can provide important competition with the first order process $1^1S \to 2^1S$ as the dominant mechanism for this process. Thus, the most serious error in the Born approximation for the $1^1S \to 2^1S$ excitation is the neglect of virtual excitation of P states (polarization).[53] This effect can be included by using the full close-coupling equations[41] (4) or by second order perturbation theory. We will include it by a method not previously applied to electronically inelastic scattering - the polarized Born approximation.[8] We replace the potential $V_{12}(r)$ by

$$V_{12}(r) + U_{12}(r) \quad , \tag{19}$$

where $U_{12}(r)$ is a generalized optical potential[54] designed to incorporate the polarization effect. For small r we must take account of

nonadiabatic effects, but the asymptotic form of $U_{12}(r)$ can be obtained using the adibatic approximation.[55-56] Making the adiabatic approximation in the initial state (electron in the field of He 1^1S) results in

$$U_{12} \sim \frac{-\alpha_{12}}{2r^4} , \quad r \to \infty \quad , \tag{20}$$

where the static transition polarizability

$$\alpha_{12} = \alpha_{12}^{(1)} = 2 \sum_{\beta} \frac{Z_{2\beta} Z_{\beta 1}}{\Delta E_1^{\beta}} \quad . \tag{21}$$

Making the adiabatic approximation in the final state (electron in the field of He 2^1S) again yields (20) but with

$$\alpha_{12} = \alpha_{12}^{(2)} = 2 \sum_{\beta} \frac{Z_{1\beta} Z_{\beta 2}}{\Delta E_2^{\beta}} \quad . \tag{22}$$

The asymptotic form (20) is not valid at all r and we will use the two-parameter forms

$$U_{12}^{A} = \frac{-\alpha_{12}}{2(r^2 + b^2)^2} \tag{23}$$

$$U_{12}^{B} = \begin{cases} -\alpha_{12}/2r^4 & r > b \quad (24a) \\ -\alpha_{12}/2b^4 & r \le b \quad (24b) \end{cases}$$

$$U_{12}^{B'} = \begin{cases} -\alpha_{12}/2r^4 & r > b \quad (25a) \\ -\alpha_{12} r/2b^5 & r \le b \quad (25b) \end{cases}$$

$$U_{12}^{C} = \begin{cases} -\alpha_{12}/2r^4 & r > b \quad (26a) \\ 0 & r \le b \quad (26b) \end{cases}$$

as approximate representations of the polarization transition potential for all r. The forms are chosen so that by making b large we can reduce the polarization potential for $r < b$ from its asymptotic form. This reduction simulates the main nonadiabatic effect. In this regard the form B′, which has not been used previously, is apparently the most realistic[57a] of the four.

The scattering amplitude in the polarized Born approximation[8] is

$$f^{B/P} = f^{B} + f^{P} \tag{27}$$

where

$$f^{P} = -\frac{1}{2\pi}\int d\vec{r}_3\, e^{i\vec{q}\cdot\vec{r}_3}\, U_{12}(r_3) \tag{28}$$

$$f^{B} = -\frac{1}{2\pi}\int d\vec{r}_3 e^{i\vec{q}\cdot\vec{r}_3}\iint d\vec{r}_1 d\vec{r}_2 \psi_2^*(\vec{r}_1,\vec{r}_2)\psi_1(\vec{r}_1,\vec{r}_2)\left[\frac{1}{r_{13}}+\frac{1}{r_{23}}\right] \tag{29}$$

$$= -(4/q^2)M$$

$$M = \int \psi_2^*(\vec{r}_1,\vec{r}_2)e^{i\vec{q}\cdot\vec{r}_1}\,\psi_1(\vec{r}_1,\vec{r}_2)d\vec{r}_1 d\vec{r}_2 \tag{30}$$

$$\vec{q} = \vec{k}_2 - \vec{k}_1 \ . \tag{31}$$

ψ_1 and ψ_2 are the initial and final state wave functions, respectively, $\vec{r}_1$ and $\vec{r}_2$ are the position vectors of the two bound electrons, $\vec{r}_3$ is the position vector of the scattering electron with initial wave number k_1 and final wave number k_2, and q is the momentum-transfer. U_{12} and f^B depend on the phases of the bound state functions in the same way; thus, the cross sections (proportional to the squared modulus of $f^{B/P}$) will be independent of the phases of the bound-state wave functions. We have consistently chosen the spatial part of the 1^1S bound state wave function ψ_1 positive. The spatial part of the 2^1S bound state wave function ψ_2 is chosen negative

at the nucleus and positive at large r_1 and r_2. With this choice of signs and the wave functions in Section III.B, M is calculated to be negative and f^B is positive for all q, and α_{12} is positive when evaluated theoretically (see Eqs. (21)-(22) and see below). Since the polarization transition potential U_{12} is spherically symmetric, (28) can be reduced to

$$f^P = -(2/q) \int_0^\infty \sin qr \, U_{12}(r) r \, dr \tag{32}$$

and the integral can be performed analytically for the potentials of Eqs. (23)-(26). We obtain

$$f^{P(A)} = (\alpha_{12}\pi/4b) \exp(-B) \tag{33}$$

$$f^{P(B)} = (\alpha_{12}/b)\left[(B^{-2} + \tfrac{1}{2})\left(\frac{\sin B}{B}\right) + (\tfrac{1}{2} - B^{-2})\cos B - \tfrac{1}{4}\pi B + \tfrac{1}{2} B \, Si(B)\right] \tag{34}$$

$$f^{P(B')} = (\alpha_{12}/b)\left[(\tfrac{1}{2} + 2B^{-2})\left(\frac{\sin B}{B}\right) + (\tfrac{1}{2} - B^{-2} + 2B^{-4})\left(\frac{\cos B}{B}\right) - 2B^{-4} - \tfrac{1}{4}\pi B + \tfrac{1}{2} B \, Si(B)\right] \tag{35}$$

$$f^{P(C)} = (\alpha_{12}/b)\left[\tfrac{1}{2} B^{-1} \sin B + \tfrac{1}{2} \cos B - \tfrac{1}{4}\pi B + \tfrac{1}{2} B \, Si(B)\right] \tag{36}$$

where

$$B = qb$$

$$Si(B) = \int_0^B \frac{\sin t}{t} \, dt \tag{37}$$

Although the potentials (23)-(26) all have the same long range form, the limiting forms of f^P at small scattering angles differ. These results are given in Appendix I.

Notice that $f^{P(A)}$ is positive for all q but the amplitudes associated with the B, B′, and C forms of the potential may be positive or negative, depending on q. However, since all the forms lead to f^P being positive at small q (see Appendix I), the polarization amplitude will interfere constructively with f^B there and will increase the small angle scattering. Since the form of f^P for large q depends on the uncertain details of $U_{12}(r)$, i.e., on its small r form, we cannot trust the predictions of this simple polarization model at large scattering angles. By using more than one form for U_{12} at smaller r we get an estimate in each case of how large a scattering angle can be treated without a better model for the polarization potential at small r.

Previous treatments of the polarization effect indicate that α_{12} should be independent of energy and equal to the static transition polarizability (21) or (22), but that the cutoff parameter b in Eqs. (23)-(26) should be energy-dependent. Mittleman[57b] discussed the polarization effect for inelastic scattering and concluded that nonadiabatic effects may be larger in this case than for elastic scattering, i.e., b may be very large.[53] Polarization corrections must become small at very high energies. Nevertheless, in treating electronically elastic scattering it has been found that use of the static polarizability and a cutoff of the magnitude of the target dimensions provides a reasonable approximation even at energies as high as 700 eV.[8,43-44,46] Holt and Moiseiwitsch's[58] second-Born calculations show that polarization corrections become small at a lower energy for inelastic scattering than for elastic scattering.

As shown above, we obtain different adiabatic polarization potentials if we consider polarizing interactions in the initial and final states. Since we do not have a good method for quantitatively estimating nonadiabatic effects, we wish to use the case which has smaller nonadiabatic corrections. Fetter and Watson[50] show that a reasonable criterion for validity of the adiabatic approximation in state j at a distance r much greater than the atomic radius is

$$b_j^{FW} \equiv k_j / < \Delta E_j^{\beta} > \ll r \quad . \tag{38}$$

In (38), $< \Delta E_j^{\beta} >$ is the effective average value of ΔE_j^{β} over all states β causing polarization. The usual approximation is $< \Delta E_j^{\beta} > \cong U_j$ where U_j is the ionization potential in state j. In our case, $U_1 = 0.90372$ a.u. and $U_2 = 0.14597$ a.u. However, we find (see below) that excitations from the 2^1S state are dominated by those to the 2^1P state. Thus, we take $< \Delta E_1^{\beta} > = U_1$, but $< \Delta E_2^{\beta} > \cong \Delta E_2^2 = 0.02213$ a.u. We can now use b_j^{FW} as an approximate estimate of b (we expect that b is at least approximately proportional to b_j^{FW} with an energy-independent constant of proportionality). The results are shown in Table IV. The table shows that the adiabatic approximation to polarizing interactions in the final state is a good approximation only for distances too large to be interesting, i.e., nonadiabatic corrections are large in this case. However, it also shows that we can use the adiabatic approximation to polarizing interactions in the initial state to obtain a useful estimate of the polarization effect. For lack of a better theory at this time, we will consider b_1^{FW} to be the theoretically most justified choice for b in Eqs. (23)-(26). At zero momentum transfer (q = 0), the scattering amplitudes f^P associated with the polarization forms A, B, B′, and C (see Eqs. (23)-(26) and Appendix I) are $\pi\alpha/4b$, $4\alpha/3b$, $5\alpha/4b$,

TABLE IV. Values of the cutoff parameter b_j^{FW} computed using the Fetter-Watson formula (Eq. 38).

E (eV)	k_1 (a_o^{-1})	k_2 (a_o^{-1})	b_1^{FW} (a_o)	b_2^{FW} (a_o)
26.50	1.40	0.66	1.54	29.72
44.00	1.80	1.31	1.99	59.24
81.63	2.45	2.12	2.71	95.69
150.00	3.32	3.08	3.67	139.35
300.00	4.70	4.53	5.20	204.77
500.00	6.06	5.94	6.71	268.23
25000.00	42.87	42.85	47.43	1936.24

and α/b, respectively. In order to make these amplitudes equal at $q = 0$, we usually use $b = (\text{const.}) \times b_1^{FW}$ where the constant is $\pi/4$, $4/3$, $5/4$, and 1 for forms A, B, B′, and C, respectively. We will also consider an empirical determination of b in Section IV.A.1.

There are at least two reasons why we might expect nonadiabatic effects to be larger for electronically inelastic scattering than for electronically elastic scattering. (1) A change of electronic state is a nonadiabatic phenomenon. (2) Elastic scattering is dominated by large ℓ_2 (large impact parameters in semiclassical language). At any given energy, the relative velocity along the line connecting target and projectile is smaller for larger impact parameters than it is for smaller ones. Consequently, electronic adiabaticity (which roughly depends on the relative velocity being smaller than the average kinetic energy of the bound electrons) is more likely when ℓ_2 is large. Inelastic scattering cross sections are smaller than elastic scattering cross sections so that they depend more on low-partial-wave scattering; thus, the adiabatic approximation should not be as accurate for inelastic scattering as for elastic scattering.

d. Polarized Born-Oppenheimer Approximation

The polarized Born-Oppenheimer approximation consists of replacing the potential (17) by

$$V_{12}(r) + U_{12}(r) + K_{12}(r) \tag{39}$$

where V_{12} is the direct transition potential, U_{12} is the (direct) polarization transition potential, and $K_{12}(r)$ is the exchange transition potential. Upon summing over partial waves, $V_{12}(r)$ and $U_{12}(r)$ lead to the direct scattering amplitude $f^{B/P}$ and $K_{12}(r)$ leads to the Oppenheimer[42] exchange scattering amplitude g^{BO},

$$g^{BO} = -\frac{1}{2\pi}\iiint e^{i\vec{k}_1\cdot\vec{r}_3 - i\vec{k}_2\cdot\vec{r}_1}\,\psi_2^*(\vec{r}_3,\vec{r}_2)\psi_1(\vec{r}_1,\vec{r}_2)\left(\frac{1}{r_{13}} + \frac{1}{r_{23}} - \frac{2}{r_3}\right)$$

$$d\vec{r}_1\, d\vec{r}_2\, d\vec{r}_3 \quad . \tag{40}$$

In the polarized Ochkur-like approximations considered below we use the potential (39) but modify the terms containing $K_{12}(r)$ in ways designed to remove some of the failings of the Oppenheimer exchange amplitude.

e. Ochkur-Like Theories and Polarized Ochkur-Like Theories

The Born-Oppenheimer (BO) approximation[42] was the first and is perhaps the most well-known method of including electron exchange, but the exchange amplitude in this approximation suffers from a number of serious deficiencies, including the lack of orthoganality between the initial and final total-system wave functions. In practice, the calculated cross section is much too large near threshold, leading to a serious violation of flux conservation.[59] The role of the electron-nucleus interaction term in a first-order theory has recently been discussed by a number of workers.[60] Although the angular dependence of the BO differential cross section is in fair qualitative agreement with the accurate theories, the magnitude is invariably too large except at the highest electron energies.[35] Only those first-order approximations to the exchange amplitude which represent improvements over the BO approximation will be employed here.

Ochkur observed[28,61] that in the case of the excitation of helium, the prior-interaction form of the BO exchange scattering amplitude (Eq. (40)), can be expanded in inverse powers of the incident electron energy. Retaining at all energies only the first term in this expansion results in what we call the prior-interaction form of the Ochkur (O) approximation. The exchange amplitude in this approximation is related to the Born approximation by

$$g^{O} = (q^2/k_1^2) f^{B} \quad . \tag{41}$$

Any expression like this one which relates the exchange amplitude to the direct amplitude by a factor independent of the electronic structure of the target will be called an Ochkur-like approximation. Although Ochkur's formula cannot be obtained from a variational expression, Rudge has obtained[29] an approximation (denoted OR) based on a variational principle in the prior-interaction form. It is designed so that it reduces to the Ochkur form at high energies, but it sometimes gives improved cross sections at lower energies. The exchange amplitude in the OR approximation is

$$g^{OR} = \frac{q^2 e^{2i\xi_{12}} f^{B}}{(k_2^2 + 2U_1)} \tag{42}$$

where

$$\xi_{12} = \tan^{-1} \frac{\sqrt{2U_1}}{k_2} \tag{43}$$

and U_1 is the ionization energy. However, the OR approximation to g combined with f^{B} or $f^{B/P}$ does not satisfy detailed balancing because of the nonsymmetric phase factor in the amplitude. Bely[62] removed this discrepancy by forming an exchange amplitude which is the absolute value of the (OR) form. We call this the symmetrized Ochkur-Rudge approximation (denoted ORB.I),

$$g^{ORB.I} = |g^{OR}| \quad . \tag{44}$$

The Ochkur and Ochkur-Rudge approximations also exist in post-interaction forms,[7] and we shall present some results based on these forms.

Vainshtein, Presnyakov, and Sobelman[63] (VPS) have suggested a different approach for the calculation of the excitation cross sections in which the emphasis is on a more complete account of the electron-electron interaction. The validity of the final expressions for the scattering amplitudes has been questioned[27a] because of the various mathematical approximations made in their derivation. Nonetheless, the method has been found to lead to approximately correct cross sections for the excitation of the H-atom,[63a] and on that basis it is worth considering. The ratio between direct and exchange amplitudes in the VPS method may be used to construct an Ochkur-like relation which is called here the transferred Vainshtein-Presnyakov-Sobelman (TVPS) approximation. The TVPS exchange amplitude takes the form

$$g^{TVPS} = C_{TVPS} \frac{q^2}{k_1^2} f^B \tag{45}$$

where

$$C_{TVPS} = \frac{F(-i\nu,\ i\nu\ 1;\ 1/4)}{F(-i\nu,\ i\nu,\ 1;\ X)} \tag{46}$$

and

$$X = \frac{2\Delta E + q^2}{2\Delta E + 3q^2}, \quad \nu = \frac{1}{k_1 + \sqrt{2U_1}} \tag{47}$$

$F(X, Y, Z; W)$ is the hypergeometric function,[64] and ΔE is the excitation energy. We present the integral cross sections obtained by using the VPS method[63] for both direct and exchange scattering.

The final model to be considered here is one constructed from the ratio of the direct and exchange amplitudes as calculated by Kang and Foland.[33,60b,65] In their treatment, care is taken to treat all the

electrons equivalently and to use the same approximations for both the direct and exchange amplitudes. Although their results do not suffer from many of the inconsistencies of other first-order theories, they had to make a number of mathematical approximations similar to those made in the VPS derivation in order to reduce their formal solutions to amplitudes which could be evaluated. By using their ratio of exchange to direct amplitudes, the transferred Kang-Foland (TKF) exchange amplitude is constructed as

$$g^{TKF} = \frac{q^2}{k_1^2} \, C_{KF} \, f^B \tag{48}$$

where

$$C_{KF} = \frac{\gamma}{\epsilon}^{i/k_1} \left(\frac{\epsilon + \beta}{\epsilon}\right)^{i/k_2} \frac{F\left(1-i/k_1, 1, \left(\frac{2i(k_1k_2 - \vec{k}_1 \cdot \vec{k}_2)}{k_1k_2}\right)\right)}{F(i/k_1, ik_2, 1; X)} \tag{49}$$

where

$$\epsilon = q^2/2, \; \beta = k_1k_2 \cos\theta - k_2^2, \; \gamma = (k_1^2 - k_2^2)/2, \tag{50}$$

and $$X = 2k_1k_2(\cos\theta - 1)/(k_1 - k_2)^2 \; .$$

The quantity $F(X,Y,Z)$ is the confluent hypergeometric function,[64] and θ is the scattering angle.

The various models for the exchange amplitude g described above are combined with the Born amplitude for direct excitation f^B to give the total scattering amplitude. In terms of these amplitudes, the differential cross section is

$$I(k_1, \theta) = \frac{k_2}{k_1} \left| f^B - g \right|^2 \; . \tag{51}$$

In the polarized Born-Ochkur-Rudge (BOR/P) approximation, the direct amplitude f^B is replaced by the polarized Born approximation direct amplitude $f^{B/P}$, and the prior-interaction Ochkur-Rudge model is used for g.

It should be noted that of the approximations discussed above, only those with total scattering amplitudes which contain g^{TKF} or g^{OR} are complex. The other models involve phases between the direct and exchange amplitudes such that the total amplitude can be taken as either real or imaginary depending on the particular transition.

B. Wave Functions

1. 1^1S Wave Function

Many approximate wave functions for the 1^1S ground state of helium have been reported in the literature. Calculations based on two of these wave functions will be presented here. One of these is the 53-term correlated wave function of Weiss.[66] The other is the self-consistent-field (SCF) function of Clementi[67]

$$\Psi_1 = \xi_o(\vec{r}_1)\ \xi_o(\vec{r}_2)\ \eta(1,2) \tag{52}$$

where η is a singlet spinor,

$$\xi_o(\vec{r}_k) = \sum_{i=1}^{2} c_{oi}\chi_{oi}(r_k) \tag{53}$$

and $\chi_{oi}(r)$ is a normalized hydrogenic 1s orbital with orbital exponent Z_{oi}. The coefficients c_{oi} and orbital exponents are given in Table V. The Weiss and Clementi wave functions are compared with each other and with some others in Table VI. For first-order scattering theories, the spatial extent ot the electron charge distribution is of primary importance in determining the accuracy of the calculated cross sections.[68-69] Therefore, as an

TABLE V. Parameters for self-consistent-field (SCF) wave functions.

State	n	i	c_{ni}	Z_{ni} [c]
1^1S [a]	0	1	0.835188	1.446
	0	2	0.189650	2.870
2^1S [b]	1	1	0.998451	1.992
	1	2	0.001185	4.812
	2	1	-0.00061	0.528
	2	2 [d]	0.001299	1.210
	1	3	-0.117763	1.992
	1	4	-0.006733	4.812
	2	3	1.176333	0.528
	2	4 [d]	-0.315588	1.210

[a] Ref. 67.

[b] Ref. 85.

[c] The orbital exponents are optimized in both the 1^1S and 2^1S calculations.

[d] The u orbital cusp is -2.0043461 a.u. and the v orbital cusp is -2.1079229 a.u. The cusp property is discussed by C. C. Roothaan and P. S. Kelly, Phys. Rev. 131, 1177 (1963).

TABLE VI. Energies and second moments for helium wave functions.

State	Ref.	Energy (hartrees)	$\langle r_1^2 + r_2^2 \rangle$ (a_0^2)	No. of parameters	Functional form eq. no.	SCF	No. of Terms
1^1S	a	-2.8475	2.1070	1	52	Yes	1
	67	-2.86167	2.3712	3	52	Yes	1
	82	-2.87251	-	6	55	No	1
	b	-2.90332	2.3872	5	54	No	4
	66	-2.90372	-	54	54	No	53
	70(a)	-2.90372	2.3870	1078	54	No	1078
2^1S							
	c	-2.1475	21.7	3	55	No	1
	75	-2.14439	38.8	3	55	No	1
	82	-2.14345	-	8	55	No	1
	Present[d]	-2.14374	33.372	10	55	Yes	1
	Present[e]	-2.14374	33.419	10	58	No	2
	f	-2.14407	33.1	13	54	No	9
	72	-2.14490	-	6	54	No	6
	g	-2.14559	32.36	not given	54	No	not given
	66	-2.14597	-	55	54	No	54
	70(b)	-2.14597	32.178	444	54	No	444

a. E. A. Hylleraas, Z. Physik 54, 347 (1929).

b. A. L. Stewart and T. G. Webb, Proc. Phys. Soc. (London) 82, 532 (1963).

c. P. M. Morse, L. A. Young, and E. S. Haurwitz, Phys. Rev. 48, 948 (1935).

d. GF wave function, not orthogonal to 1^1S wave function, see Ref. 85.

e. Orthogonal to 1^1S wave function.

f. A. S. Coolidge and H. M. James, Phys. Rev. 49, 676 (1936).

g. H. O. Knox and M. R. H. Rudge, J. Phys. B (Atom. Molec. Phys.) 2, 521 (1969). See H. O. Dickinson and M. R. H. Rudge, ibid., 3, 1284 (1970).

additional check on the accuracy of the calculations to be presented in Section III.C, the expectation value $< r_1^2 + r_2^2 >$ is also included in Table VI. Comparison with the exact results of Pekeris[70a] shows that the Clementi wave function is quite accurate, at least for this expectation value.

2. 2^1S Wave Function

The 2^1S state of helium presents a more difficult problem since it is not the lowest state of its symmetry (^1S). The standard variational principle[71] guarantees only that the energy calculated for a wave function approximating this state is an upper bound if this wave function is orthogonal to the exact ground state (1^1S) wave function. This is an obstacle because the exact 1^1S function is not known. This difficulty can be overcome by writing a linear variational function

$$\Psi = \sum_{i=1}^{N} c_i \xi_i \qquad (54)$$

where all the ξ_i have ^1S symmetry and setting up the secular equations for the coefficients. The system of equations has N orthogonal solutions (a solution is specified by a set of c_i). Hylleraas and Undheim[72] and MacDonald[73] have shown that the solution which yields the second lowest energy is an upper bound to the second lowest state of ^1S symmetry. This procedure has been used by several authors to approximate the helium wave functions, and some examples are given in Table VI. Kim and Inokuti[5] have calculated generalized oscillator strengths using the accurate Weiss wave function of this form, and we have used their results to calculate scattering cross sections (see the next section).

It has been shown by various researchers that, when approximate wave functions are used to calculate physical quantities (such as the matrix

elements (30) used in this paper) which do not explicitly depend on electron correlation, a self-consistent-field wave function may be as good as or better than a correlated wave function of the same number of parameters.[74] Since many-parameter correlated wave functions are difficult to work with and interpret and since the good wave functions available for molecules and heavy atoms are often SCF wave functions, we want to study the effect of using these wave functions on scattering calculations. We consider the orbital approximation

$$\Psi_2 = \frac{1}{\sqrt{2}} [u(\vec{r}_1)\, v(\vec{r}_2) + v(\vec{r}_1)\, u(\vec{r}_2)]\, \eta(1,2) \quad . \qquad (55)$$

This form for the 2^1S wave function was first considered by Fock,[78] who derived equations for the nonorthogonal SCF orbitals u and v. Fock's equations were solved numerically by Trefftz, Schlüter, Dettmar, and Jörgens.[79] However, these equations are complicated by the nonorthogonality of u and v,[75-76] and the first analytic wave function of the form (55) was not SCF.[75] In an attempt to approximately insure an upper bound on the energy of the 2^1S state, some workers[75-77] have orthogonalized their approximate wave functions to approximate wave functions for the 1^1S state. One way to do this is to use the "fixed core" modification[80-82] to obtain a non-SCF wave function of form (55). This method is also called the improved virtual orbital method.[83]

The form (52) is equivalent for helium to the form of the wave function in a more general, new SCF method - the GF method.[84] The SCF wave function of form (55) so obtained can be shown[84] to yield an upper bound to the true 2^1S energy. Cartwright and Goddard[85] have calculated an analytic GF wave function for the 2^1S state. In this wave function

$$u(\vec{r}_k) = \sum_{n=1}^{2} \sum_{i=1}^{2} c_{ni}\chi_{ni}(r_k) \qquad (56)$$

$$v(\vec{r}_k) = \sum_{n=1}^{2} \sum_{i=3}^{4} c_{ni}\chi_{ni}(r_k) \quad . \qquad (57)$$

The χ_{ni} are normalized Slater atomic orbitals of principal quantum number n and orbital exponent Z_{ni}. The coefficients and screening constants are given in Table V.

To insure reasonable values for calculated transition moments (see next section) we found it necessary to consider a 2^1S wave function which was orthogonal to our approximate 1^1S wave function. The new 2^1S wave function $\Psi(2^1S)$ still yields an upper bound on the true 2^1S energy. The new wave function is

$$\Psi(2^1S) = \frac{1}{\sqrt{1-S^2}} [\Psi_2(2^1S) - S\,\Psi_1(1^1S)] \qquad (58)$$

where $\Psi_2(2^1S)$ is given by equations (55), (56), and (57) and

$$S = \langle \Psi(2^1S) | \Psi_1(1^1S) \rangle = -0.01498479 \quad . \qquad (59)$$

The properties of this orthogonalized wave function (58) are compared with some other calculations in Table VI. The table shows that the GF wave function gives charge distributions in good agreement with the exact calculations of Pekeris[70b] for the excited state. The table also shows that the properties of the GF wave function are not much changed by orthogonalization to the approximate 1^1S wave function.

C. Generalized Oscillator Strengths

The differential cross section (Eq. (51)) can be written in the first Born approximation or one of the Ochkur-like approximations in terms of the generalized oscillator strength $\Phi(q)$. For example, in the Born approximation

$$I(k_1,\theta) = (k_2/k_1)(2/q^2\Delta E)\Phi(q) \tag{60}$$

where

$$\Phi(q) = \frac{8\Delta E}{q^2}\,|M|^2 \tag{61}$$

(see Eq. (30)). The effect on the calculated cross sections of the use of approximate wave functions has been discussed by numerous authors.[5,7,68,74]

Accurate generalized oscillator strengths for the $1^1S \rightarrow 2^1S$ transition have been calculated by Kim and Inokuti[5] using the Weiss[66] correlated wave functions and also by Bell, Kennedy, and Kingston[86] using the same wave functions. The results of these two calculations generally agree to three significant figures. The generalized oscillator strengths obtained using the orthogonal SCF wave functions discussed above with both the theoretical and experimental values of ΔE used in Eq. 61 are compared in Table VII with the values tabulated by Bell et al.[86] Also included in the table are the results obtained for the nonorthogonalized 2^1S wave function and the recent results of Schneider,[87] who calculated this quantity utilizing linear response theory. Figure 9 is a plot of the data given in Table VII to illustrate more clearly the differences in the generalized oscillator strengths. One notes that the result obtained with the nonorthogonal 2^1S SCF wave function is extremely poor for $q \leq 1.5$. The result from the orthogonal SCF wave function is smaller than the accurate result of Bell et al.[86]

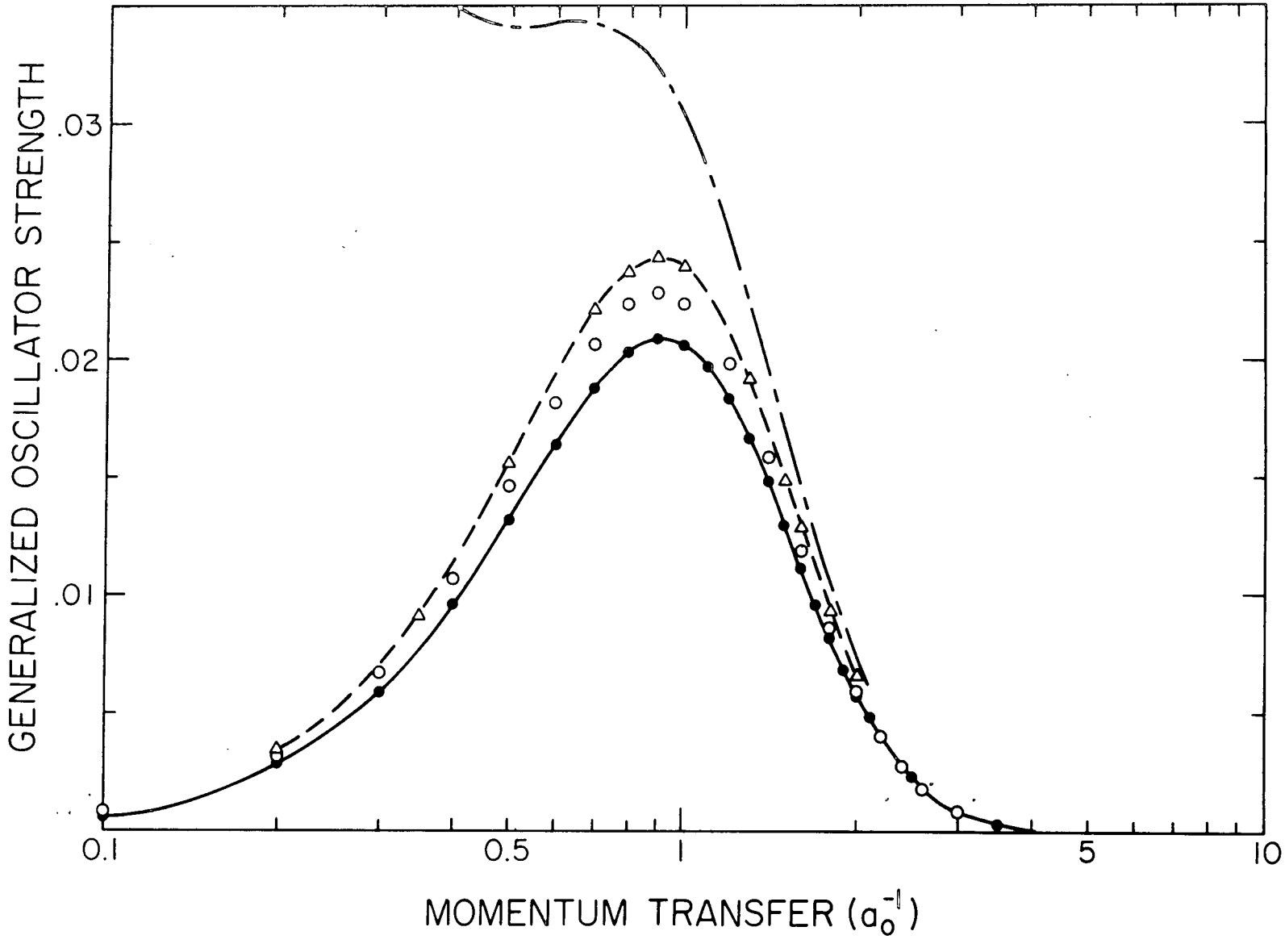

Fig. 9. Generalized oscillator strength for the He($1^1S \rightarrow 2^1S$) transition as a function of the momentum transfer. The solid curve is obtained using the present orthogonal wave functions with $\Delta E = 0.7576$ hartrees; the open circles are from Bell, Kennedy, and Kingston (Ref. 86); the dashed curve is from Schneider (Ref. 87); and the dot-dash curve is that calculated using the nonorthogonal 2^1S wave function.

TABLE VII. Generalized oscillator strengths in the length formulation. (The numbers in parentheses are powers of 10 by which the preceding numbers are to be multiplied.)

q(a.u.)	Orthog. GF[a]	Orthog. GF[a]	Nonorthog. GF[a]	Schneider[b]	BKK[c] (accurate)	BK[d] Case A	BK[d] Case B	Kennedy[e]
0.001	7.2027(-8)	6.8283(-8)	1.3609(+3)	~ 0				
0.01	7.4671(-6)	7.0789(-6)	1.3629(+1)					8.3622(-6)
0.10	7.3634(-4)	6.9806(-4)	1.5627(-1)		8.241(-4)	7.38(-4)	8.43(-4)	8.2406(-4)
0.20	2.8208(-3)	2.6742(-3)	5.5747(-2)	3.3588(-3)	3.154(-3)	2.83(-3)	3.22(-3)	3.1538(-3)
0.40	9.5234(-3)	9.0284(-3)	3.4955(-2)		1.061(-2)	9.53(-3)	1.08(-2)	1.0607(-2)
0.50	1.3147(-2)	1.2464(-2)	3.4198(-2)	1.5540(-2)	1.460(-2)			
0.70	1.8761(-2)	1.7786(-2)	3.4201(-2)	2.2032(-2)	2.070(-2)			
0.80	2.0276(-2)	1.9222(-2)	3.3567(-2)	2.3722(-2)	2.228(-2)	2.01(-2)	2.21(-2)	2.2276(-2)
0.90	2.0861(-2)	1.9777(-2)	3.2263(-2)	2.4314(-2)	2.282(-2)			
1.00	2.0616(-2)	1.9544(-2)	3.0346(-2)	2.3936(-2)	2.245(-2)	2.03(-2)	2.19(-2)	2.2450(-2)
1.10	1.9704(-2)	1.8680(-2)	2.7959(-2)					
1.20	1.8315(-2)	1.7363(-2)	1.5280(-2)		1.976(-2)	1.78(-2)	1.90(-2)	
1.30	1.6633(-2)	1.5768(-2)	2.2480(-2)	1.9105(-2)				
1.40	1.4816(-2)	1.4045(-2)	1.9702(-2)		1.582(-2)			
1.50	1.2987(-2)	1.2312(-2)	1.7054(-2)	1.4835(-2)				
1.60	1.1234(-2)	1.0650(-2)	1.4609(-2)	1.2806(-2)	1.188(-2)	1.05(-2)	1.11(-2)	
1.80	8.1541(-3)	7.7302(-3)	1.0463(-2)	9.3686(-3)	8.526(-3)			
2.00	5.7544(-3)	5.4553(-3)	7.3267(-3)	6.5311(-3)	5.946(-3)	5.16(-3)	5.41(-3)	

TABLE VII (cont.)

q(a.u.)	Orthog. GF[a]	Orthog. GF[a]	Nonorthog. GF[a]	Schneider[b]	BKK[c] (accurate)	BK[d] Case A	BK[d] Case B	Kennedy[e]
3.00	8.9353(-4)	8.4708(-4)	1.1317(-3)		8.605(-4)			
4.00	1.5533(-4)	1.47261(-4)	1.9828(-4)		1.406(-4)			
5.00	3.3034(-5)	3.1317(-5)	4.2439(-5)		2.896(-5)			
ΔE (a.u.)[f]	0.7576[g]	0.7182[h]	0.7576[g]		0.75775[h]	0.7599[h]	0.729[h]	0.7578[h]
$\lim_{q\to 0} \frac{\Phi(q)}{q^2}$	7.4671(-2)	7.079(-2)	1.3629(+5)			7.5(-2)	8.6(-2)	8.3261(-2)

[a] Present.

[b] Ref. 87.

[c] Ref. 86.

[d] K. L. Bell and A. E. Kingston, J. Phys. B 1, 521 (1968).

[e] D. J. Kennedy, J. Phys. B 1, 526 (1968).

[f] Value of ΔE used in Eq. (61).

[g] Experimental value.

[h] Theoretical value.

for all values of $q \leq 2.4$ a.u., and the same conclusions reached in the study of the 2^1P excitation[7] concerning the reliability of SCF wave functions also apply here. On the other hand, the results obtained by Schneider[87] are larger than the accurate values for all values of q. Since a separate wave function was not calculated by Schneider in applying linear response theory, the differences between his results and the accurate values cannot be analyzed in the same manner.

All our calculations of 2^1S DCS's and $2^1S/2^1P$ DCS ratios using the methods which include polarization were carried out using SCF wave functions, i.e., Ψ_1 (Eq. 52) for the 1^1S state, $\Psi(2^1S)$ (Eq. 58) for the 2^1S state, and the 2^1P wave function of Eq. 33 of Ref. 7 with the experimental value of ΔE. When it is not stated otherwise, calculations of DCS's and ratios which do not include polarization are performed using the accurate $1^1S \rightarrow 2^1S$ generalized oscillator strengths.[5,86]

D. Theory of the Transition Polarizability

The transition polarizabilities are defined by Eqs. (21) and (22). Although the perturbation theory of off-diagonal matrix elements is less well developed than the perturbation theory of diagonal matrix elements, any of the standard techniques of perturbation theory can be applied to evaluate these quantities. That is, we could use direct summation, the Z^{-1} expansion,[88-89] or Buckingham's variational-perturbational method for obtaining first-order perturbed functions.[90-93] The direct summation technique has the advantage of showing which P states make important contributions and giving quantitative estimates of the errors involved in neglecting certain groups of P states in the eigenfunction expansion of the wave function (see Eqs. (3)-(4)). The variation-perturbation methods have the advantage that they can be used to compute very accurate values of the transition

polarizabilities. The variation-perturbation method for $\alpha_{12}^{(1)}$ proceeds by writing

$$\alpha_{12}^{(1)} = -(2/F^2) < \Psi_2 | H_1 | \Psi_1^p > \tag{62}$$

$$H_1 = -F(z_1 + z_2) \tag{63}$$

where Ψ_1^p is the perturbed helium ground state wave function for the perturbation H_1. Ψ_2 is the helium 2^1S wave function, and F is the electric field produced by the scattering electron. The variation-perturbation method for $\alpha_{12}^{(2)}$ proceeds by writing

$$\alpha_{12}^{(2)} = -(2/F^2) < \Psi_1 | H_1 | \Psi_2^p > \tag{64}$$

where Ψ_2^p is the first-order perturbed helium 2^1S wave function for the same perturbation. If the perturbed wave functions are calculated in terms of the usual eigenfunction expansion, we obtain (21) and (22).

The $Z_{j\beta}$'s in Eqs. (10), (21), and (22) can be evaluated from various wave functions. The best available results are given in Table VIII. The matrix elements in the table and the corresponding energy differences between the states show that perturbation of the ground state involves several excited P states in an important way. However, perturbation of the 2^1S state mixes in essentially only the 2^1P state.

Accurate values of the transition polarizabilities have been computed by Drake[94] by the variation-perturbation method using 50-term correlated wave functions. The construction of the basis sets used for this calculation was described by Drake and Dalgarno.[95] Drake finds $\alpha_{12}^{(2)} = 101.6\ a_o^3$ and $\alpha_{12}^{(1)} = 1.584\ a_o^3$. From the discussion in Section III.A.3.c, it is

TABLE VIII. Matrix elements $Z_{i\beta}$ and energy differences ΔE_j^β which enter into equations (21)-(22). All values are in hartree atomic units.

β	$Z_{1\beta}$	ΔE_1^β	$Z_{2\beta}$	ΔE_2^β
2	0.4206[a]	0.77988[a]	2.916[c]	0.022131[c]
3	0.2080[a]	0.84859[a]	-0.902[c]	0.090840[c]
4	0.131[b]	0.87287[a]	-0.470[c]	0.115019[c]

[a] Ref. 5, Table V.

[b] Y. -K. Kim and M. Inokuti, Phys. Rev. 184, 38 (1969), calculated from Table I.

[c] Y. -K. Kim and M. Inokuti, Phys. Rev. 181, 205 (1969), calculated from Table I.

apparent that the latter value is the appropriate one to use in the present model.

It is interesting to consider calculations which include both the initial state polarization and the final state polarization interaction with the very large values of the cutoff parameter suggested by the Fetter-Watson criterion (see Table IV). Although $\alpha_{12}^{(2)}$ is much larger than $\alpha_{12}^{(1)}$, b_2^{FW} is so large that the correction is very small. In fact, adding this interaction does not even change the first few significant figures of the calculated DCS.

IV. COMPARISON OF THEORETICAL AND EXPERIMENTAL DIFFERENTIAL CROSS SECTIONS

A. Ratios

In this section we consider the ratio of the DCS for excitation of the 2^1S state to that for excitation of the 2^1P state.

1. Energy Dependence

The intermediate and low energy ratio data exhibit two trends which are qualitatively predicted by the calculations. First, the low angle ($\theta < 15°$) ratios increase with decreasing impact energy (see particularly Figs. 2, 10, 11, and 12), and second, the large angle ($\theta > 60°$) ratios increase with increasing impact energy (see particularly Figs. 2 and 13). Figures 10-13 show that the theory and experiment are in better agreement for the ratios at small θ than at large θ. They also show that the theory predicts the energy dependence of the ratios better than it predicts the ratios themselves. The Born approximation (either with or without correcting for exchange in one of the Ochkur-like theories) is about a factor of 3 too low for the $2^1S/2^1P$ ratios at 0°. This ratio is underestimated because of the neglect of polarization. Polarization is much more important for the excitation of the 2^1S state than the 2^1P state as explained in Section III.A. Including polarization in the calculation of the DCS for the 2^1S state using the theoretically most justified polarization model ($\alpha \equiv \alpha_{12}^{(1)} = 1.584\ a_o^3$, $b = (5/4)b_1^{FW}$, and form B′ for the polarization cutoff function, see Section III) gives DCS ratios at 0° in much better agreement with experiment (see Fig. 10). This result indicates that including polarization in the description of the 2^1S excitation is necessary to describe the 2^1S and 2^1P excitation processes to the same degree of accuracy.

C2

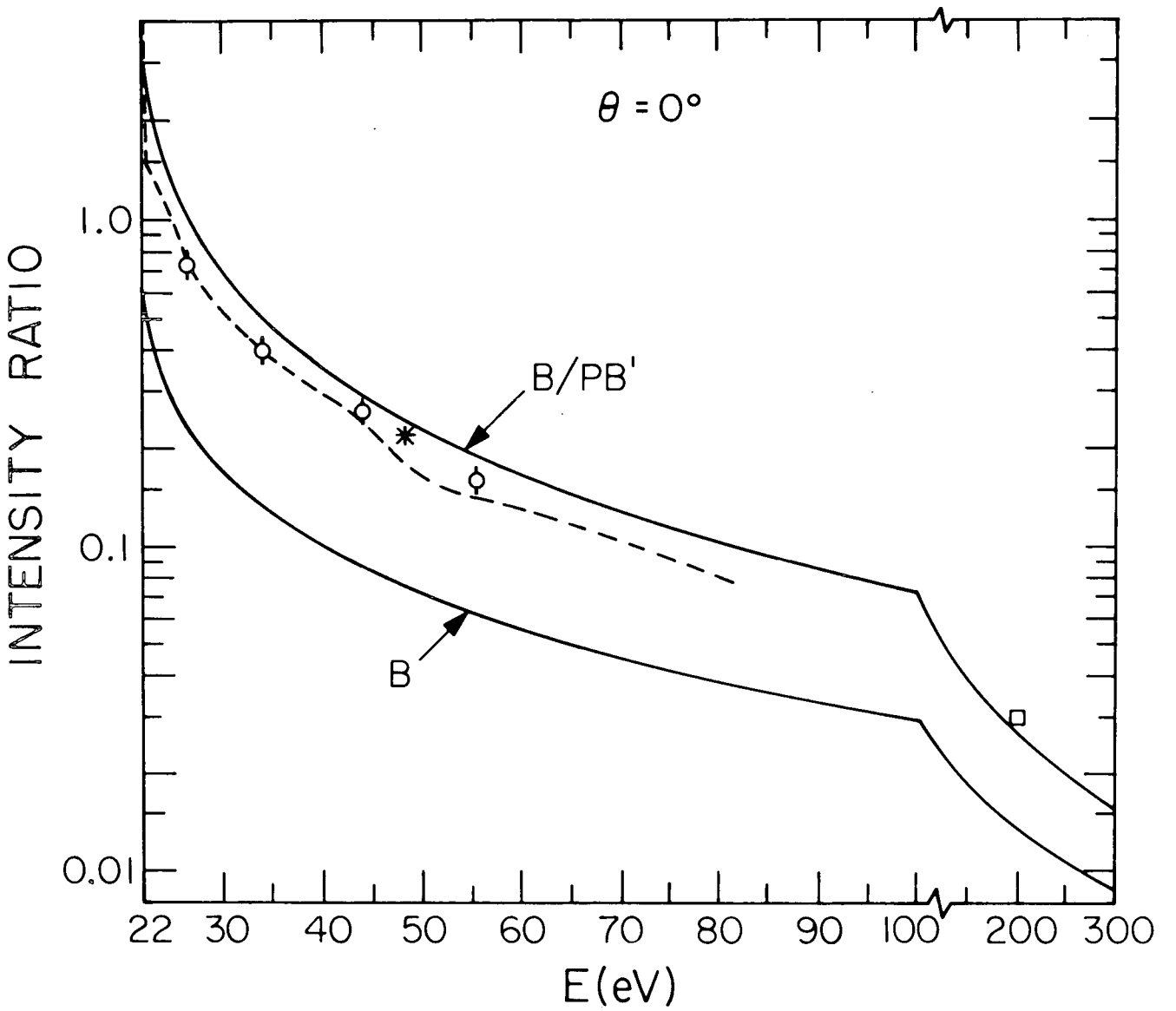

Fig. 10. $2^1S/2^1P$ intensity ratio at a scattering angle of 0° as a function of impact energy. The dashed line is the (interpolated) experimental results of Chamberlain et al. (Ref. 19), the circles (with error bars) are the present experimental results, the asterisk is the result of Lassettre et al. (Ref. 18). The curves are calculated in the indicated approximation. $\alpha = 1.584\ a_0^3$ and $b = (5/4)\ b_1^{FW}$ at each energy. (Note the change in the impact energy scale at energies above 100 eV.)

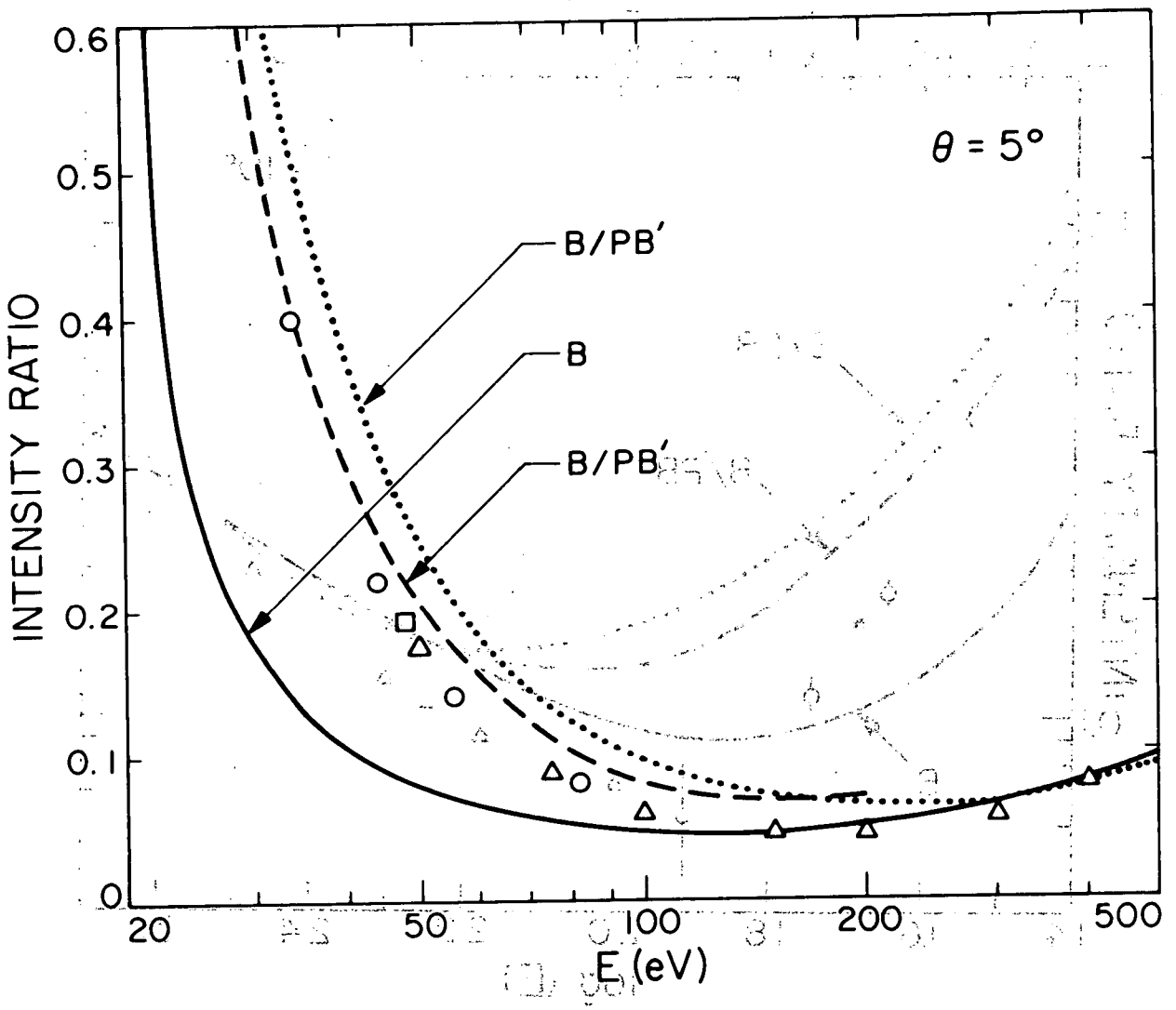

Fig. 11. $2^1S/2^1P$ intensity ratios versus energy at $\theta = 5°$. The circles are interpolated from the present experimental results, the square is an experimental value from Ref. 25, and the triangles are experimental values from Ref. 14. The curves are calculated in the Born (B) and polarized Born (B/PB′) approximations. The dotted curve is calculated with $\alpha = 1.584\ a_o^3$ and $b = (5/4)\ b_1^{FW}$ at each energy; the dashed curve is calculated with $\alpha = 1.584\ a_o^3$ and with b equal to the value determined empirically (see text).

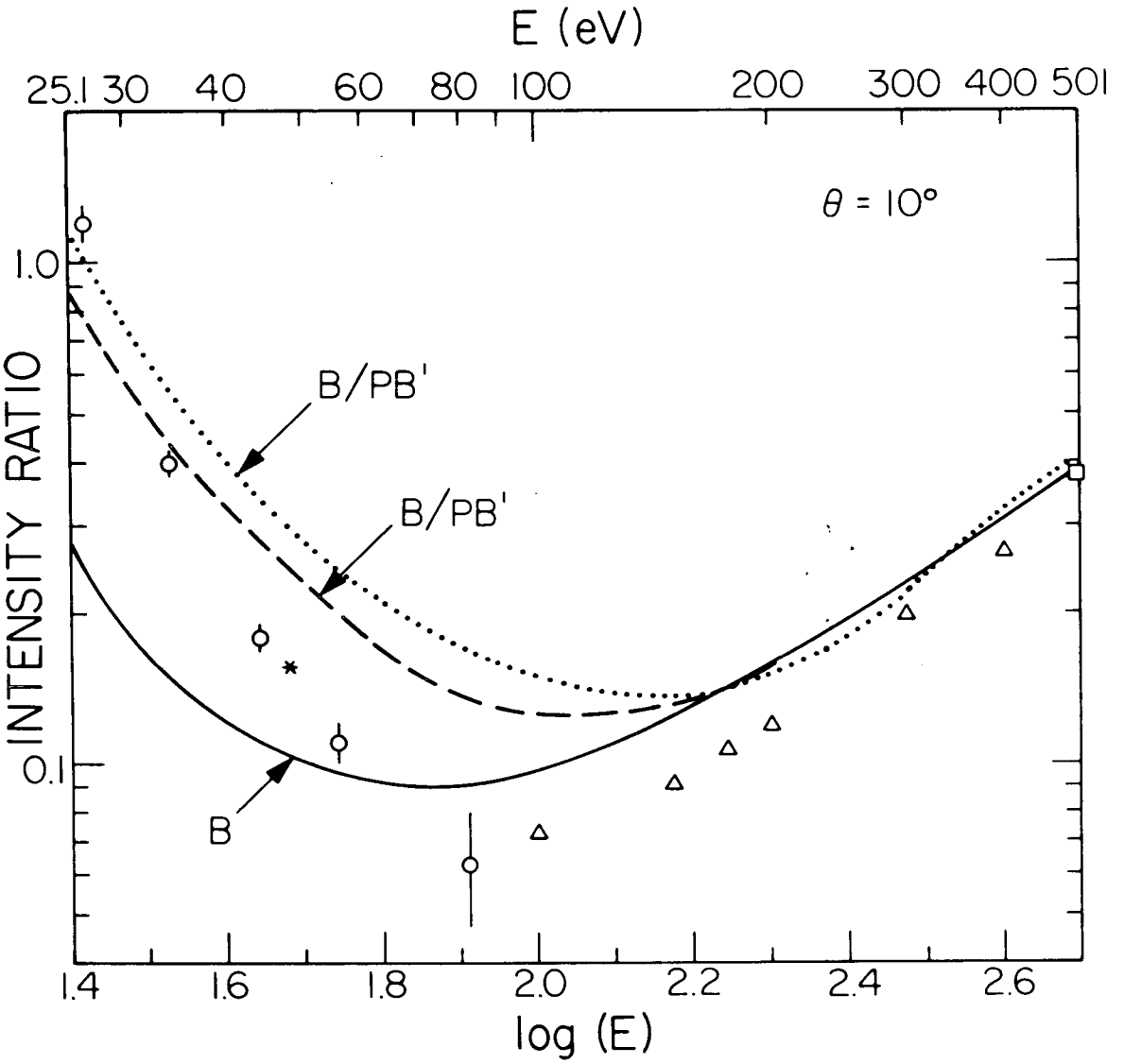

Fig. 12. $2^1S/2^1P$ intensity ratio at a scattering angle of 10° as a function of impact energy. The triangles are the experimental data of Vriens et al. (Ref. 2), the asterisk is the result of Lassettre et al. (Ref. 25), and the square is interpolated from the results of Silverman and Lassettre (Ref. 10). The curves are calculated in the approximations as indicated. The dotted curve is calculated with $\alpha = 1.584$ a_o^3 and $b = (5/4)\, b_1^{FW}$ at each energy. The dashed curve is calculated with $\alpha = 1.584\ a_o^3$ and with b equal to the value determined empirically from the $2^1S/2^1P$ ratios at 0° at each energy.

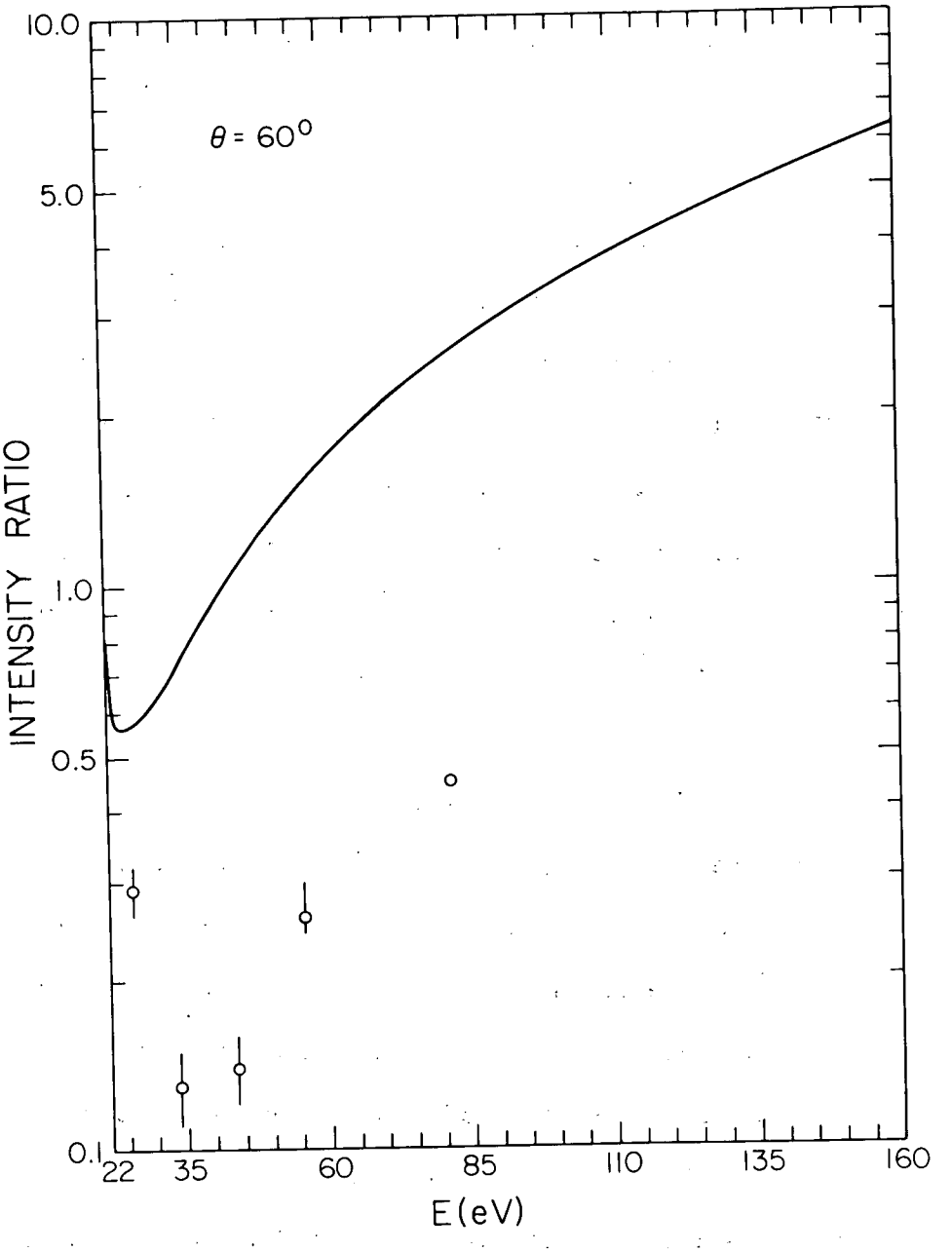

Fig. 13. Ratio of the differential cross section for excitation of the 2^1S state to that for excitation of the 2^1P state as a function of incident energy at $\theta = 60°$. The curve is calculated in the symmetrized Born-Ochkur-Rudge approximation (BORB.I). The circles are the present experimental results. The error limits are the average deviation for 3-6 runs. No error estimate has been made for the 81.6 eV point.

The 0° ratios are predicted more accurately by the first Born approximation at very high energies than at lower ones. Boersch, Geiger, and Schröder[23] obtain a $2^1S/2^1P$ intensity ratio of $(1.43 \pm 0.27) \times 10^{-4}$ at 25 keV and $\theta = 0°$. This ratio is calculated to be 1.03×10^{-4} and 1.05×10^{-4} using the Born approximation with the accurate[5,86] and SCF (with the experimental ΔE) oscillator strengths, respectively. The inclusion of polarization in the 2^1S state slightly improves the agreement between experiment and theory. With $\alpha = 1.584\ a_o^3$ and $b = (5/4)b_1^{FW}$, and B/PB′ approximation yields a $2^1S/2^1P$ ratio of 1.10×10^{-4}. Calculations using the other polarization forms give results within a few percent of this value. The polarization potential is highly nonadiabatic at this energy (note the large b_1^{FW} in Table IV), and, hence, it contributes relatively little to the scattering even at 0°.

The calculations including polarization are not in exact agreement with experiment for the 0° ratio (see Fig. 10). If, however, with a fixed α we let the cutoff parameter b in the polarized Born approximation for the excitation of the 2^1S state be an empirical quantity, we can adjust it at each energy to make the calculated $2^1S/2^1P$ DCS ratio at 0° equal the experimentally measured one. The value of b determined in this manner depends on the form chosen for the polarization potential curoff function (Eqs. (23)-(26)). These results are shown in Fig. 14 which compares these empirically determined cutoff parameters to the theoretically justified b_1^{FW}. The agreement is very good. Thus, somewhat surprisingly, we can use the Fetter-Watson criterion to obtain a good estimate of the cutoff parameter b.

Figures 11 and 12 show the polarized Born predictions for the DCS ratio as a function of energy at 5° and 10° scattering angles, respectively. The inclusion of polarization has little effect at high energy where the

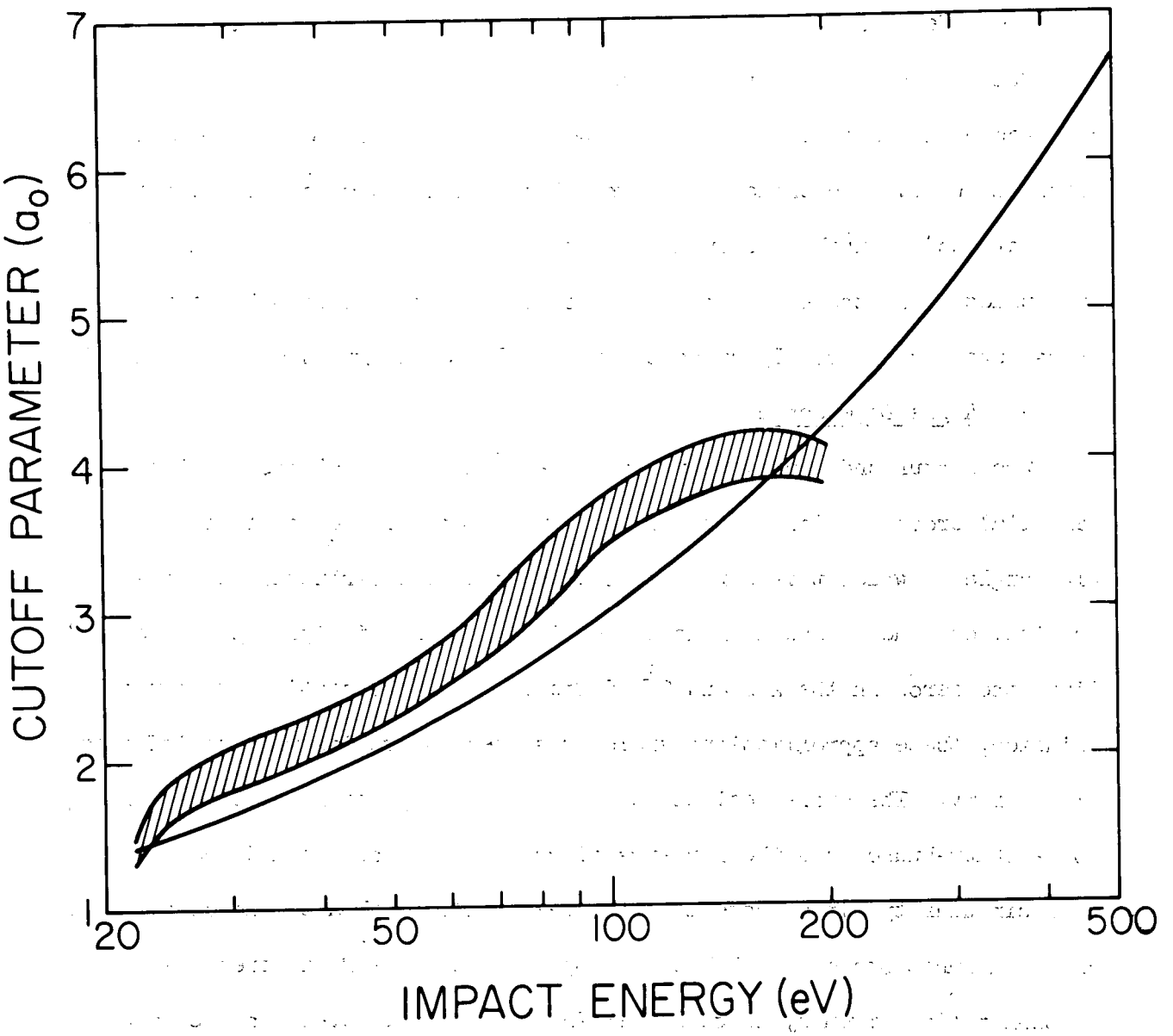

Fig. 14. Cutoff parameter (b) vs. impact energy. The solid line is $b = b_1^{FW} = k_o/0.90372$. The shaded area encloses the range of b values determined empirically from the $2^1S/2^1P$ cross section ratios at 0°. The empirically determined b values for the A, B, B′, and C forms of the polarization potentials are scaled by multiplying them by $4/\pi$, 3/4, 4/5, and 1, respectively. The lowest value at each energy corresponds to the C form of the polarization potential and the highest to the A form. The scaled b values for the B, B′, and C forms differ by only 1-2% at each energy.

first Born approximation is accurate, but at lower energies it improves agreement with experiment significantly.

The effects of exchange and of distortion of the scattering electron wave function are small at small scattering angles. However, these effects are presumably large at 60°. Also, the short-range form of the polarization potential (i.e., the choice of polarization cutoff function in the present calculations) is much more important at $\theta = 60°$ than it is at small scattering angles. For these reasons the present calculations do not predict the cross sections accurately at scattering angles as large as 60° (see Fig. 13).

2. Angle Dependence

The Ochkur and the symmetrized Born-Ochkur-Rudge methods predict differential cross sections which have a zero except very close to threshold. (The angle at which this zero occurs depends on the particular energy-loss and incident energy and approaches 90° in the limit of high impact energy.) Since the zeros in the 2^1S and 2^1P differential cross sections do not quite coincide, these approximations yield cross section ratios with an infinite singularity. The cross section ratios predicted by the Born, unsymmetrized Born-Ochkur-Rudge, and the Born-transferred-Kang-Foland methods do not have this singularity since these methods yield DCS's which are monotonically decreasing functions of θ. Table IX compares the $2^1S/2^1P$ differential cross section ratios given by these latter four methods at several angles and energies. The low-angle, high-energy ratios predicted by the methods which predict a singularity in the ratios also agree with those presented in Table IX since the zero in the differential cross section near 90° at high energy has little effect on the low-angle ratios.

The present calculations are shown to be in excellent agreement with the high energy ratio data of Silverman and Lassettre[10] at 500 eV (see Fig.

TABLE IX. $2^1S/2^1P$ differential cross section ratios calculated in the Born (B), Born-Ochkur-Rudge prior (BOR), Born-Ochkur-Rudge post (BORP), and Born-transferred Kang-Foland (BTKF) approximations.

Scattering angle (deg)	Method			
	B	BOR	BORP	BTKF
		E = 25 eV		
0	0.276	0.267	0.289	0.275
30	0.349	0.338	0.365	0.346
60	0.543	0.528	0.573	0.535
90	0.834	0.819	0.902	0.810
120	1.16	1.15	1.30	1.13
150	1.41	1.41	1.63	1.40
180	1.51	1.51	1.75	1.50
		E = 30 eV		
0	0.170	0.168	0.173	0.169
30	0.289	0.285	0.297	0.288
60	0.620	0.609	0.650	0.617
90	1.18	1.16	1.29	1.16
120	1.81	1.78	2.08	1.77
150	2.27	2.24	2.66	2.24
180	2.44	2.41	2.86	2.42
		E = 60 eV		
0	0.0557	0.0557	0.0558	0.0556
30	0.397	0.396	0.400	0.397
60	1.66	1.65	1.72	1.66
90	3.70	3.66	4.21	3.71
120	6.07	5.99	6.98	6.04
150	8.23	8.13	9.03	8.09
180	9.12	9.02	9.87	8.96
		E = 300 eV		
0	0.00898	0.00898	0.00898	0.00898
30	2.83	2.83	2.84	2.84
60	17.5	17.5	17.7	17.5
90	52.2	52.1	61.4	52.7
120	92.8	92.4	96.6	94.7
150	124	123	126	126
180	135	135	137	137

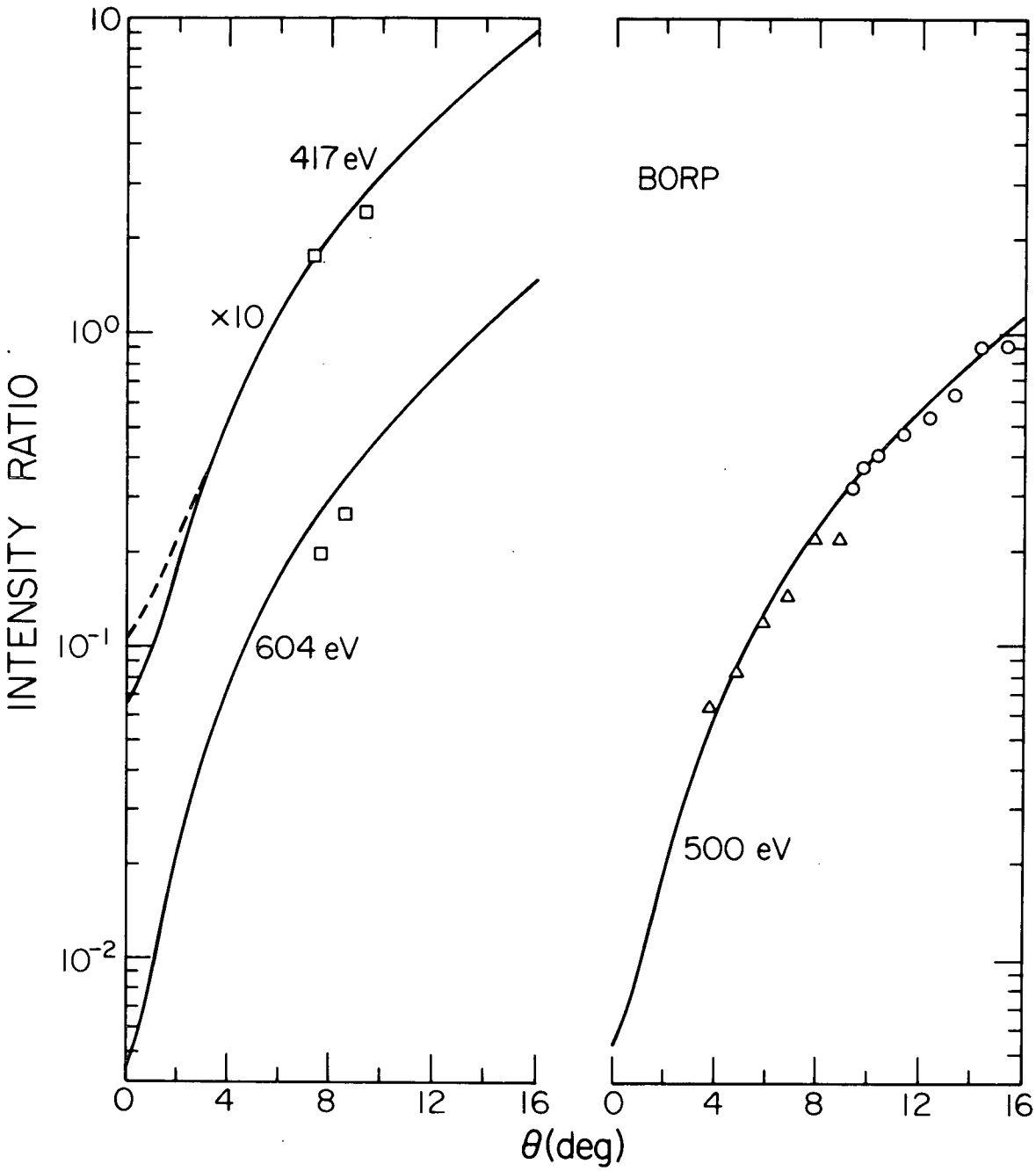

Fig. 15. $2^1S/2^1P$ intensity ratios vs. scattering angle. The squares (417 and 604 eV) and triangles (511 eV) are the results of Lassettre et al. (Ref. 9), and the circles (500 eV) are the results of Silverman and Lassettre (Ref. 10). The dashed curve is calculated in the B/PC approximation with $\alpha = 1.584\ a_o^3$ and $b = b_1^{FW} = 6.13\ a_o$. The solid curves are calculated in the post Born-Ochkur-Rudge approximation (BORP). The results of the BORP and the first Born approximation are indistinguishable in the energy and angle range of this figure.

15), with that of Lassettre, Krasnow, and Silverman[9] at 511 eV and 417 eV (see Fig. 15), and with the experimental results of Vriens, Simpson, and Mielczarek[2] at 400 eV (see Fig. 16) and 300 eV (see Fig. 17). Apparently, theory and experiment[9] differ at 604 eV. The lack of high energy experimental data for $\theta > 15°$ precludes a more rigorous test of these first-order methods for large-angle, high-energy scattering. At high energies, polarization is significant only at relatively small scattering angles. The data presently available do not cover the low-angle region well enough to allow a definitive test of the importance of polarization at these energies.

As the impact energy is lowered to 225 eV and below, the ratios calculated either with or without polarization increase more rapidly with increasing angle than do the experimental ones (see Fig. 17). However, even at impact energies as low as 81.6 eV (see Fig. 3), the calculated ratios are within about a factor of 5 of the experimental ones to angles as large as 80° and exhibit a variation with angle which is qualitatively correct. At energies below 81.6 eV, the ratios calculated without polarization differ markedly in both magnitude and shape from the experimental ones (see Figs. 1 and 2). However, the inclusion of polarization in the calculation significantly improves the agreement between theory and experiment at small angles (see Figs. 1, 16, and 18).

Figures 18 and 19 show the effect on the calculated intensity ratios of varying the polarization potential. As the value of α is increased, the ratio curves become steeper functions of scattering angle for angles greater than about 30°, and a minimum develops at lower angles. These changes directly reflect the changes in the 2^1S DCS, since the 2^1P DCS used to construct all these ratios is the same. The important effect of polarization on the angle dependence of the 2^1S DCS is discussed in the next section.

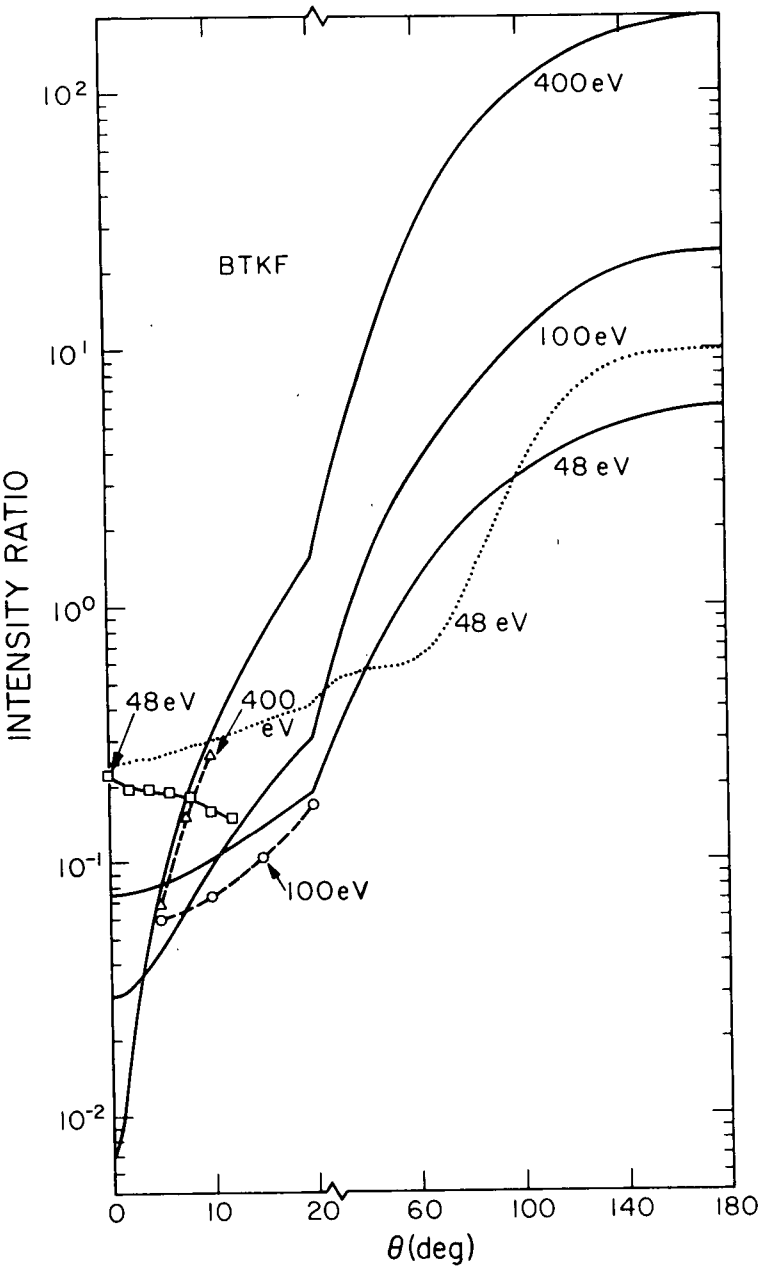

Fig. 16. $2^1S/2^1P$ intensity ratios. The triangles and circles are the experimental results of Vriens et al. (Ref. 2) at 400 and 100 eV, respectively. The squares are the experimental results of Lassettre et al. (Ref. 25) at 48 eV. The solid curves are calculated in the BTKF approximation at the indicated energy. The dotted curve is calculated in the B/PB′ approximation with $\alpha = 1.584\ a_o^3$ and b empirically determined to be $2.08\ a_o$. A curve for the Born approximation at 400 eV would be indistinguishable from the BTKF curve on the scale of this figure.

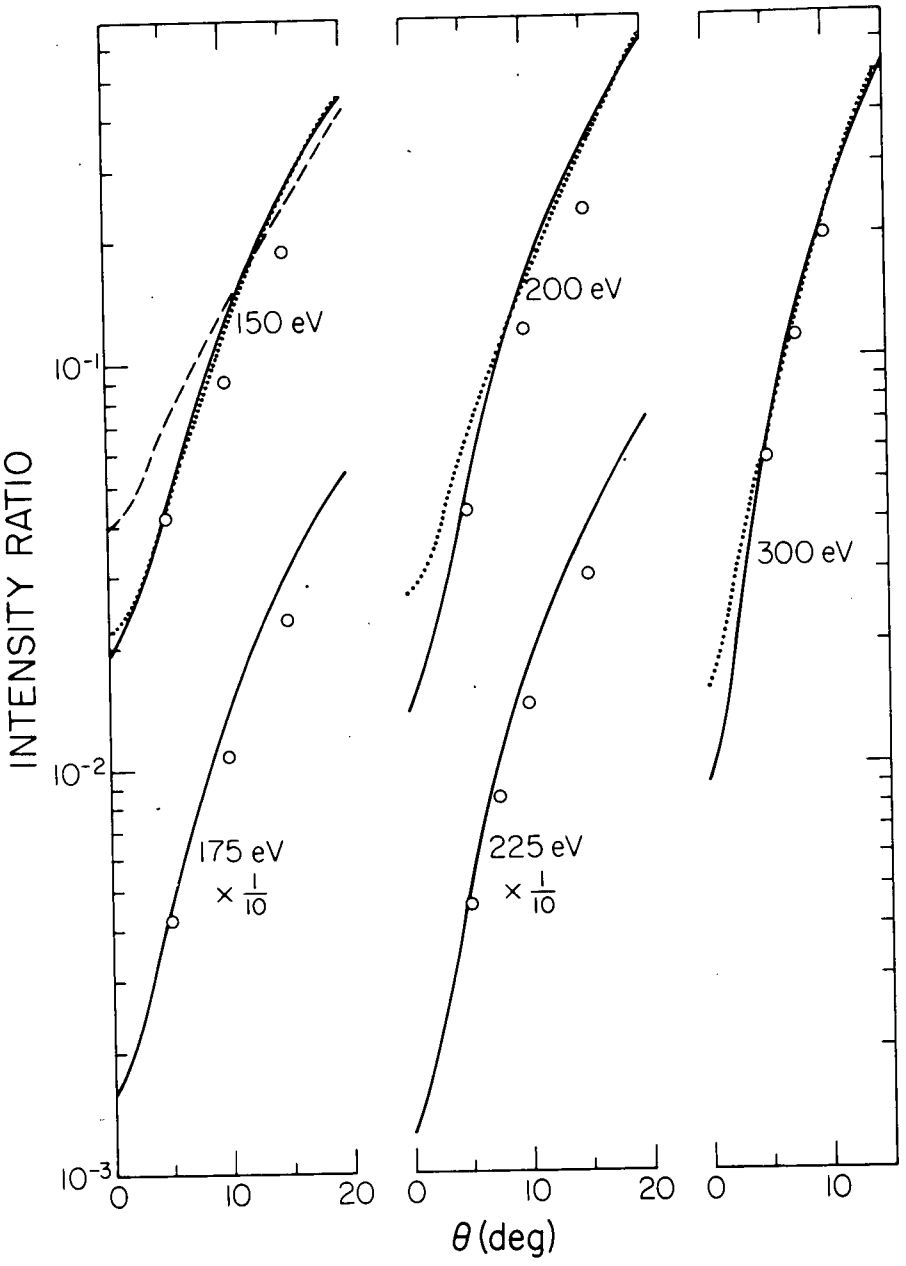

Fig. 17. $2^1S/2^1P$ intensity ratios as a function of scattering angle at the indicated energies. The circles are the experimental results of Vriens et al. (Ref. 2). The solid curves are calculated in the Born-transferred Kang-Foland approximation (BTKF). The dashed and dotted curves are calculated in the polarized Born approximation (B/PB′) with $\alpha = 1.584\ a_o^3$. $b = (5/4)\ b_1^{FW} = 4.59\ a_o$ for the dashed curve, $b = 2(5/4)\ b_1^{FW} = 9.18\ a_o$ for the dotted curve at 150 eV; $b = (5/4)\ b_1^{FW} = 5.30\ a_o$ for the dotted curve at 200 eV, and $b = (5/4)\ b_1^{FW} = 6.50\ a_o$ for the dotted curve at 300 eV.

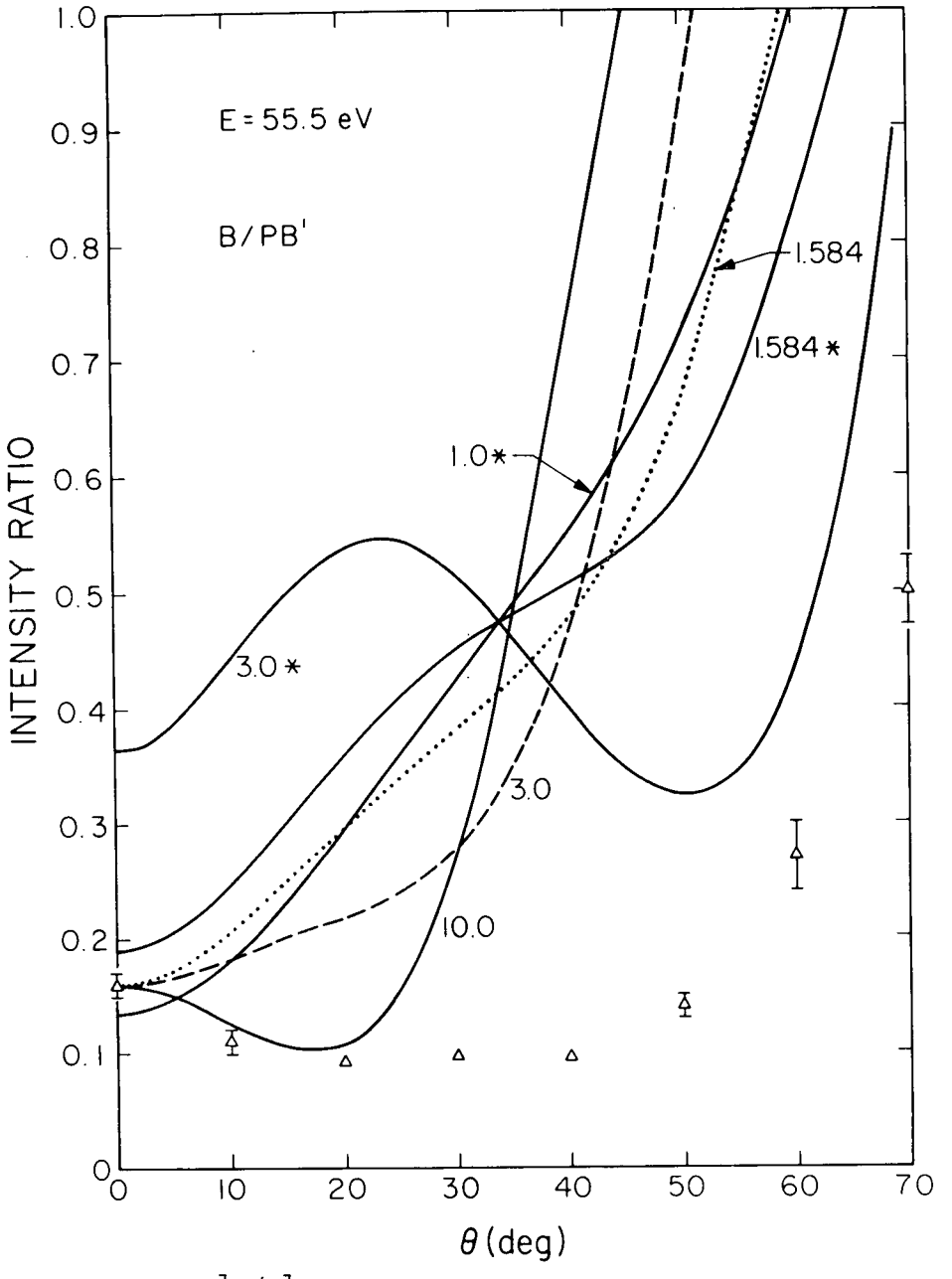

Fig. 18. $2^1S/2^1P$ intensity ratios at E = 55.5 eV. The 2^1S differential cross section is calculated in the B/PB′ approximation, and the 2^1P differential cross section is calculated in the Born approximation. SCF wave functions are used in both calculations. The curves are labeled with the value of α used in the 2^1S cross section calculations. The cutoff parameter in the polarization potential is $b = (5/4)\, b_1^{FW} = 2.79\, a_o$ for those curves marked with an asterisk and was determined empirically from the $2^1S/2^1P$ cross section ratios at 0° for the others. The triangles (with error bars, except when the error is small) are the present data.

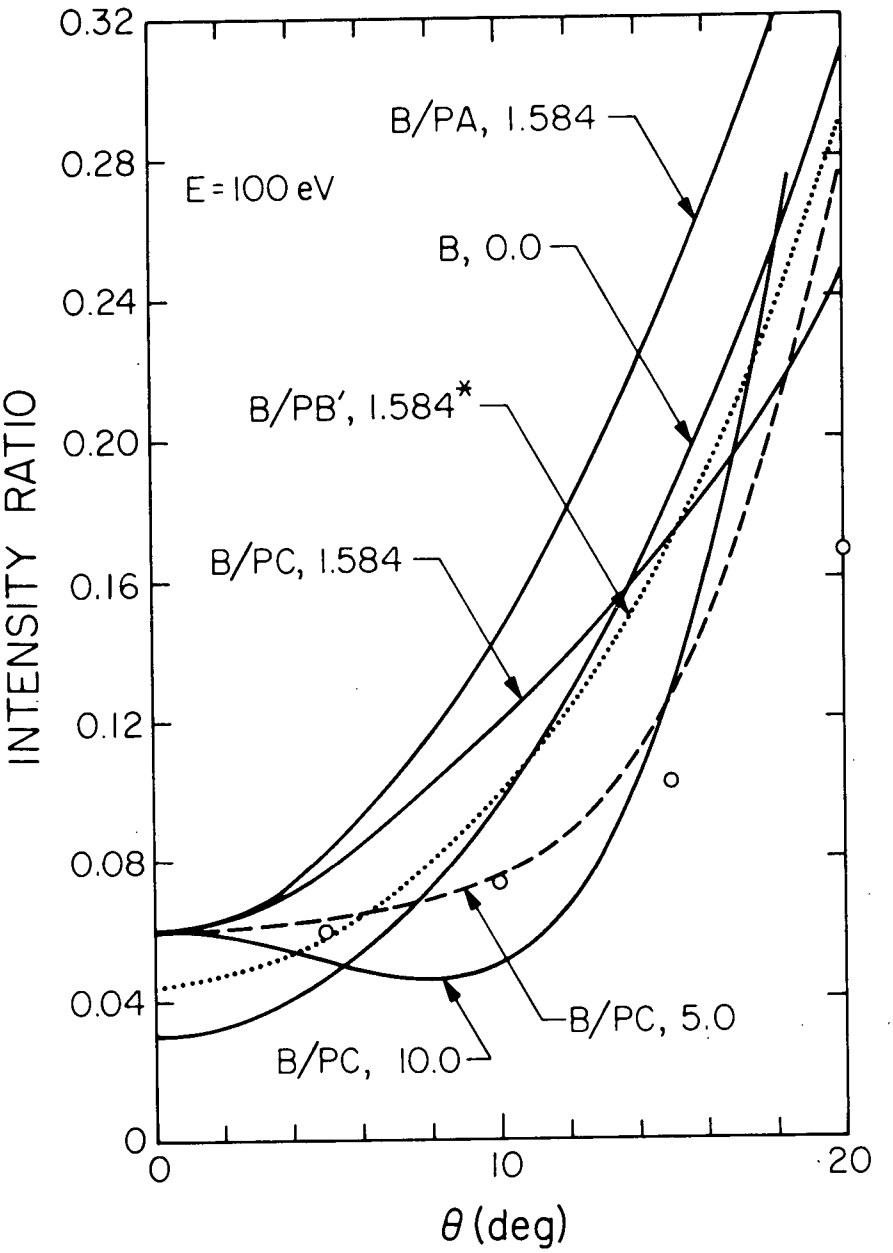

Fig. 19. $2^1S/2^1P$ intensity ratios at E = 100 eV. The 2^1S differential cross sections are calculated in the polarized Born approximation using the indicated form of the polarization potential (and value of α). The 2^1P cross sections are calculated in the Born approximation. SCF wave functions are used. The cutoff parameter in the polarization potential for the curve marked with an asterisk is 1.5 (5/4) b_1^{FW} = 5.62 a_o and the other values are determined empirically (see text and Fig. 13) to be 6.04 a_o for α = 10.0 a_o^3, 5.17 a_o for α = 5.0 a_o^3, 3.46 a_o for α = 1.584 a_o^3 and form C, and 3.02 a_o for α = 1.584 a_o^3 and form A. The circles are the data of Ref. 2.

B. Differential Cross Sections - Angle Dependence

The experimental and calculated DCS's for the 0°-90° angular range are shown in Figs. 4-8 for several energies below 100 eV (26.5, 34, 44, 55.5, and 81.6) and in Fig. 20 for the 0°-20° range at several higher energies (100, 150, 175, 200, 225, 300, and 400 eV). Although the Ochkur and the symmetrized Born-Ochkur-Rudge DCS's have zeroes at some scattering angles, the different first-order calculations predict approximately the same angular behavior, which can be simply characterized in most of the cases as monotonically decreasing as the scattering angle increases and becoming steeper as the impact energy increases. The agreement between the theoretical and the available experimental results becomes much better at impact energies of 81.6 eV and above.

The best agreement between the experimental and theoretical angular dependence is obtained for the B/PB′ calculations as shown on Figs. 5, 6, and 7 by the dotted curves. These curves are easily seen to be much steeper than the Born (B) curves due to the inclusion of polarization. Unfortunately, at the smaller angles the magnitudes of the B/PB′ curves exhibit the poorest agreement with experiment. (For ease of comparison of their angular dependence with experiment, they were renormalized to the experimental DCS's at 10° by multiplying the calculated values by a factor of 0.281, 0.230, and 0.193 for the energies of 34, 44, and 55.5 eV, respectively.)

The plane wave theories used here overestimate the magnitude of the differential cross section as they did for excitation of the 2^1P state.[7] However, in that case we found that the Born approximation and the Ochkur-like approximations gave approximately the correct angle dependence of the DCS for momentum-transfers less than about 1.6 a.u. This corresponds to about 40° in the intermediate energy range. Figures 4-7, however, show

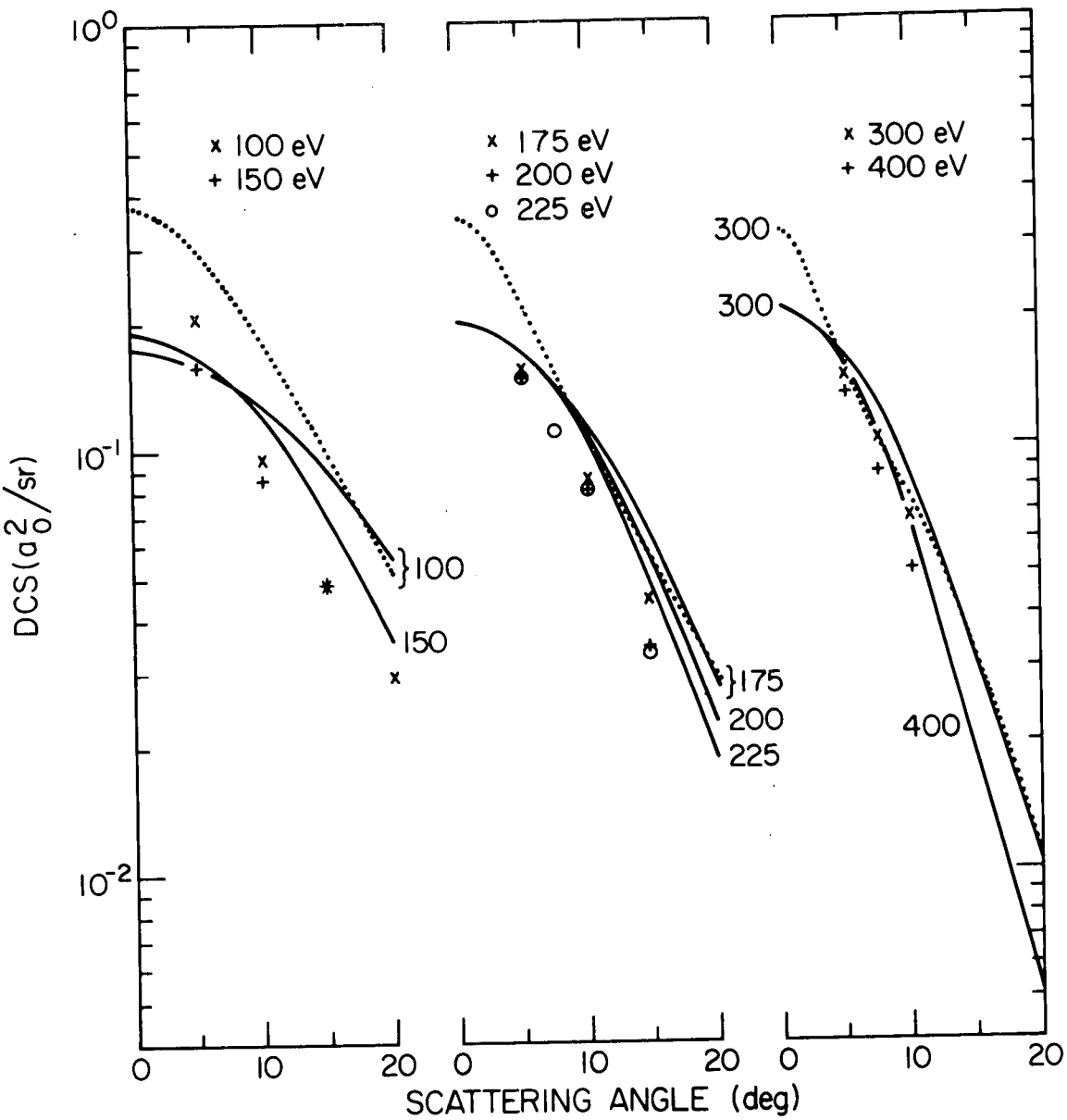

Fig. 20. 2^1S differential cross sections. The solid curves are the DCS calculated in the post Born-Ochkur-Rudge approximation (BORP) and the symbols represent the data of Ref. 2. The impact energies in eV are indicated next to the curves and symbols. The dotted curves are calculated in the polarized Born approximation (B/PB′) with $\alpha = 1.584\ a_0^3$ and $b = (5/4)\ b_1^{FW}$ at each energy.

that the Born approximation and the Ochkur-like approximations (neglecting polarization) do not predict the correct angular dependence for excitation of the 2^1S state even at angles considerably less than 40°. The inclusion of dipole-polarization, making the adiabatic approximation in the initial state, brings theory and experiment into better qualitative agreement for the angle dependence. In Appendix III we discuss the angle range over which plane wave theories agree with experiment for elastic scattering by He, Hg, and H_2, as well as the 2^1P and 2^1S excitations.

Because of the possibility of determining transition polarizabilities empirically from experiment, it is important to examine the effect of the choice of polarization potential on the DCS's. This is explicitly shown in Figs. 21-24 for E = 34, 44, 55.5, and 81.6 eV, respectively. The calculations shown in these figures were carried out in the BOR/P and B/P approximations with different types of cutoff functions and with different values of α and b. At low impact energies (e.g., 34 eV) we can draw the following general conclusions: In the BOR/PA calculations the angle dependence of the DCS's is not very sensitive to changes in either α or b. In the BOR/PC calculations, as the value of α is increased the DCS curves become steeper at low angles, and a minimum and a maximum develop in the curve at intermediate angles. These minima and maxima shift to lower angles as α is increased. The behavior of the DCS's calculated in the BOR/PB and BOR/PB' approximations is intermediate between those of the BOR/PA and BOR/PC approximations. Attempts at determining the transition polarizability from the present data indicate that it cannot be determined with any accuracy.

The best agreement with experiment at 34 eV is obtained with polarization form C and with $\alpha \approx 7\ a_o^3$. This value of α is considerably larger than the theoretically justified value of $1.584\ a_o^3$. However, the value of α

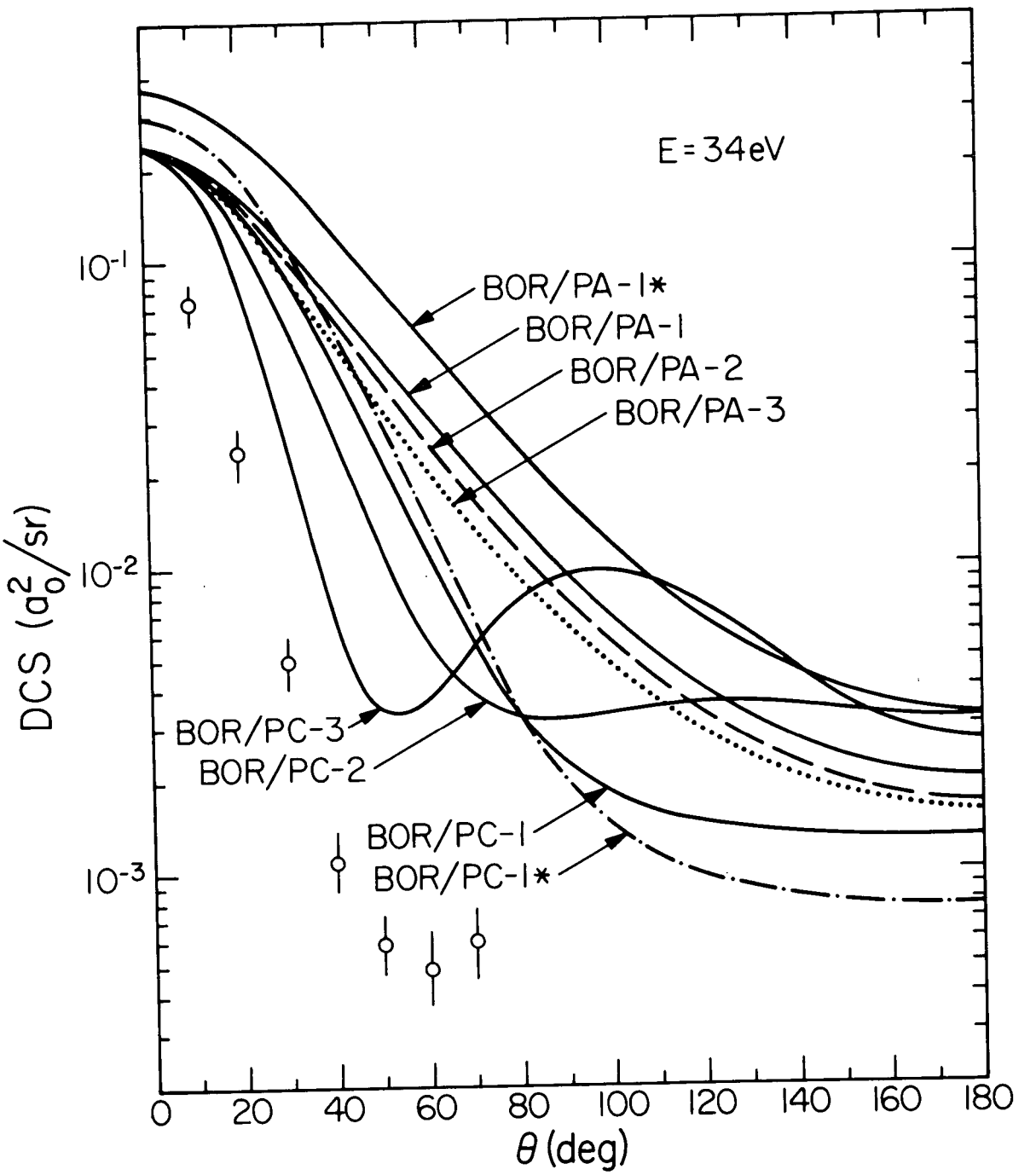

Fig. 21. 2^1S differential cross sections at E = 34 eV calculated in the polarized Born-Ochkur-Rudge approximation (BOR/P) with form A and form C polarization potentials. The numbers 1, 2, and 3 after the designations refer to $\alpha = 1.584\ a_o^3$, $\alpha = 3.0\ a_o^3$, and $\alpha = 7.0\ a_o^3$, respectively. The cutoff parameter used in the polarization potential is b_1^{FW} for the BOR/PC-1* and $(\pi/4)\ b_1^{FW}$ for the BOR/PA-1* curves, and is determined empirically (see text) for the others. The circles with error bars represent the present data.

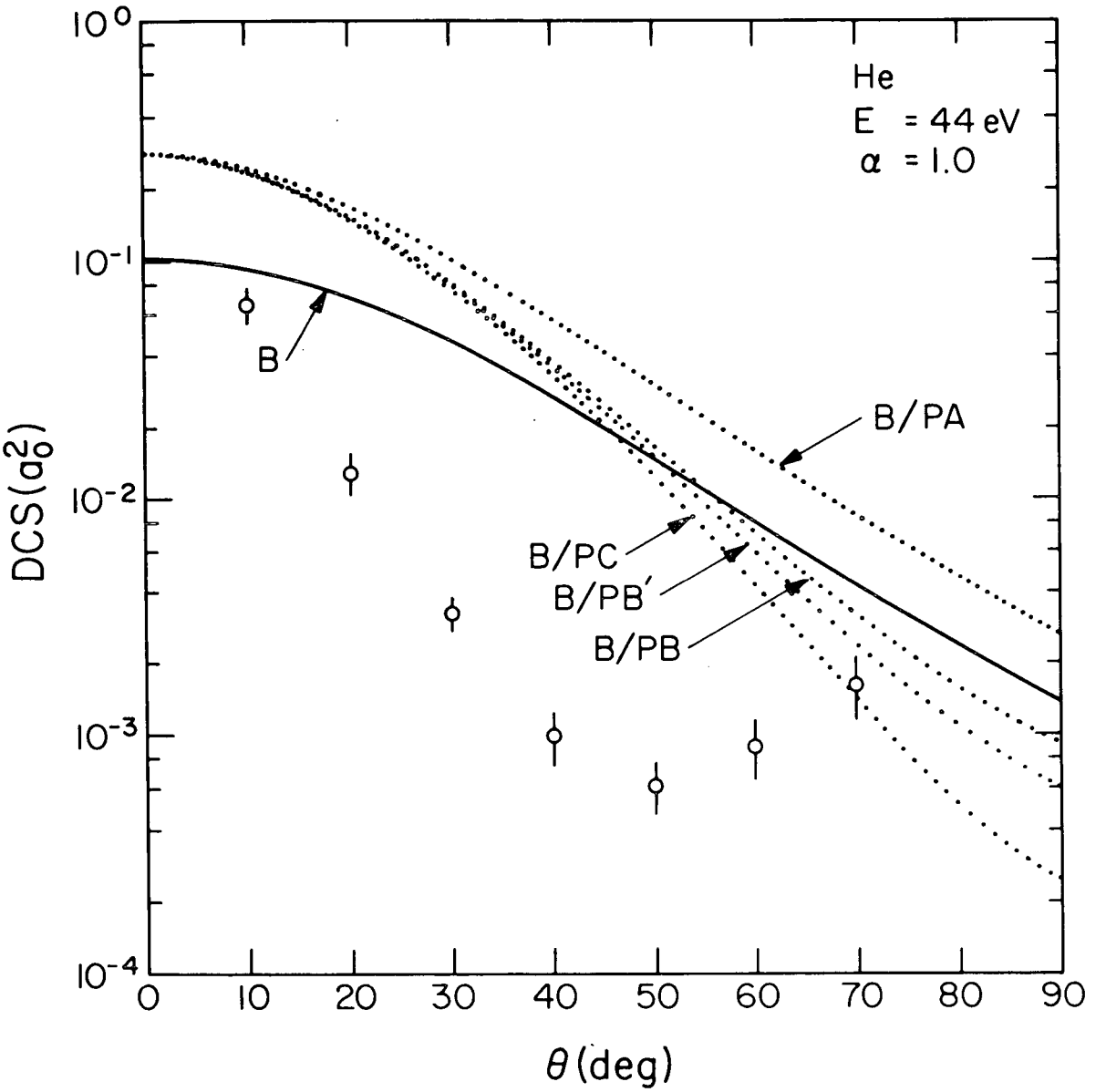

Fig. 22. 2^1S differential cross sections at E = 44 eV with $\alpha = 1.0\ a_o^3$. The curves are calculated in the indicated approximation. The empirically determined cutoff parameter b is used in each calculation which includes polarization. The circles with error bars are the present experimental results at this energy.

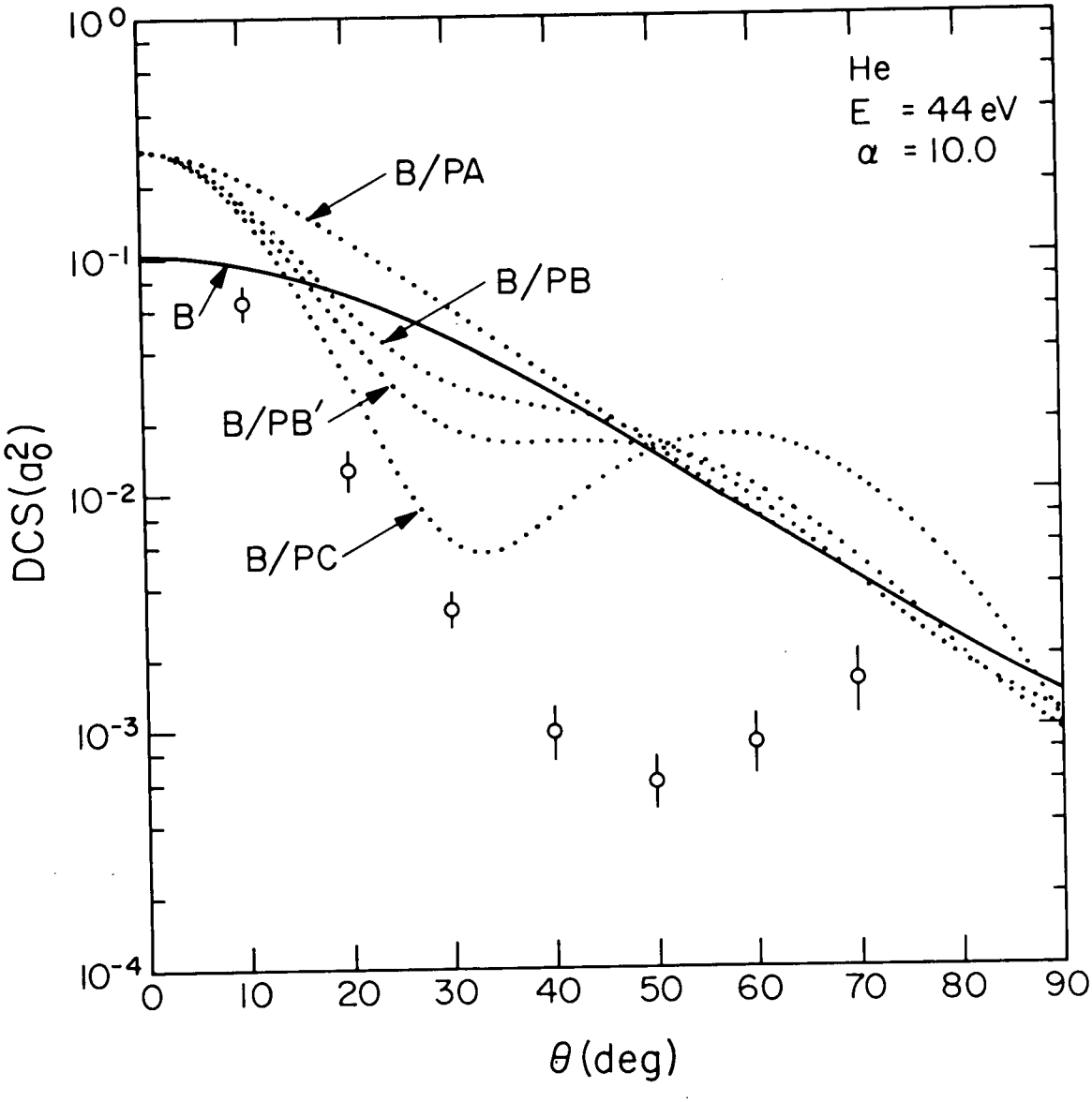

Fig. 23. Same as Fig. 22 except $\alpha = 10.0\ a_0^3$.

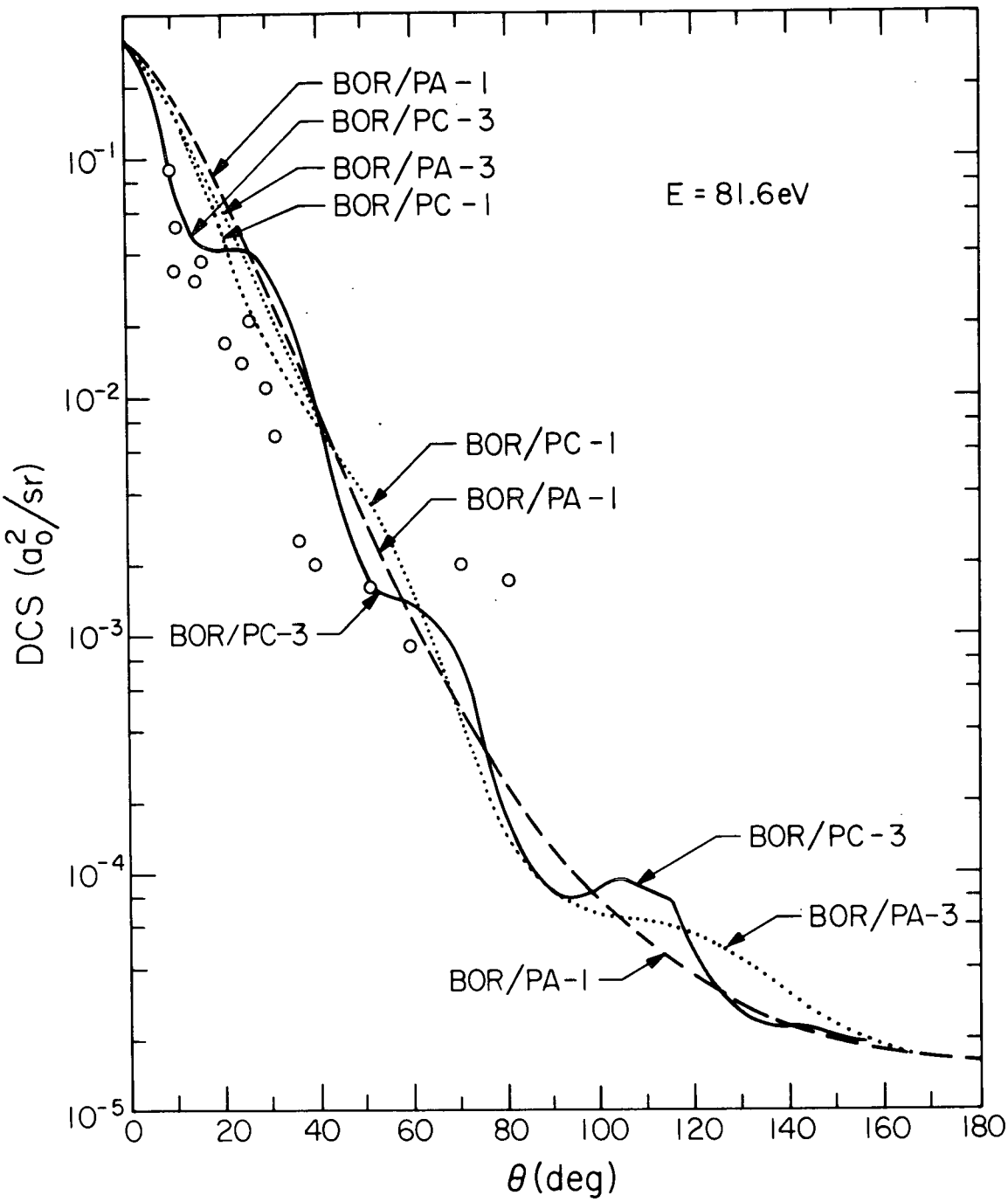

Fig. 24. 2^1S differential cross sections at 81.6 eV calculated in the polarized Born-Ochkur-Rudge approximation (BOR/P) with form A and form C polarization potentials. The numbers 1 and 3 after the symbols refer to $\alpha = 1.584\ a_o^3$ and $\alpha = 7.0\ a_o^3$, respectively. The cutoff parameter used in the polarization potential is determined from the experimental $2^1S/2^1P$ intensity ratios at $\theta = 0°$ (see text). The BOR/PA-3 curve is shown only up to $\theta = 40°$ because at higher angles it cannot be distinguished from the BOR/PA-1 curve on the scale of this figure. Curves for BOR/PA and BOR/PC with $\alpha = 3.0\ a_o^3$ are not shown since they are intermediate between the two cases shown. The circles are the present data.

required for the best agreement with experiment decreases with increasing energy in contrast to the expected energy independence of this quantity (see Section III.D). These observations appear to indicate that the polarization potential should go to zero at small r faster than form B′ does.

At higher impact energies (81.6 eV) all the calculated curves fall into a relatively narrow band, and they predict the magnitude of the DCS's in agreement with experiment out to about 70°. The calculations are not expected to be reliable at large scattering angles because of uncertainties in the proper short range form of the polarization potential. At energies near 100 eV and higher the influence of α and b is significant only at small scattering angles, where the lack of experimental data precludes a definitive test of these calculations.

V. COMPARISON OF THEORETICAL AND EXPERIMENTAL INTEGRAL CROSS SECTIONS

The integration of our experimental 2^1S differential cross sections to obtain 2^1S integral cross sections is discussed in Section II, and the results (circles with error bars) are plotted in Fig. 25. The high energy (200, 225, 300, and 400 eV) experimental integral cross sections obtained by Vriens, Simpson, and Mielczarek[2] are shown in this figure (triangles). The cross sections at 100, 150, and 175 eV (diamonds) were obtained by integrating the 2^1S differential cross section fits given by these authors. These latter results are subject to some uncertainty since only a small range of angles ($\theta \leq 20°$) was studied. We obtained the remaining experimental cross sections in Fig. 25 (squares) by an analysis of the excitation function measurements of Dugan, Richards, and Muschlitz[26] as discussed below.

Dugan, Richards, and Muschlitz[26] measured the relative electron-impact excitation function R(E) for production of the 2^1S state for $26 \leq E \leq 136$ eV. Their excitation function includes contributions from radiative decay to the 2^1S state by higher states (cascade) excited by electron impact, i.e.,

$$Q(E) \cong \lambda\, R(E) - \sum_{n=2} Q_n A(n^1P - 2^1S) \qquad (65)$$

where the last term is the cascade correction, λ is independent of E and normalizes their relative data to the absolute scale, $Q_n(E)$ is the integral cross section for excitation of the n^1P state, A is the branching fraction for $n^1P \rightarrow 2^1S$ radiative decay, and Q(E) is the 2^1S integral cross section. The branching fractions for n = 2-8 are calculated from the table given by

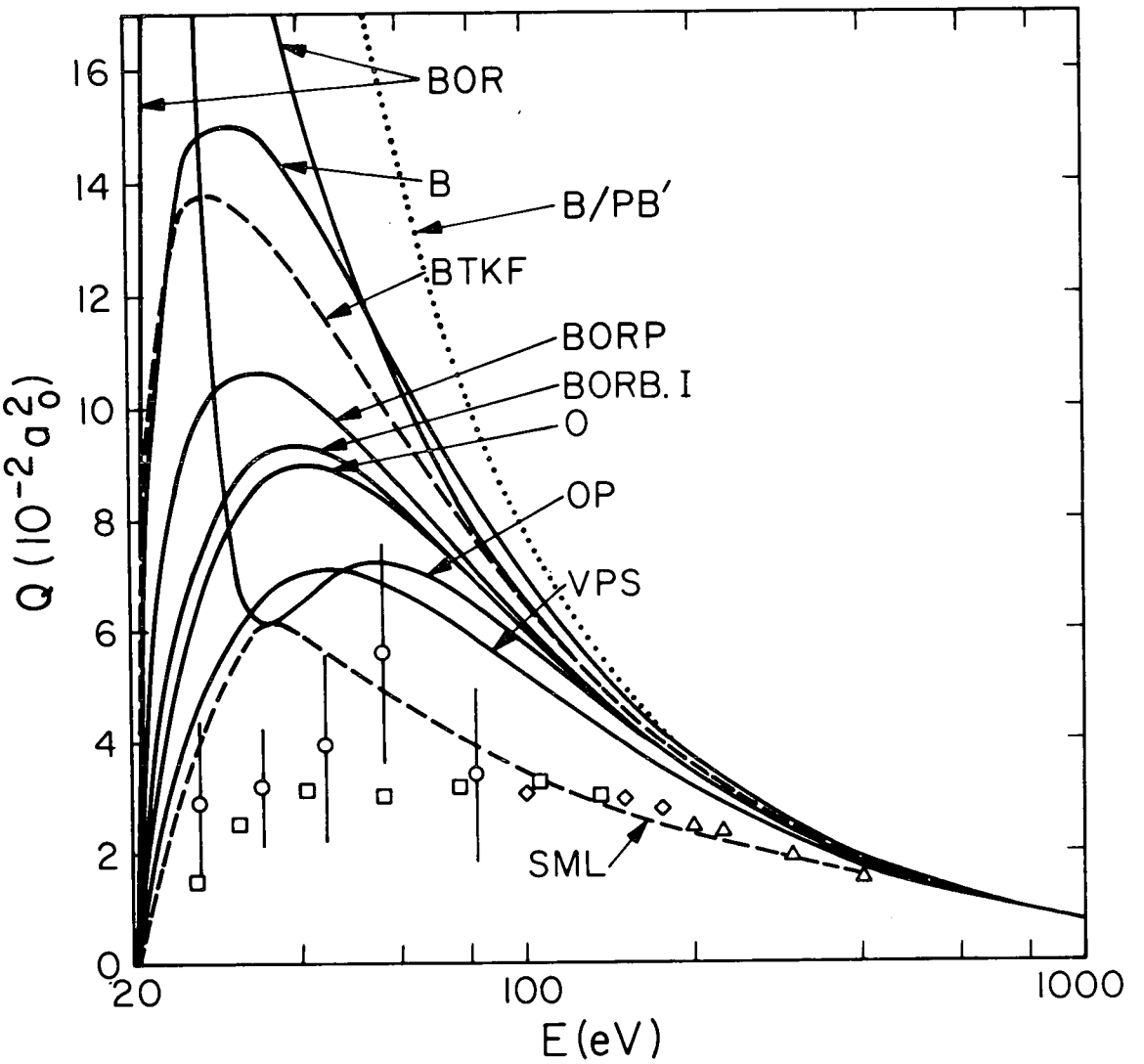

Fig. 25. $1^1S \rightarrow 2^1S$ integral cross sections as a function of impact energy. The squares are the experimental results of Dugan et al. (Ref. 26) (corrected for cascade, see text); the triangles and diamonds are those of Vriens et al. (see text) (Ref. 2); and the circles (with error bars) are the present experimental results (see text). The curve labeled SML is obtained by scaling the 3^1S excitation function data of St. John, Miller, and Lin (Ref. 97) (see text). The other curves are calculated using the indicated approximations. The curves labeled O and OP are calculated using the Born direct amplitude and the Ochkur approximation in the prior and post formulations, respectively, for the exchange amplitude. For the polarized Born approximation (B/PB′), $\alpha = 1.584\ a_0^3$ and $b = (5/4)\ b_1^{FW}$ at each energy. The low energy rise in the B/PB′ cross section (not shown) is steeper than that of the Born-Ochkur-Rudge approximation (BOR).

Gabriel and Heddle.[96] Since the 3^1P state is the largest contributor to the cascade correction, we assume that

$$Q_n(E) = \left(\frac{3}{n}\right)^3 Q_3(E) \qquad n = 2,4,5... \tag{66}$$

We then obtain

$$Q(E) \cong \lambda\, R(E) - 0.0527\, Q_3(E) \quad . \tag{67}$$

We use the absolute values of $Q_3(E)$ of St. John, Miller, and Lin.[97] The value of λ in Eq. (67) is determined by requiring that Q (136 eV) = 0.030 a_o^2, which is chosen to be in reasonable agreement with the lower energy data of Vriens, Simpson, Mielczarek.[2] The resulting cross section values Q(E) are plotted (squares) in Fig. 25.

The curve in Fig. 25 labeled SML is obtained by assuming that the shape of the 2^1S integral cross section curve is the same as the 3^1S one measured by St. John, Miller, and Lin[97] as a function of the incident energy in threshold units ($E/\Delta E(1^1S - n^1S)$). The ordinate for this curve is determined by normalizing it to the E = 300 eV integral cross section data of Vriens, Simpson, and Mielczarek.[2]

The different measurements for the 2^1S integral cross section shown in Fig. 25 are in good accord with each other with the possible exception of the result deduced from the SML data below about 50 eV.

The other curves in Fig. 25 represent the various theoretical models discussed in Section III, both with and without polarization as indicated. The total cross sections calculated with the BOR and B/PB′ ($\alpha = 1.584\ a_o^3$) models reach maxima of about 0.21 and 0.37 a_o^2, respectively, within an eV of 26 eV. Figure 26 presents some additional integral cross sections calculated using several forms of the polarization potential. This figure

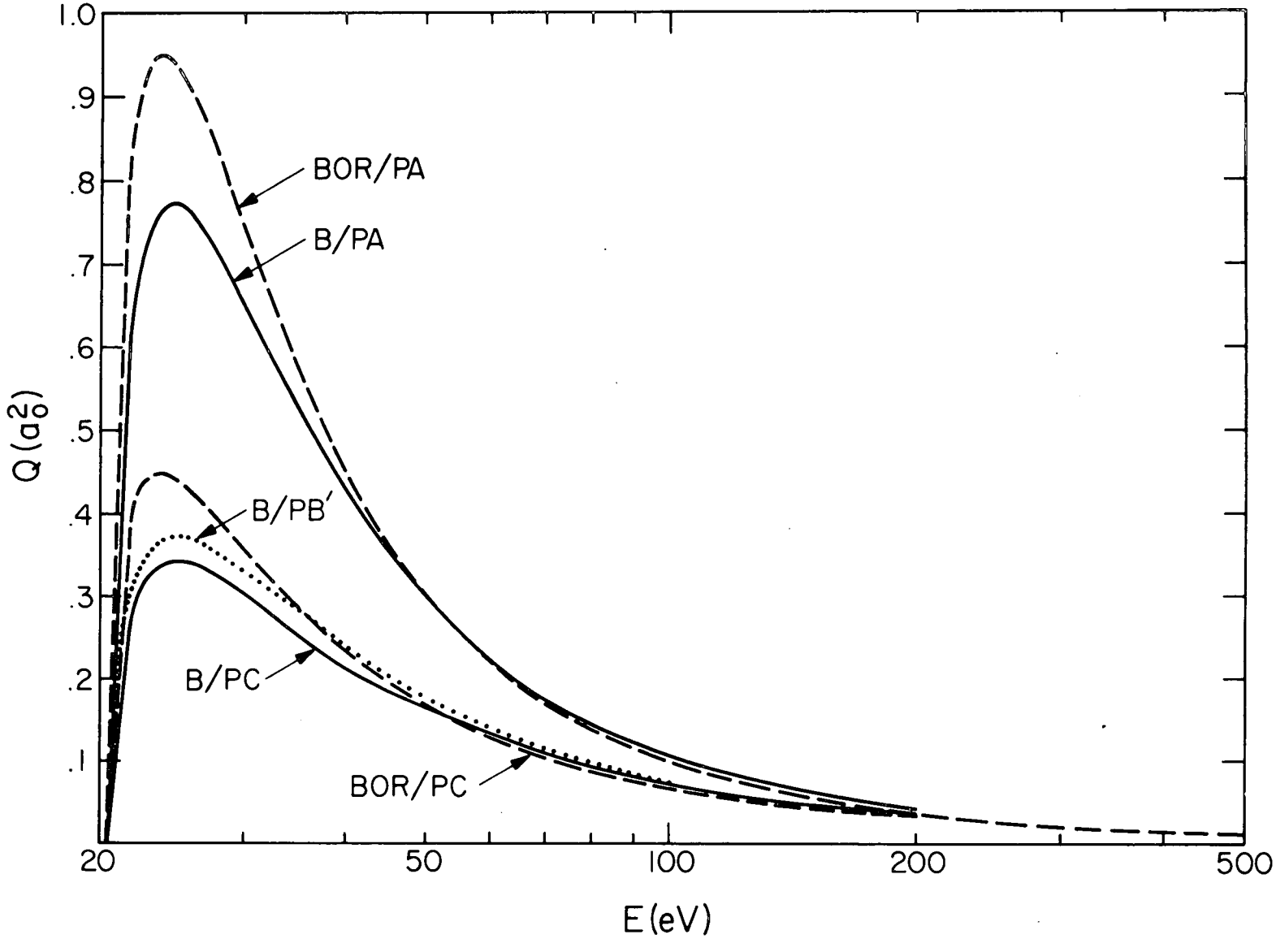

Fig. 26. 2^1S integral cross sections calculated in the indicated approximation including polarization. $\alpha = 1.584\ a_0^3$ for all curves. $b = b_1^{FW}$ for polarization potential form C, $b = (5/4)\ b_1^{FW}$ for form B′ and $b = (\pi/4)\ b_1^{FW}$ for form A at each energy.

shows the sensitivity of the magnitudes of the B/P cross sections to the form of the short range part of the polarization potential.

The cross sections predicted by the first-order theories apparently agree well with experiment for energies greater than about 400 eV but are too large at lower energies. This behavior has been observed by several other investigators. Lassettre[98] used the Born approximation and a generalized oscillator strength fitting procedure to obtain the 2^1S integral cross section at all energies based on experimental generalized oscillator strengths measured only at high energies. His cross section curve lies very close to the BTKF curve in Fig. 25 and somewhat below the Born approximation results based on the accurate generalized oscillator strengths of Kim and Inokuti.[5] Schneider[87] used a generalized oscillator strength calculated using linear response theory to calculate an integral cross section at 500 eV. His value is just slightly (10%) larger than that given by the pure Born result using the SCF wave functions. As in the case of the 2^1P excitation,[7] the VPS, OP, O, and BORB.I approximations give considerable improvement over the Born approximation in the shape of the cross section and the VPS and OP are only about 50% larger than the maximum in the experimental cross section. Over the whole energy range, the VPS and OP approximations to the integral cross section give the best agreement with experiment. This fact could be useful in empirical work. As a general rule, the inclusion of polarization in a given first-order theory results in an even larger integral cross section.

Figure 27 compares the near-threshold behavior of the 2^1S integral cross sections predicted by the present first-order methods and by close-coupling calculations with the lowest energy experimental data from Fig. 25. The triangles are the results of a three-state (1^1S, 2^1S, 2^3S) close-coupling

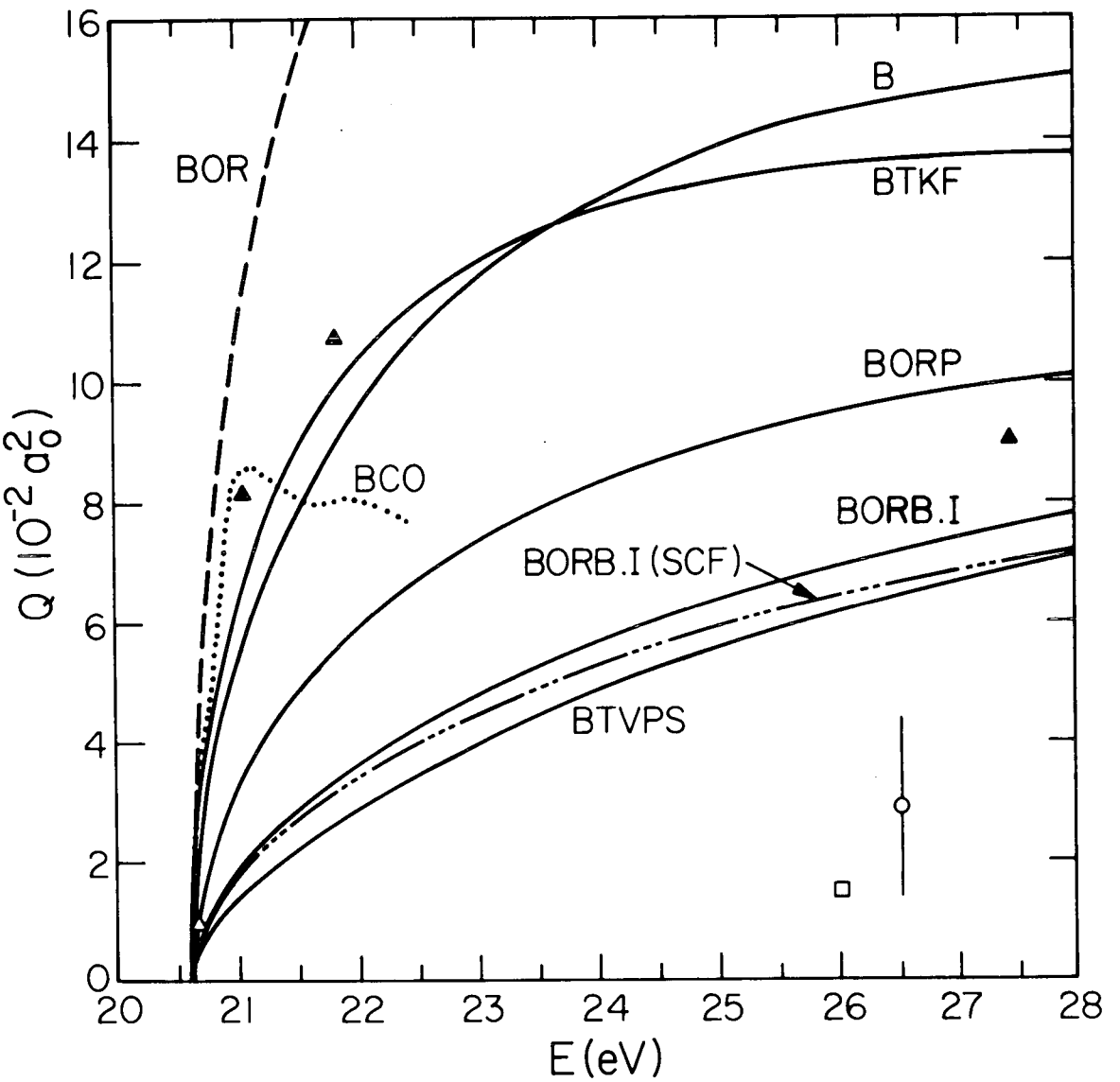

Fig. 27. $1^1S \rightarrow 2^1S$ integral cross sections as a function of impact energy near threshold. The square and circle (with error bar) are the experimental results of Dugan et al. (Ref. 26) and the present work, respectively. The triangles are the theoretical results obtained by Marriott (Ref. 99). The curve labeled BCO is the theoretical result of Burke et al. (Ref. 41). The other curves are the present theoretical results, calculated using the indicated approximations.

calculation performed by Marriott.[99] Since he used a threshold of 20.58 eV, his energy scale was multiplied by 20.61/20.58 before plotting the cross sections. The five-state (1^1S, 2^1S, 2^3S, 2^3P, 2^1P), close-coupling calculation by Burke, Cooper, and Ormonde[41] is labeled as BCO in the figure. The experimental data points are significantly smaller than all the calculated cross sections, including the Marriott close-coupling results. The five-state close-coupling calculations have not yet been reported over a large enough energy range, nor have experimental data been reported at low enough energies, to permit a more definitive comparison. The first-order theories are of course not expected to be reliable in the energy range of Fig. 27. The differences between the curves labeled BORB.I and BORB.I(SCF) are due entirely to differences in the bound-state wave functions used in the two calculations.

VI. SUMMARY AND DISCUSSION

Experimental and quantum mechanical results are presented for the integral and differential cross sections (DCS's) for excitation of the 2^1S state and for the ratio of DCS's for excitation of the 2^1S and 2^1P states in the impact energy range 26.5-81.6 eV. To explain the angle dependence of the small-scattering-angle ($\theta \lesssim 40°$) DCS for E = 34-81.6 eV for either transition it is unnecessary to include an accurate treatment of the distortion of the scattering-electron wave function or of exchange of the incident electron with the bound electrons. This property of the scattering is accurately predicted using plane-wave scattering functions and an effective potential (optical potential) to represent the interaction of the scattering electron with the target. For the 2^1P excitation, the potential may be determined in the static approximation (unperturbed initial and final state), but for the 2^1S excitation it is necessary to include the induced dipole in the description of the target. Although the adiabatic polarization model was previously shown to be an adequate way to include the effect of the induced dipole on elastic scattering at impact energies at least up to a few hundred eV, this model is not adequate for the $1^1S \rightarrow 2^1S$ transition. Evidently, nonadiabatic effects are more important for inelastic scattering than for elastic scattering. We use Fetter and Watson's theoretical criterion for the applicability of the adiabatic approximation to evaluate a cutoff parameter for including some nonadiabatic effects in the polarization model. This procedure gives results in better agreement with experiment than those obtained by including only the static interaction.

The present calculations agree better with higher energy ($E \geq 100$ eV) experimental DCS's than do previous theoretical treatments (the first Born approximation).

The calculated magnitudes of the differential cross sections are in poor agreement with experiment at intermediate energies. The agreement is worse in the present case than in the case of the 2^1P excitation.[7]

The usefulness of self-consistent-field (SCF) single-configuration wave functions for describing the target is examined. We find, on comparing the results to those from more accurate calculations, that SCF wave functions reproduce many facets of the more accurate calculations with good accuracy.

The results of this study indicate that the procedures applied to helium in this paper should also be useful for more complicated atoms and diatomic molecules. The criteria developed here for the importance of polarization can be used to discuss in a consistent way the DCS's for elastic scattering of electrons by He and H_2 and for excitation of the 2^1S and 2^1P states of He.[106]

Finally, we examine, using our experimental results, the reliability and correct interpretation of experiments carried out before 1940. It is found that in some cases that data is still useful.

APPENDIX I: SMALL MOMENTUM-TRANSFER FORMS OF THE POLARIZATION AMPLITUDES

If the polarization amplitudes (Eqs. (33)-(36)) are expanded in a power series in the momentum-transfer q and if second and higher order terms are ignored, the following expressions for the amplitudes are obtained.

$$ {}_fP(A) \underset{q\to 0}{\approx} \frac{\pi\, \alpha_{12}}{4b} (1 - B) $$

$$ {}_fP(B) \underset{q\to 0}{\approx} \frac{4\, \alpha_{12}}{3b} \left(1 - \frac{3\pi B}{16}\right) $$

$$ {}_fP(B') \underset{q\to 0}{\approx} \frac{5\, \alpha_{12}}{4b} \left(1 - \frac{\pi B'}{5}\right) $$

$$ {}_fP(C) \underset{q\to 0}{\approx} \frac{\alpha}{b} \left(1 - \frac{\pi B}{4}\right) $$

where

$$ B = qb. $$

APPENDIX II. COMPARISON OF THEORY AND RECENT EXPERIMENTS WITH OLDER EXPERIMENTAL WORK

Investigations of the angular dependence of inelastic scattering by helium carried out prior to 1940[100] suffer primarily from a lack of adequate energy resolution. The most intense inelastic feature in the energy-loss spectrum was usually observed to peak at an energy-loss of about 21.1 eV and was attributed to excitation of the 2^1P state. It is evident from the results of more recent investigations[37] that this peak contained significant contributions from excitation of the other n = 2 states (i.e., 2^3S, 2^1S, and 2^3P states), particularly at larger scattering angles and lower impact energies. In some cases, these older differential cross section data are also affected by double scattering and improper effective path length corrections. In general, these early investigators collected data over a wide range of angles. These data cannot be readily reproduced with good resolution. It is of interest to re-examine these data in the light of more recent results.

As an example, we will consider the data of Nicholl and Mohr[100a] since they were careful to operate under conditions for which double scattering did not occur. Their basic experimental measurement is the peak (21.1 eV energy-loss) scattered electron intensity as a function of θ. This intensity is multiplied by sin θ to obtain a differential cross section in arbitrary units. The energy resolution in their experiment appears to be about 1.5 eV (see Fig. 3 of Ref. 100b). Since their observed 21.1 eV energy-loss

feature contained contributions from all of the n = 2 excitation cross sections and since these cross sections have quite different angular dependencies, it is to be expected that the shape of this feature varied with changes in the scattering angle. With a knowledge of the n = 2 cross section ratios[37] and the assumption of a Gaussian energy distribution (full-width at half-maximum equal to 1.5 eV) for the incident beam, we can estimate the ratio of peak height to peak area which was obtained in the experiments of Nicholl and Mohr. At 34 eV, this ratio changes by only about 6% for scattering angles between 10° and 70°.

The data of Nicholl and Mohr at 40 eV are shown in Fig. 28 (triangles). These data are compared with the sum of all n = 2 differential cross sections at 40 eV (circles) obtained by interpolation of the cross section ratios of Ref. 37 and the 2^1P differential cross sections of Ref. 7. In addition, theoretical calculations of the various n = 2 cross sections are included in the figure.

The two sets of experimental data in Fig. 28 are in good agreement. Similar comparisons at other energies (e.g., the data of Hughes and McMillan[100c] with those of Vriens *et al.*[2]) also show good agreement. Apparently these early measurements provide reasonably good estimates of the angular dependence of the sum of all n = 2 differential excitation cross sections over a wide range of scattering angles and incident energies.

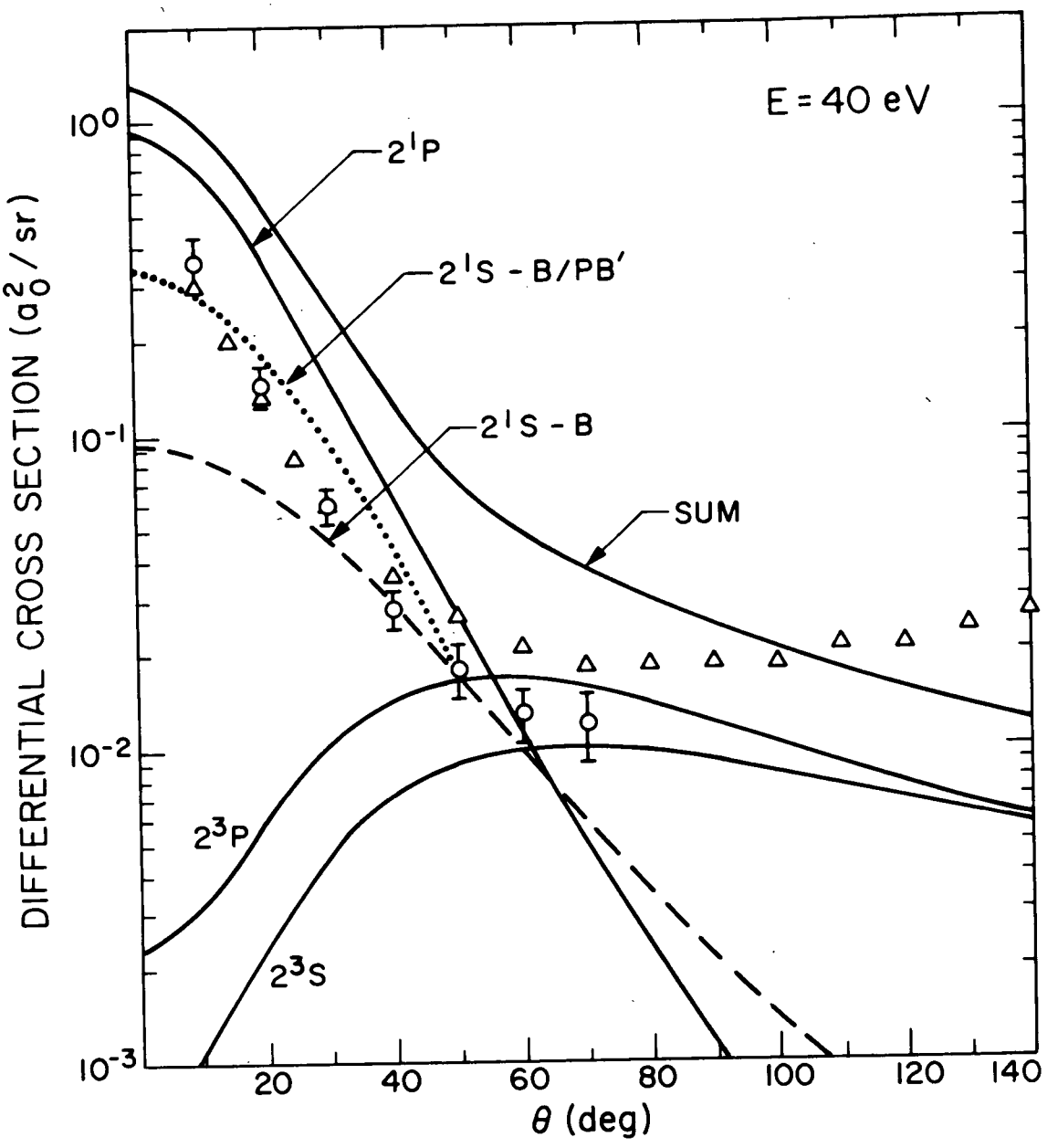

Fig. 28. Differential cross sections vs. scattering angle at E = 40 eV. The triangles represent the data of Ref. 100a and the circles (with error bars) represent the sum of all n = 2 excitation cross sections as derived in Appendix II. The former data are normalized to the latter at θ = 30°. The curves are the results of theoretical calculations for transitions from the 1^1S state to the indicated final states. The curves labeled 2^3S and 2^3P are calculated in the Ochkur-Rudge approximation and are taken from Ref. 101. The curve labeled 2^1P is calculated in the Born approximation and is taken from Ref. 7. The curves labeled 2^1S are the present results calculated using the Born (B) and polarized Born (B/PB′) approximations and SCF wave functions. For the latter, $\alpha = 1.584\ a_o^3$ and $b = (5/4)\ b_1^{FW} = 2.37\ a_o$. The results of the B/PB′ approximation are not shown for $\theta > 50°$. The curve labeled SUM is the sum of the calculated 2^3S, 2^3P, 2^1S, and 2^1P cross sections in which polarization in the 2^1S calculation is included for angles ≤ 50° and ignored for larger angles.

APPENDIX III: THE ANGLE RANGE OVER WHICH PLANE WAVE THEORIES AGREE WITH EXPERIMENT

Both Rice et al.[38-39] and Miller, Mielczarek, and Krauss[102] have attempted to use the experimentally measured angle dependence of the DCS as an indicator of the state symmetries involved in a transition which produces a particular energy-loss peak.

The method used by Rice and co-workers is empirically based on the comparison of measured DCS ratios as a function of angle for various types of transitions.[103] However, Miller et al. attempt to match the angle dependence of the experimental DCS to that of a Born approximation calculation. They argue that a dip in the experimental DCS means the transition is of the type for which the Born approximation DCS has a dip. If such reasoning is to be used confidently, we must be reasonably certain that the Born approximation predicts the correct angle dependence of the DCS in certain situations. Further, in order to decide whether plane wave calculations for different types of transitions can be useful in guiding the method of Rice et al., we must determine the range of angles for which plane wave calculations predict the correct angle dependence of the DCS.

Table X summarizes some of the presently available data on the range over which the Born and polarized Born approximations predict the approximately correct angle dependence of the differential cross sections. Columns 1, 2, and 3 list the target, transition, and impact energy, respectively. Column 4 contains the maximum angle θ_{max} for which plane wave theory and

experiment have approximately the same shape. This angle is determined by normalizing theory to experiment at $\theta = 20°$ and finding the angle at which they deviate by 50%. Columns 5, 6, and 7 contain, respectively, the momentum-transfer $q(\theta_{max})$, the experimental DCS $I^{exp}(\theta_{max})$, and the calculated DCS $I^{calc}(\theta_{max})$ evaluated at $\theta = \theta_{max}$.

The plane wave cross sections agree qualitatively with experiment at small θ, where many partial waves contribute appreciably to the DCS. At large θ the scattering is due mainly to the lowest few partial waves, where distortion of the plane wave may be appreciable. To obtain a rough estimate of the contribution to scattering involving large distortion, we present in Column 8 one-half the maximum theoretical cross section for s-wave scattering I^s. The s-wave limit for the DCS is $1/k^2$ for elastic scattering and $1/4k^2$ for inelastic scattering.[104] Finally, Columns 9 and 10 list, respectively, the experimental and calculated DCS's divided by $I^s/2$.

In a previous paper[7] we noted that for excitation of the 2^1P state, the angle dependence of the DCS was predicted out to $q \approx 1.6$ a.u. The more extensive collection of data presented in Table X shows that for elastic scattering the plane-wave theories often predict the angle dependence correctly out to even larger q. The data also indicate a systematic trend in which the angle dependence of the DCS is correctly predicted out to larger q at higher energies than at lower ones. Further, the magnitudes of the experimental and theoretical DCS's agree better at higher energy. In discussing scattering from a central potential of finite range, Schiff[105] suggests that the Born approximation can be used at all angles provided the incident energy is high enough while at lower energies the small-angle scattering may be given correctly when the large-angle scattering is not. Such a trend is consistent with the present results.

TABLE X

The range of angles over which plane-wave theories predict approximately the correct angle dependence of the differential cross section for elastic and inelastic scattering. The column headings are defined in Appendix IV. The theoretical cross sections for elastic scattering and excitation of the He 2^1S state are calculated in the polarized Born approximation. Those for excitation of the 2^1P state of helium are calculated in the Born approximation. In cases where the theory and experiment still satisfy our criterion for agreement at the largest angle for which experimental data are available, we can only obtain lower bounds on columns 4 and 5 and upper bounds on columns 6-7, 9-10.

Target	Transition	E (eV)	θ_{max} (deg)	q_{max} (a.u.)	I^{exp} (a_o^2/sr)	I^{calc} (a_o^2/sr)	$I^s/2$ (a_o^2/sr)	$2I^{exp}/I^s$	$2I^{calc}/I^s$
He	elastic	39[a]	≥80	≥2.18	≤0.23	≤0.23	0.174	≤1.3	≤1.3
		81.6[a]	50	2.07	0.18	0.27	0.084	2.1	3.2
		500[b]	≥60	≥6.06	≤0.011	≤0.011	0.014	≤0.78	≤0.78
He	$1^1S \rightarrow 2^1S$	34	22[c]	0.76	0.020	0.18	0.050	0.40	3.6
		44	26[c]	0.85	0.007	0.11	0.039	0.18	2.8
		55.5	42	1.36	0.0016	0.013	0.031	0.052	0.42
		81.6	45	1.77	0.002	0.0052	0.022	0.091	0.24
		100[d]	≥20	≥0.94	≤0.029	≤0.051	0.017	≤1.7	≤3.0
		175[d]	≥15	≥0.93	≤0.044	≤0.055	0.0097	≤4.5	≤5.7
		300[d]	≥10	≥0.82	≤0.069	≤0.074	0.0057	≤12	≤13
		400[d]	≥10	≥0.95	≤0.052	≤0.061	0.0042	≤12	≤14

TABLE X (cont.)

Target	Transition	E	θ_{max}	q_{max}	I^{exp}	I^{calc}	$I^s/2$	$2I^{exp}/I^s$	$2I^{calc}/I^s$
He	$1^1S \rightarrow 2^1P$	34[e]	40	1.04	0.017	0.084	0.050	0.34	1.7
		44[e]	58	1.56	0.0072	0.010	0.039	0.18	0.26
		55.5[e]	45	1.44	0.014	0.019	0.031	0.45	0.61
		81.6[e]	49	1.91	0.0067	0.0027	0.022	0.30	0.12
		100[f]	≥20	≥0.94	≤0.18	≤0.20	0.017	≤11	≤12
		175[f]	≥15	≥0.94	≤0.19	≤0.22	0.0097	≤20	≤23
		300[f]	≥10	≥0.82	≤0.35	≤0.37	0.0057	≤61	≤65
		400[f]	≥10	≥0.95	≤0.20	≤0.21	0.0042	≤48	≤50
Hg	elastic	300[g]		≥1.61	≤7.5	≤33[h]	0.028	≤268	
		400[g]		≥1.86	≤4.7	≤20[h]	0.017	≤276	
		500[g]		≥2.1	≤3.3	≤12[h]	0.014	≤236	
H_2	elastic[i]	7	115	1.21	2.0	1.3	0.97	2.1	1.3
		10	120	1.48	1.0	0.65	0.68	1.5	0.96
		13.6	≥80	≥1.29	≤1.2	≤1.2	0.50	≤2.4	≤2.4
		20	100	1.86	0.5	0.30	0.34	1.5	0.88
		45	≥80	≥2.34	≤0.15	≤0.12	0.15	≤1.0	≤0.80
		60	120	3.64	0.043	0.03	0.11	0.39	0.27
		81.6	≥80	≥3.15	≤0.058	≤0.05	0.084	≤0.69	≤0.60
		30	100	2.28		0.14	0.23		0.61
		50	110	3.14		0.05	0.14		0.36
		100	105	4.30		0.018	0.068		0.26

TABLE X (cont.)

[a] Reference 106.

[b] J. P. Bromberg, J. Chem. Phys. 50, 3906 (1969).

[c] These angles, obtained by interpolation, are so close to 20 degrees that they imply there is very little quantitative agreement in the angle dependence of theory and experiment.

[d] Experimental data of Ref. 2 and polarized Born approximation calculations of present work.

[e] Reference 7.

[f] Experimental data of Ref. 2 and Born approximation results of Ref. 7.

[g] J. P. Bromberg, J. Chem. Phys. 51, 4117 (1969).

[h] These values are $(36.5/18.65)^2$ times greater than the values in g due to an error in that calculation.

[i] Reference 46.

The entries in Column 9 of Table X are near unity for the elastic scattering data and possibly the $1^1S \rightarrow 2^1P$ DCS's. Thus, s-wave scattering may account for the values of θ_{max} obtained in these cases. However, the angle dependence of the $1^1S \rightarrow 2^1S$ DCS's is predicted to angles at which the cross section is considerably lower than our estimate of the maximum probable s-wave contribution. Possibly our use of $\frac{1}{2}I^S$ for this estimate is not as realistic in this case. In general, Column 9 provides a less energy-dependent criterion for the validity of the plane wave theories than do either Columns 4 or 5.

Table X shows that plane wave theories are more successful for elastic scattering than for inelastic scattering. This success is probably due to the larger contributions to the cross sections from higher partial waves in the elastic case. For the two inelastic transitions in the table, the Born approximation is less valid for the 2^1S excitation than for the 2^1P one. This is probably due to the much greater difficulties in estimating the effective potential for the 2^1S case. This points up the importance of further study of the nonadiabatic polarization transition potential.

REFERENCES

1. E. N. Lassettre and E. A. Jones, J. Chem. Phys. 40, 1222 (1964).
2. L. Vriens, J. A. Simpson, and S. R. Mielczarek, Phys. Rev. 165, 7 (1968).
3. N. F. Mott and H.S.W. Massey, The Theory of Atomic Collisions (Clarendon Press, Oxford, 1965), 3rd ed., pp. 484-488, 499, and references therein.
4. H.S.W. Massey and E.H.S. Burhop, Electronic and Ionic Impact Phenomenon (Clarendon Press, Oxford, 1969), 2nd ed., Vol. I, (a) pp. 480-496 and (b) Chap. XVIII.
5. Y.-K. Kim and M. Inokuti, Phys. Rev. 175, 176 (1968).
6. A. Skerbele and E. N. Lassettre, J. Chem. Phys. 53, 3806 (1970).
7. D. G. Truhlar, J. K. Rice, A. Kuppermann, S. Trajmar, and D. C. Cartwright, Phys. Rev. A1, 778 (1970). The normalization of the experimental absolute 2^1P differential cross sections presented there should be modified as discussed in Section II of this paper.
8. D. G. Truhlar and J. K. Rice, J. Chem. Phys. 52, 4480 (1970).
9. E. N. Lassettre, M. E. Krasnow, and S. M. Silverman, J. Chem. Phys. 40, 1242 (1964).
10. S. M. Silverman and E. N. Lassettre, J. Chem. Phys. 40, 1265 (1964).
11. A. Skerbele and E. N. Lassettre, J. Chem. Phys. 45, 1077 (1966).
12. J. A. Simpson, M. G. Menendez, and S. R. Mielczarek, Phys. Rev. 150, 76 (1966).
13. D. Andrick, H. Ehrhardt, and M. Eyb, Z. Physik 214, 388 (1968).
14. G. E. Chamberlain, S. R. Mielczarek, and C. E. Kuyatt, Phys. Rev. A2, 1905 (1970).
15. G. E. Chamberlain, J. A. Simpson, S. R. Mielczarek, and C. E. Kuyatt, J. Chem. Phys. 47, 4266 (1967).

16. J. A. Simpson and S. R. Mielczarek, J. Chem. Phys. 39, 1606 (1963).

17. E. N. Lassettre, A. S. Berman, S. M. Silverman, and M. E. Krasnow, J. Chem. Phys. 40, 1232 (1964).

18. E. N. Lassettre, V. D. Meyer, and M. S. Longmire, J. Chem. Phys. 41, 2952 (1964).

19. G. E. Chamberlain, H. G. M. Heideman, J. A. Simpson, and C. E. Kuyatt, IVth International Conference on the Physics of Electronic and Atomic Collisions: Abstracts of Papers (Science Bookcrafters, Hastings-on-Hudson, 1965), p. 378.

20. J. P. Doering, J. Chem. Phys. 45, 1065 (1966).

21. J. P. Doering and A. J. Williams, J. Chem. Phys. 47, 4180 (1967).

22. J. P. Doering, private communication (1967).

23. H. Boersch, J. Geiger, and B. Schröder, Vth International Conference on the Physics of Electronic and Atomic Collisions: Abstracts of Papers (Nauka, Leningrad, 1967), p. 481.

24. A. Skerbele and E. N. Lassettre, Vth International Conference on the Physics of Electronic and Atomic Collisions: Abstracts of Papers (Nauka, Leningrad, 1967), p. 495.

25. E. N. Lassettre, A. Skerbele, M. A. Dillon, and K. J. Ross, J. Chem. Phys. 48, 5066 (1968).

26. J. L. G. Dugan, H. L. Richards, and E. E. Muschlitz, J. Chem. Phys. 46, 346 (1967).

27. B. L. Moisiewitsch and S. J. Smith, Rev. Mod. Phys. 40, 238 (1968), (a) p. 254 and references therein.

28. V. I. Ochkur, Soviet Phys.-JETP 18, 503 (1964).

29. M. R. H. Rudge, Proc. Phys. Soc. (London) 85, 607 (1965).

30. O. Bely, Proc. Phys. Soc. (London) 87, 1010 (1966).

31. D. S. F. Crothers, Proc. Phys. Soc. (London) 87, 1003 (1966).

32. L. Presnyskov, I. Sobelman, and L. Vainshtein, in Atomic Collision Processes, edited by M. R. C. McDowell (North-Holland Publishing Co., Amsterdam, 1964), p. 243.

33. I.-J. Kang and W. D. Foland, Phys. Rev. 164, 122 (1967).

34. R. A. Bonham, J. Chem. Phys. 36, 3260 (1962).

35. D. G. Truhlar, D. C. Cartwright, and A. Kuppermann, Phys. Rev. 175, 113 (1968).

36. D. G. Truhlar and A. Kuppermann, VIth International Conference on the Physics of Electronic and Atomic Collisions: Abstracts of Papers (M.I.T. Press, Cambridge, 1969), p. 247.

37. J. K. Rice, A. Kuppermann, and S. Trajmar, J. Chem. Phys. 48, 945 (1968).

38. A. Kuppermann, J. K. Rice, and S. Trajmar, J. Phys. Chem. 72, 3894 (1968).

39. J. K. Rice, Ph.D. Thesis, California Institute of Technology, Pasadena (1969).

40. B. L. Scott, Phys. Rev. 140, A699 (1965).

41. P. G. Burke, J. W. Cooper, and S. Ormonde, Phys. Rev. 183, 245 (1969).

42. J. R. Oppenheimer, Phys. Rev. 32, 361 (1928).

43. (a) S. P. Khare and B. L. Moisiewitsch, in Atomic Collision Processes, edited by M. R. C. McDowell (North-Holland, Amsterdam, 1964), p. 49.
(b) S. P. Khare and B. L. Moisiewitsch, Proc. Phys. Soc. (London) 85, 821 (1965).

44. R. W. LaBahn and J. Callaway, Phys. Rev. 180, 91 (1969).

45. S. P. Khare and P. Shobha, in VIth International Conference on the Physics of Electronic and Atomic Collisions: Abstracts of Papers, edited by I. Amdur (M.I.T. Press, Cambridge, Mass., 1969), p. 844.

46. S. Trajmar, D. G. Truhlar, and J. K. Rice, J. Chem. Phys. 52, 4502 (1970).

47. L. Castillejo, I. C. Percival, and M. J. Seaton, Proc. Roy. Soc. (London) 254, 259 (1960).

48. M. H. Mittleman and J. L. Peacher, Phys. Rev. 173, 160 (1968).

49. C. J. Kleinman, Y. Hahn, and L. Spruch, Phys. Rev. 165, 53 (1968).

50. A. L. Fetter and K. M. Watson, Adv. Theor. Phys. 1, 115 (1965).

51. P. G. Burke, in Scattering Theory: New Methods and Problems in Atomic, Nuclear, and Particle Physics, edited by A. O. Barut (Gordon and Breach, New York, 1969), p. 193.

52. See, e.g., M. J. Seaton, Proc. Phys. Soc. (London) 77, 174 (1961).

53. D. G. Truhlar, J. K. Rice, S. Trajmar, and D. C. Cartwright, Bull. Am. Phys. Soc. 15, 786 (1970).

54. See H. C. Volkin, Phys. Rev. 155, 1177 (1965) and references therein.

55. R. T. Pu, Univ. of Calif. Lawrence Radiation Laboratory Technical Report UCRL-10878 (Berkeley, 1963).

56. R. J. Damburg and S. Geltman, Phys. Rev. Letters 20, 485 (1968).

57. a) See, e.g., N. F. Lane and R. J. W. Henry, Phys. Rev. 173, 183 (1968).
b) M. H. Mittleman, Ann. Phys. 14, 94 (1961).

58. A. R. Holt and B. L. Moisiewitsch, J. Phys. B1, 36 (1968).

59. D. R. Bates, A. Fundaminsky, and H. S. W. Massey, Phil. Trans. Roy. Soc. (London) A243, 93 (1950).

60. The core terms in the approximate scattering amplitude have been discussed from opposing viewpoints by (a) J. B. Day, L. S. Rodberg, G. A. Snow, and J. Sucher, Phys. Rev. 123, 1051 (1961); I.-J. Kang and W. D. Foland, Phys. Rev. 164, 122 (1967); Ref. 65. (b) M. R. H. Rudge, J. Phys. B (2) 1, 130 (1968); Ref. 3, Chap. XV. The quantitative effects of the core on the cross sections have been discussed for the excitation of hydrogen and helium in Refs. 28 and 35.

61. R. A. Bonham (Ref. 34) gave an earlier derivation of this approximation but considered it useful only at high energies while Ochkur considered the expression useful at all energies.

62. O. Bely, Il Nuovo Cimento 10 49, 66 (1967).

63. (a) L. Vainshtein, L. Presnayakov and I. Sobelman, Sov. Phys.--JETP 18, 1383 (1964); (b) L. Vainshtein, V. Opykhtein, and L. Presnyakov, Sov. Phys.--JETP 20, 1542 (1965).

64. Handbook of Mathematical Functions, edited by M. Abramowitz and I. A. Stegun (NBS AMS 55 (1964)), Section 15.

65. I.-J. Kang, Phys. Rev. 179, 101 (1969).

66. A. W. Weiss, J. Res. Natl. Bur. Std. 71A, 163 (1967).

67. E. Clementi, "Tables of Atomic Functions," IBM Technical Report (1965). Also, W. A. Goddard III, unpublished.

68. R. P. Hurst, Acta Cryst. 13, 634 (1960).

69. D. C. Cartwright and A. Kuppermann, Phys. Rev. 163, 86 (1967).

70. (a) C. L. Pekeris, Phys. Rev. 115, 1216 (1959). (b) C. L. Pekeris, Phys. Rev. 126, 143 (1962).

71. A. Messiah, Quantum Mechanics (North-Holland Publishing Co., Amsterdam, 1966), Vol. II, Chap. XVIII.

72. E. A. Hylleraas and B. Undheim, Z. Phys. 65, 759 (1930).

73. J.K.L. MacDonald, Phys. Rev. 43, 830 (1933).

74. W. Kolos and K. Pecul, Ann. Phys. (N.Y.) 16, 203 (1961).

75. R. Marriott and M. J. Seaton, Proc. Phys. Soc. 70A, 296 (1957).

76. C. S. Sharma and C. A. Coulson, Proc. Phys. Soc. 80, 81 (1962).

77. M. Cohen and P. S. Kelly, Can. J. Phys. 43, 1867 (1965).

78. V. Fock, Z. Phys. 61, 126 (1930).

79. E. Trefftz, A. Schlüter, K-H Dettman, and K. Jörgens, Z. Astrophys. 44, 1 (1957).

80. L. P. Smith, Phys. Rev. 42, 176 (1932).

81. M. Cohen and P. S. Kelly, Can. J. Phys. 44, 3227 (1966).

82. M. Cohen and R. P. McEachran, Proc. Phys. Soc. 92, 37 (1967).

83. W. J. Hunt and W. A. Goddard III, Chem. Phys. Lett. 3, 414 (1969).

84. W. A. Goddard III, Phys. Rev. 157, 81 (1967).

85. D. C. Cartwright and W. A. Goddard III (unpublished).

86. K. L. Bell, D. J. Kennedy, and A. E. Kingston, J. Phys. B 2, 26 (1969).

87. B. Schneider, Phys. Rev. A2, 1873 (1970). The authors thank Dr. Schneider for providing a copy of this work prior to publication.

88. G.W.F. Drake and M. Cohen, J. Chem. Phys. 48, 1168 (1968).

89. A. L. Stewart, J. Phys. B 2, 309 (1969).

90. E. G. Wikner and T. P. Das, Phys. 107, 497 (1957).

91. M. Yoshimine and R. P. Hurst, Phys. Rev. 135, A612 (1964).

92. Y. M. Chan and A. Dalgarno, Proc. Phys. Soc. 85, 227 (1965).

93. P. Sitz and R. Yaris, J. Chem. Phys. 49, 3546 (1968).

94. G.W.F. Drake, private communication.

95. G.W.F. Drake and A. Dalgarno, Astrophys. J. 157, 459 (1969).

96. A. H. Gabriel and D.W.O. Heddle, Proc. Roy. Soc. (London) A258, 124 (1960).

97. R. M. St. John, F. L. Miller, and C. C. Lin, Phys. Rev. 134, A888 (1964).

98. E. N. Lassettre, J. Chem. Phys. 43, 4479 (1965).

99. R. Marriott, in Atomic Collision Processes, edited by M.R.C. McDowell (North-Holland Publishing Co., Amsterdam, 1964), p. 114.

100. See, for example, (a) F. H. Nicoll and C.B.O. Mohr, Proc. Roy. Soc. (London) A142, 320 (1933); (b) C.B.O. Mohr and F. H. Nicoll, ibid. A138, 229 (1932);

(c) A. L. Hughes and J. H. McMillen, Phys. Rev. 44, 20 (1933); (d) E. G. Dymond, Phys. Rev. 29, 433 (1927); (e) M. Goodrich, Phys. Rev. 52, 259 (1937).

101. D. C. Cartwright, Ph.D. Thesis, California Institute of Technology, Pasadena (1967).

102. K. J. Miller, S. R. Mielczarek, and M. Krauss, J. Chem. Phys. 51, 26 (1969).

103. As an example of the application of this method, see S. Trajmar, J. K. Rice, P.S.P. Wei, and A. Kuppermann, Chem. Phys. Lett. 1, 703 (1968).

104. Ref. 3, pp. 325-326.

105. L. I. Schiff, Quantum Mechanics (McGraw-Hill Book Co., Inc., N. Y., 1955), 2nd ed., pp. 169-170. We thank S. Lipsky for helpful discussion of this point.

106. D. G. Truhlar, J. K. Rice, S. Trajmar, and D. C. Cartwright, Chem. Phys. Lett. 9, 299 (1971).